Oxygenation of 3,5-di-*tert*-Butylphenol: Reaction, Optimization and Mechanism

By Yuxuan Li

A Thesis

In the Department

Of

Chemistry and Biochemistry

Presented in Partial Fulfillment of the Requirements

for the Degree of Master of Science (Chemistry)

at Concordia University

Montreal, Quebec, Canada

August 2018

CONCORDIA UNIVERSITY
School of Graduate Studies

This is to certify that the thesis prepared

By: Yuxuan Li

Entitled: Oxygenation of 3,5-di-*tert*-butylphenol: reaction, optimization and mechanism

and submitted in partial fulfillment of the requirements for the degree of

Master of Science in Chemistry

complies with the regulations of the University and meets the accepted standards with respect to originality and quality.

Signed by the final examining committee:

Dr. Louis Cuccia Chair

Dr. Pat Forgione Examiner

Dr. John Oh Examiner

Examiner

Dr. Xavier Ottenwaelder Supervisor

Approved by:

Chair of Department or Graduate Program Director

Dean of Faculty

Date: August 31st 2018

Abstract

Oxygenation of 3,5-di-*tert*-butylphenol: reaction, optimization and mechanism

Yuxuan Li, MSc

Concordia University, 2018

The copper-catalyzed aerobic oxygenation of phenols is an attractive green method for the preparation of reactive and synthetically useful *ortho*-quinones. Recently, the Lumb group has developed fully catalytic conditions to perform this reaction with unsurpassed simplicity and efficiency. This reaction employs catalytic amounts of copper(I) and *N,N'*-di-*tert*-butylethylenediamine (DBED) as the supporting ligand. Our group unveiled the mechanism of this reaction with 4-*tert*-butylphenol, and showed that the oxygenation proceeded via side-on peroxodicopper(II) core (^{S}**P**) and copper(II)-semiquinone (**SQ**) intermediates. However, not all substrates behave equally under these or similar reaction conditions, with some substrates undergoing oxygenation with subsequent C–O coupling, some undergoing only oxygenation, and some undergoing radical-based C–C coupling. In order to better understand the selectivity of the reaction, we screened a library of ligands with different nitrogen donors and denticities on the substrate that only undergoes to *ortho*-oxygenation (3,5-di-*tert*-butylphenol). We present an extensive mechanistic study on the oxygenation reaction, including characterization of intermediates and kinetic studies. We employ UV-Vis spectroscopy between –120 and 25 °C as the main technique due to the colour of the reaction intermediates and products. We show that ligands that are successful at providing a good yield of quinones at room temperature are those who stabilize a ^{S}**P** core at low temperature. This core is the same as that in oxy-tyrosinase, the enzyme acting in the first step of melanin biosynthesis. Overall, this correlation provides a link between stoichiometric bio-inorganic studies at low temperatures and catalytic activity at room temperature, opening avenues for further reaction improvement.

Acknowledgements

First and foremost, I would like to express my gratitude to my supervisor, Dr. Xavier Ottenwaelder, whose insightful use of Da-Man and You're Fired points has been my life for these past years. The door to Dr. X office was always open whenever I ran into a trouble spot or had questions about my research.

I would also like to thank my committee members, Dr. John Oh and Dr. Pat Forgione. Without their patient and passionate participate, the defence could not be successfully conducted.

I thank all the XoRG members, former and present, kind-hearted and talented people who were always there for me: Mohammad S. Askari, Farshid Effaty, Nooshin Sheibany, Federica Gennarini, Laura Andrea Rodríguez Solano, Laura Chaloner, Kenrick Cabral-Cerqueira, Saida Latreche, Peter Gillich, Alexia Piercey, Mark Kit, and Michael Glazerman. For who helped me survive the horror of graduate life, I could not hold on to it without your supporting.

I would also like to thank Alain Tessier, with his incredible technique to help me out with the mass spectrometer problems in order to finish the KIE study. And a special thanks to Dr. Hein Schaper and Dr. Garry Hanan for the stopped-flow supporting in UdeM.

Last but definitely not least, a great gratitude to my dearest family and friends: Kai, Vincent, Marjorie, Gang, Ping and Peng for providing me with unfailing support and continuous encouragement throughout the years of my study; and teaching me to always look forward and never give up.

All the memories I made at Concordia will never be taken for granted, and I will be grateful forever for your love.

Contributions from Colleagues

Science is multidisciplinary that cannot be done alone. Significant portions of this research were only possible because of collaborations, even though most of the work has been done by myself, some key data involved in the thesis were obtained with/by my colleagues.

Mohammad S. Askari	Training, discussions on the mechanism and editing.
Farshid Effaty	Help with stopped flow data collection, editing.
Federica Gennarini	Electrochemistry measurements and analysis on **SQ** complexes.
Peter Gillich	Crystallizations and preliminary NMRs of **L-SQ**.
Mark Kit	Deuterated 3,5-DBP synthesis and KIE measurement.
Ohhyeon Kwon (McGill)	Bulk reactions with monodentate and a few bidentate ligands.
Alexia Piercey	Preliminary NMRs of **L-SQ**.

Table of Contents

List of Figures

List of Schemes

List of Charts

List of Tables

List of Abbreviations

2,4-DBP	2,4-di-*tert*-butylphenol
2,4-DBPNa	Sodium 2,4-di-*tert*-butylphenolate
2-MeTHF	2-methyltetrahydrofuran
3,5-DBP	3,5-di-*tert*-butylphenol
4-BP	4-*tert*-butylphenol
A	Phenolatobis(μ-oxo)dicopper(III)
bisOH	Bis(μ-hydroxo)dicopper(II)
C	μ-catecholato-μ-hydroxodicopper(II)
$Cu^{I}PF_6$	$[Cu(CH_3CN)_4](PF_6)$
CPET	Coupled Proton-Electron Transfer
CO	Catechol Oxidase
DCM	Dichloromethane
DBQ	3,5-di-*tert*-butylquinone
DBED	N,N'−di−*tert*−butylethylenediamine
Et_3N	Triethylamine
ED	Ethylenediamine
ET	Electron Transfer
Equiv.	Equivalents
EXAFS	Enhanced X-ray absorption fine structure
HAT	Hydrogen-Atom Transfer
HMB	Hexamethylbenzene
k	Rate Constant
K	Equilibrium Constant
KIE	Kinetic Isotopic Effect
MS	Molecular Sieves
L	Ligand
MeCN	Acetonitrile
MeOH	Methanol
NMR	Nuclear Magnetic Resonance
O	bis(μ-oxo)dicopper(III)
OAT	Oxygen-Atom Transfer
ORTEP	Oak Ridge Thermal Ellipsoid Plot
PD	Propylenediamine

^{S}P	μ-η^2:η^2-peroxodicopper(II)
^{T}P	*Trans*-μ-1,2-peroxodicopper(II)
Q2	Coupled quinone
ε	Molar absorptivity
SAR	Structure-Activity Relationship
SCE	Saturated Calomel Electrode
S_EAr	Electrophilic Aromatic Substitution
SQ	copper(II)-semiquinone
TfO	Triflate
TMPD	*N,N,N'N'*-tetramethylpropylenediamine
X	Benzoxepine
UV-Vis	Ultraviolet-Visible

Chapter 1: Introduction

This thesis deals with the catalytic aerobic oxygenation of phenols into *ortho*-quinones, a process inspired by the first step of melanin biosynthesis (melanogenesis). After an introduction on melanogenesis and the key enzyme tyrosinase, model copper complexes will be described, including those enabling the desired oxygenation reaction in stoichiometric or catalytic fashion. The goal of the thesis is to probe one such reaction on a specific substrate, 3,5-di-*tert*-butylphenol, in terms of both reaction screening and mechanistic probing.

1.1 Biosynthesis of Melanin

Melanin pigments are found in most organisms, considered as a shield against UV light and different types of ionizing radiations.[1] It is also prevalent in fungi and fruits, e.g. the browning of mushrooms or fruits upon exposure to air. Investigation of melanogenesis started back to 1886, when Bertrand identified the amino acid tyrosine as a melanin precursor.[2] In 1926, Raper isolated the intermediate dopaquinone,[3] and in 1985, an enzymatic process involving tyrosinase-catalyzed conversion of tyrosine to dopaquinone was reported that yields both the red pheomelanin and the black eumelanin.[4] A simplified scheme of the melanogenesis process is provided in Scheme 1-1. In biological organisms, tyrosinase activates O_2 as the oxygen-atom source, catalyzes the conversion of L-tyrosine into L-dopaquinone via *ortho*-oxygenation, and water is the only by-product. Tyrosinase is no longer needed once dopaquinone is formed; subsequent steps are straightforward or catalyzed by non-redox tautomerases.[5] Therefore, the oxygenation of tyrosine into dopaquinone is the key to replicating this type of reaction.

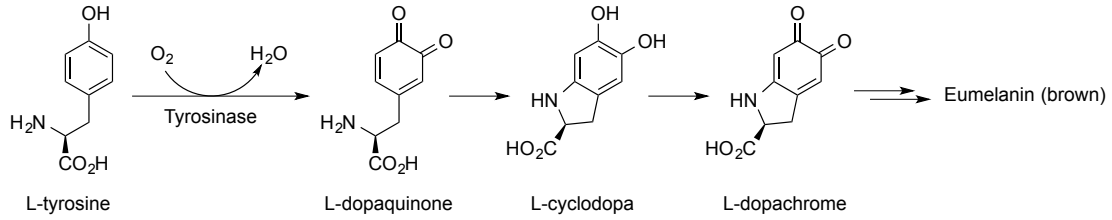

Scheme 1-1. Main reactions involved in melanogenesis.

Aerobic catalysis exponentially rises up because oxygen could act as either an electric sink (oxidase activity) or a source of oxygen atom that could able to coordinate into the product (oxygenase activity).[6] Another advantage of using oxygen as an oxidant is its non-toxic byproducts, being either reduced to water, occasionally via H_2O_2 (oxidase), or coordinate into a substrate structure (oxygenase).[6]

1.2 Tyrosinase

Tyrosinase has long received momentous attention because *ortho*-quinones and catechols are useful organic synthons. Tyrosinase is a type-III coupled binuclear Cu enzyme – the term "coupled" or "type-III" refers to the presence of magnetic coupling between the Cu(II) ions in the oxidized form of the enzyme.[2,7] In its reduced form, tyrosinase contains two Cu(I) 4.0-4.6 Å apart in its activate site, each coordinated to three histidine residues (Scheme 1-2).[8]

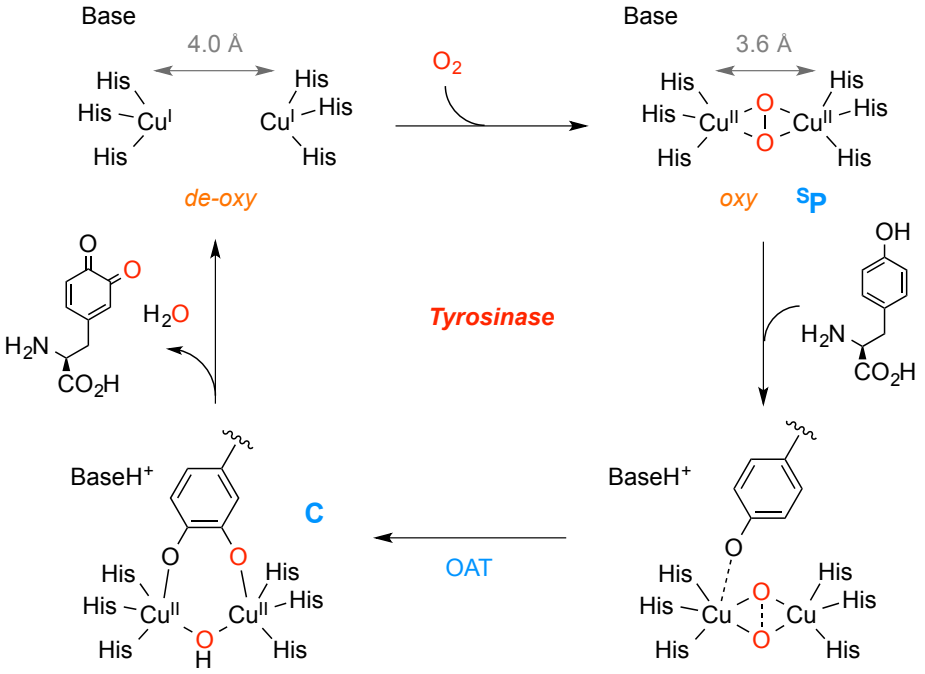

Scheme 1-2. Simplified mechanism of the *ortho*-oxygenation of L-tyrosine by tyrosinase during melanogenesis, with the key μ-η^2:η^2-peroxodicopper(II) (**^{S}P**) and μ-catecholato-μ-hydroxodicopper(II) (**C**) intermediates. The nature of the basic residue in the active site is still debated. OAT = Oxygen-Atom Transfer.

The Cu(I) centres in the deoxy state are able to bind O_2 in a characteristic side-on fashion forming peroxodicopper(II) moiety (**^{s}P**) by each donating one electron to O_2, thereby reducing it into a peroxide, O_2^{2-}, and each reaching a Cu(II) oxidation state. This side-on binding mode was confirmed by X-ray structures of oxytyrosinase in 2006 and later (Cu···Cu ca. 3.6 Å and O–O ca. 1.22 Å).[9-10]

The proposed mechanism of tyrosinase reaction proceeds via the side-on peroxodicopper(II) oxidant. The substrate, tyrosine, gets deprotonated in situ by a still-debated protein residue, and the resulting phenolate is proposed to bind into the Cu coordination sphere. The key step of the reaction is the oxygen-atom transfer (OAT) between the electrophilic Cu_2O_2 moiety and the electron-rich phenolate. Consistent with Hammett and kinetic isotopic effect (KIE) analyses,[11-12] the mechanism is proposed to proceed via electrophilic aromatic substitution pathway. The result is O–O bond cleavage, C–O formation and proton transfers generate a catecholato complex, **C**, in which the catecholate is proposed to bind both Cu(II) ions. Further oxidation of the catecholate by the Cu(II) ions liberates the quinone product and regenerates the de-oxy state of the enzyme, i.e. Cu(I) stage. The substrate oxygenation uses one oxygen atom from O_2 (i.e. monooxygenase activity), while the other oxygen atom is incorporated into a water molecule.

The mechanism of tyrosinase is a paradigm that extends to other reactions. For example, the O_2 transporter hæmocyanin is now seen as a version of tyrosinase that has blocked substrate access.[13] In addition, the aerobic two-electron transfer oxidation of catechols to quinones can be catalyzed by tyrosinase or structurally similar catechol oxidase (CO) enzymes.[8] As melanogenesis is a key process in hair and skin pigmentation, the cosmetic industry is keen to uncover the potential of this process to develop new hair-dying or skin-tone-modifying products.[14] Therefore, there has been a longstanding interest in understanding and mimicking the reactivity of coupled binuclear Cu core that are able to react with O_2. Thus, chemists have strived to obtain small-molecule models that mimic the enzymatic system in order to probe the enzymatic mechanism indirectly and to develop new organic synthetic tools.[6, 15]

1.3 Model Cu/O_2 Complexes

1.3.1 Bonding modes of Cu/O_2 species

Interaction of Cu(I) complexes with O_2 can result in different types of O_2 bonding and geometries. The nature of the resulting Cu/O_2 species is highly dependent on the structure of the ligand supporting the Cu centre and, to a lesser extent, the counterion (Scheme 1-3).[10-16] Only with ligands that are sufficiently electron-rich (e.g. tertiary di, tri and tetra-amines) will the reaction lead to an electron transfer to O_2 and the characterization of a Cu/O_2 intermediate. Most of these intermediates are, however, only stable at very low temperatures, typically –78°C, and decay readily by self-oxidation on the ligand or oxidization of adventitious impurities or solvent. With mononuclear Cu(I) precursors, a 1:1 Cu/O_2 intermediates ($^{S/E}$**S**) forms first, which quickly reacts with another equivalent of the starting Cu(I) complex to form the 2:1 Cu/O_2 species ($^{S/T}$**P** and **O**) (Scheme 1-3). The binuclear species are more prevalent due to the easier reduction of O_2 by $2e^-$ than by $1e^-$.[17-18]

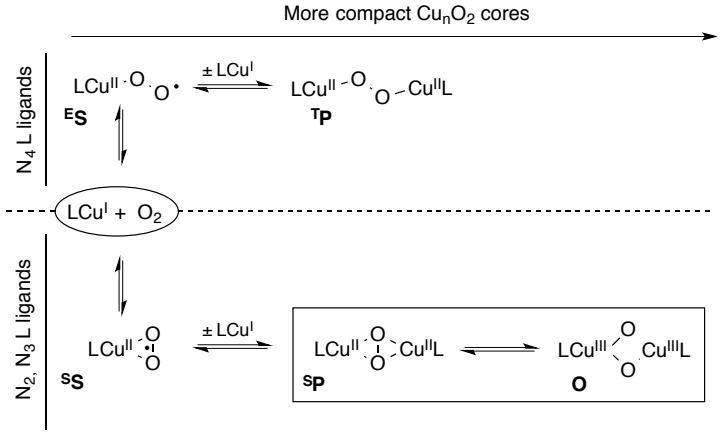

Scheme 1-3. Most prevalent mononuclear and binuclear Cu/O_2 species formed upon exposing a L-Cu(I) complex (L = bi/tridentate (bottom) or tetradentate (top) nitrogen-donor ligand) with O_2 at low temperature in aprotic solvents.[10]

In the following sections, only binuclear ^{S}**P** and **O** complexes will be discussed because they pertain to the tyrosinase mimicry. Importantly, ^{S}**P** and **O** species are valence isomers, i.e. they are constitutional isomers with the same molecular formula and only differ by the oxidation

states of Cu and the O_2 moiety: $Cu(II)_2$ and O_2^{2-} in ^{S}**P** vs. $Cu(III)_2$ and $(O^{2-})_2$ in **O**. In the majority of cases, ^{S}**P** and **O** species are strong oxidants and, for that reason, are only stable at –50°C or below. This inherent instability makes structural characterization of these species difficult. The method of choice to characterize their electronic structure is UV-Vis absorption spectroscopy, as both species exhibit characteristic charge-transfer bands.

1.3.2 Electronic structure of side-on peroxodicopper(II) ^{S}P

In general, bidentate and tridentate ligands favour the formation of side-on Cu/O_2 species. The first examples of a side-on peroxodicopper(II) intermediate (^{S}**P**) were reported by Kitajima who used a variety of substituted anionic tris(pyrazolyl)borate, $Tp^{R,R'}$ (R = Me, *i*Pr, Ph; R' = Me, *i*Pr, the $Tp^{iPr,iPr}$ is shown in Scheme 1-4) The complexes form intermediates spectroscopic parameters that closely resemble the oxygenated hæmocyanin, another oxygen carrier copper protein found in molluscs and arthropods.[19-20] X-ray characterization of this complex predates the first X-ray structure of oxy-tyrosinase (2006). It is the comparison of the UV-Vis features of the complex with that of oxy-tyrosinase that enabled to propose the side-on binding mode in the enzyme for the first time. This was a seminal achievement in biomimetic inorganic chemistry.

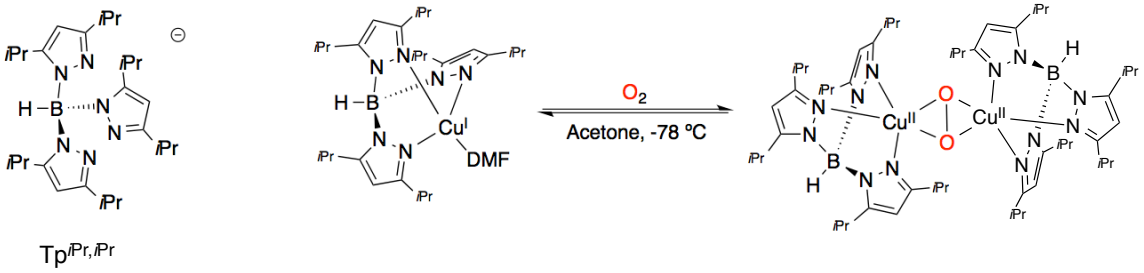

$Tp^{iPr,iPr}$

Scheme 1-4. The ^{S}**P** formation from Cu(I) complex with $Tp^{iPr,iPr}$ as supporting ligand.[18]

UV-Vis spectra of ^{S}**P** species all exhibit an intense absorption band at 350-370 nm (18 000 – 25 000 $M^{-1}cm^{-1}$) and another less intense feature around 510-550 nm (≈ 1 000 $M^{-1}cm^{-1}$).[10] Solomon established that the transitions responsible for the observed bands are $\pi_\sigma^* \rightarrow d$ (350 nm) and $\pi_v^* \rightarrow d$ (530 nm) charge-transfer transitions (Figure 1-1), the more intense $\pi_\sigma^* \rightarrow d$ arising from better overlap of orbitals within the same plane.[21]

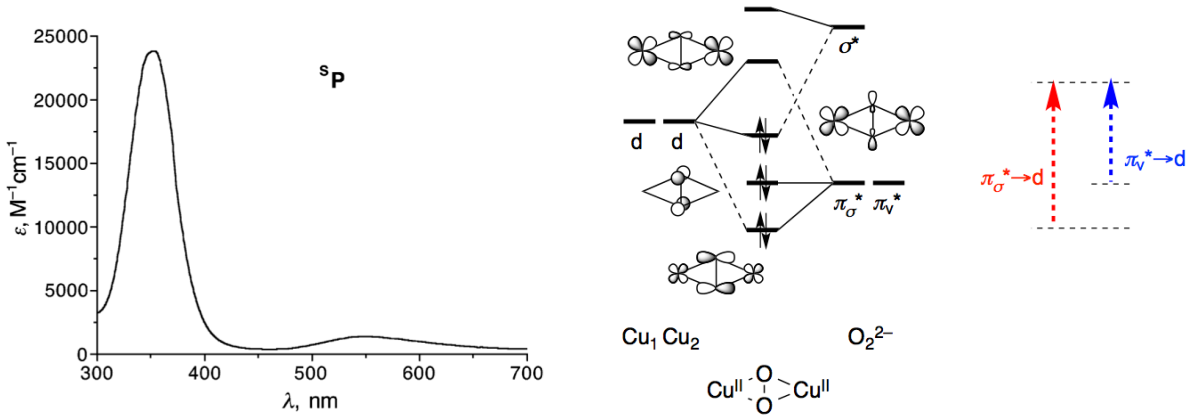

Figure 1-1. Typical UV-Vis spectrum and simplified molecular orbital diagram for a **^{S}P** species, with electronic transitions displayed on the right.[10]

1.3.3 Electronic structure of bis(*μ*-oxo)dicopper(III) species O

In 1995, Tolman et al. described a new Cu_2/O_2 motif, a bis(*μ*-oxo)dicopper(III) species, **O**. in which the O–O bond is completely cleaved. The bis(*μ*-oxo) complex is made from the $4e^-$ reduction of O_2 into two O^{2-} and the oxidation of two Cu(I) to Cu(III). Many bidentate and tridentate ligands support the **O** species over its **^{S}P** isomer, especially those favouring the square–planar coordination geometry preferred by d^8 Cu(III) ions.[10, 16]

UV-Vis spectra of **O** species all exhibit two intense charge–transfer bands at ca. 300 nm (~20,000 $M^{-1}cm^{-1}$) and 400 nm (~25,000 $M^{-1}cm^{-1}$) (Figure 1-2).[10] The O–O bond cleavage in **O** triggers a dramatic energy decrease of the σ* orbital, compared with the situation in a **^{S}P** species. Based on computational studies by Solomon, the band at 300 nm is assigned to a $\pi_\sigma^* \rightarrow$ d transition, and the band at 400 nm to a $\sigma^* \rightarrow$ d transition.[12]

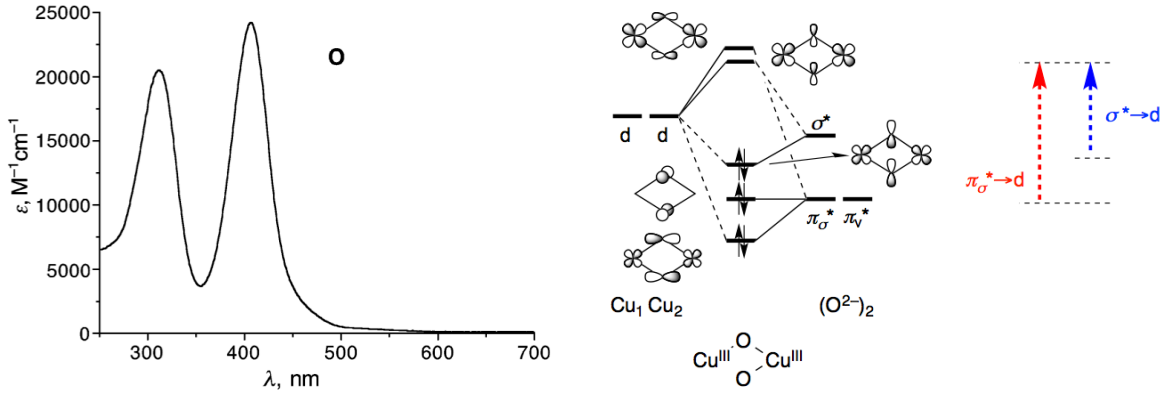

Figure 1-2. Typical UV-Vis spectrum and simplified molecular orbital diagram for a **O** species, with electronic transitions displayed on the right.[10]

1.3.4 Isomerism and equilibrium between ^{S}P and O isomers

The ^{S}**P** and **O** species are isoelectronic isomers that differ by the oxidation states of the Cu ions and the O_2 moiety (valence isomers, also known as electromers). The most striking difference between these isomers is the compactness of the Cu_2O_2 core, related in the Cu···Cu distance: 3.6 Å in ^{S}**P** and 2.8 Å in **O**, as measured by X-ray structures, enhanced X-ray absorption fine structure (EXAFS) and computational studies (Scheme 1-5).[22] As a result, more crowded supporting ligands tend to favour the ^{S}**P** formation and the least sterically demanding ligands are required to support the **O** core.

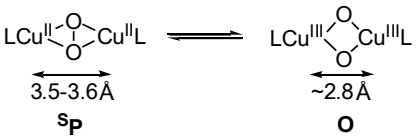

Scheme 1-5. Equilibrium between ^{S}**P** and **O**, with typical Cu···Cu distances.[22]

In 1996, Tolman et al. revealed the presence of an equilibrium between ^{S}**P** and **O** isomers when the ligand and reaction conditions are carefully chosen.[23] In 2000, Stack and co−workers used increasingly sterically demanding ligands to disfavour the **O** isomer and find conditions where the ^{S}**P** and **O** isomers have similar thermodynamic stabilities, leading to an equilibrium

mixture.[24] Examples of ligands supporting either or both isomers are drawn in Chart 1-1. These ligands are all based on aliphatic and/or heteroaromatic nitrogen donors.

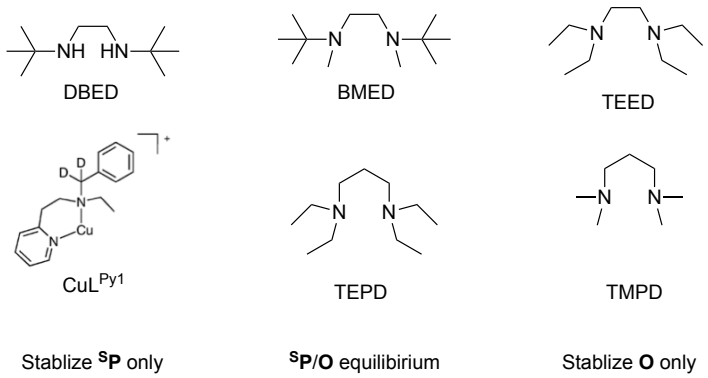

Chart 1-1. Examples of ligands supporting either or both **^{S}P** and **O** isomers.[10]

Beside the all-important steric effects, the last two decades of studies have provided some general trends for controlling the equilibrium position: (1) tridentate ligands favours **^{S}P** while bidentate ligands favours **O**;[25] (2) polar solvents tend to favour **O**;[25] (3) more coordinating anions (up to the basicity of carboxylates) favour **^{S}P** by axial anion coordination to the Cu(II) ion, which can accommodate square-pyramidal coordination more readily than a Cu(III) ion.[26] Stack has also recently revealed that the **O** core is made even more thermodynamically stable inasmuch as the proton affinity (not the pKa) of the ligand increase (i.e. these ligands are intrinsically stronger donors).[27] This is particularly striking feature as imidazoles, found in the tyrosinase active site, are actually better donors and will thermodynamically stabilize **O** species even more than tertiary amines.[28-30] Therefore, even though an **O** species has not yet been observed directly in biological systems, the facility of the **^{S}P**/**O** equilibrium, where only small bond length and oxidation changes occur, gives credit to the hypothesis of a transient **O** intermediate in the tyrosinase catalytic cycle.[30]

1.4 Aerobic Oxidation of Phenols

1.4.1 Thermodynamic and kinetic considerations

As electron-rich aromatics, phenols are prone to oxidations. However, because of their relatively high redox potentials (around 1.5 V vs. SCE),[31] a single-electron transfer is usually prohibited ($E^o(O_2/H_2O)$ = 0.98 V vs. SCE at pH0) and phenols tend to undergo coupled proton/electron transfers (CPET, also known as PCET for proton-coupled electron-transfer) or hydrogen-atom transfer (HAT, i.e. a $H^\bullet$ abstraction) under a large set of oxidation conditions. These processes generate a phenoxyl radical species that is responsible for the lack of selectivity in oxidation products (Scheme 1-6).[6]

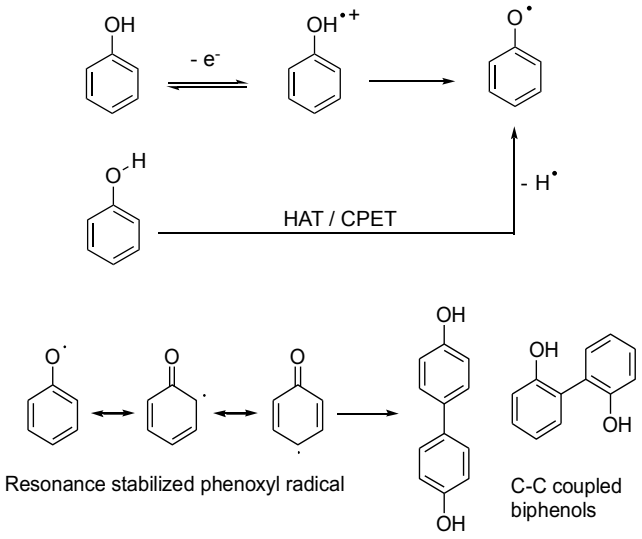

Scheme 1-6. Selectivity issue due to the HAT/CPET, phenoxyl radicals (up) and C-C coupling (bottom).[6,31]

The reaction carried out by tyrosinase is a phenol oxygenation, not an oxidation per se (Scheme 1-7). Therefore, simple redox arguments are not valid as this reaction involves bond making and cleavage. A simple thermodynamic calculation shows that the reaction of phenol and O_2 to make *ortho*-quinone and H_2O is an enthalpically favoured process (Scheme 1-8). The problem of selectivity towards oxygenation over radical-based reactions is therefore a kinetic issue. This problem is further complicated by the fact that O_2 is in a triplet spin state (S = 1). Most of the organic compounds being diamagnetic (S = 0), their reaction with O_2 is spin-

forbidden.[32] A catalyst, generally metal-based, is therefore required to reduce O_2 and activate it for further processes. Among the many metal complexes reported for activating O_2, Cu(I) species will be the only one discussed in this thesis because tyrosinase is a copper-containing enzyme.

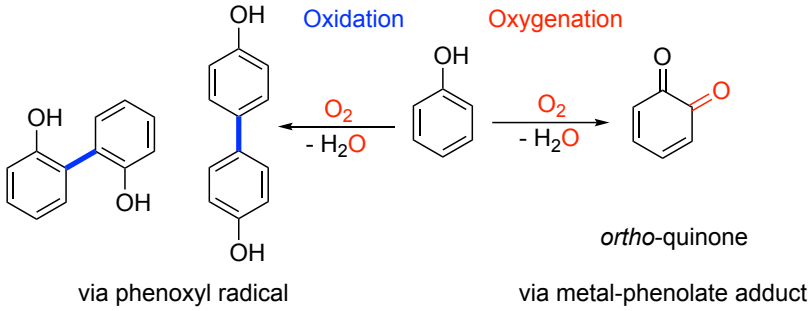

Scheme 1-7. Illustration of the selectivity issues upon oxidation/oxygenation of phenols.[33]

Scheme 1-8. Simple enthalpic analysis of the oxygenation of a phenol.

1.4.2 Inner-sphere vs. outer sphere reactivity

Enzymes are able to catalyze the difficult reactions efficiently with high selectivity that arouses the interest of bioinorganic chemists. The high substrate specificity and selectivity of the enzymes stem from the fact that the substrate is bound to or near the active site before reaction occurs. This ensures proper orientation of the substrate, proximity of the reactive sites (that of the enzyme and that of the substrate), and minimal side-reactions. One of the major difficulties when developing molecular catalysts is indeed to make sure that the substrate is close to the catalyst when the latter gets activated.

In the case of phenol oxidations, radical pathways are thought to stem from outer-sphere reactivity, i.e. the substrate encounters the activated catalytic species and an outer-sphere

electron-transfer occurs. To avoid this deleterious route, an inner-sphere pathway is desired, wherein the phenolic species is already bound to the catalyst upon activation of the latter. For this reason, researchers have long assumed that the phenol must be deprotonated, since a negatively charged phenolate is a much better coordinating species and would enter the coordination sphere more readily.

Tyrosinase brings together Cu(I) with nitrogen coordination, O_2 and a phenol, which, according to the above, should become deprotonated. Therefore, much efforts have been devoted to the reaction of phenolates and Cu(I) precursors with nitrogen-based ligands (aliphatic amines or heteroaromatics). For decades, 2,4-di-*tert*-butylphenol (2,4-DBP) has been the substrate of choice, because the two *tert*-butyl groups block the C2 and C4 positions and only the C6 (*ortho*) position is available for reaction (Chart 1-2). In addition, the diphenol resulting from C6−C6' coupling of 2,4-DBP is stable, which helps analysis of reaction conversion. To avoid the C−C coupling side-reaction, the sodium phenolate salt (2,4-DBPNa) was chosen preferentially, of course under stoichiometric conditions.

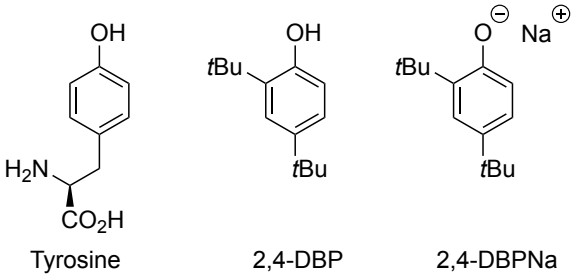

Chart 1-2. Structures of tyrosine, 2,4-di-*tert*-butylphenol (2,4-DBP), and sodium 2,4-di-*tert*-butylphenolate (2,4-DBPNa).

1.4.3 Stoichiometric studies

Many stoichiometric reactions between Cu/O_2 intermediates and phenols/phenolates have been reported over the last few decades. Most of the reactions with phenolates lead to desired products, either catechol or quinone or both, whereas with neutral phenols outer-sphere one-electron transfer leading to phenoxyl radicals takes place, leading to C−C/C−O coupling

products.[6,34] This work was reviewed extensively.[34-37,8,38] Here we only provide the main conclusions.

In 1996, Casella reported the first small-molecule model system of tyrosinase, using complex $[Cu_2(L66)]^{2+}$ (Scheme 1-9).[39] Reversible formation of an **^{S}P** species is observed at −80°C in dry acetone, which was capable of oxygenating electron-poor phenolates to catechols as well as converting electron-rich catechols into quinones.

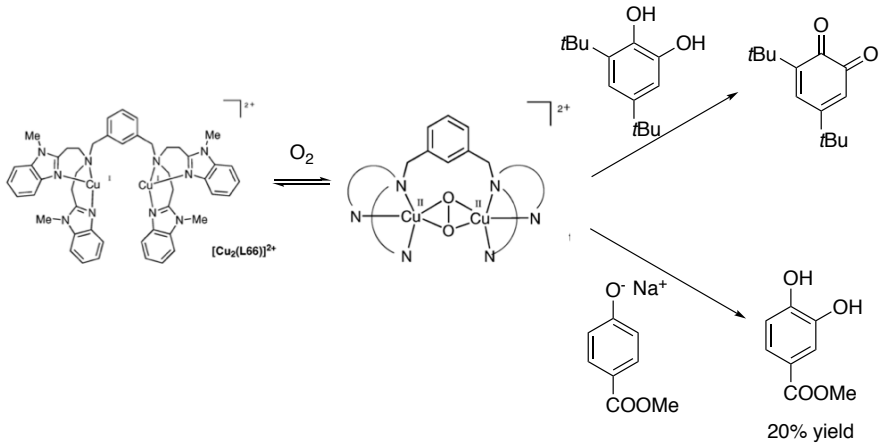

Scheme 1-9. Reactivity of $[Cu^{I}_2(L66)]^{2+}$ towards O_2 and subsequent reaction with external phenolate and catechols.[39]

In 2001, Itoh et al reported tyrosinase-like reactivity from an **^{S}P** species[40] based on the L^{Py2} ligand system (Scheme 1-10).[41] The reaction was performed in anhydrous acetone at −94°C, catechol complex was observed after injecting Lithium phenolate once the **^{S}P** was stabilized, 60% of catechol was isolated after acidic workups, but neither *ortho*-quinone nor C–C / C–O coupling dimer was obtained from the final product. This is the first time that researchers showed the evidence of intermolecular reactions between the **^{S}P** intermediate and the phenolate.

In contrast to the reaction with phenolate with yields the catechol, the reactivity towards external neutral phenols yielded the bisphenol compound, which was considered an undesired

side-products based on the radical pathway.[31] Moreover, the reaction with phenols are relatively slow, it requires 6 - 24 h, especially for the more electron poor phenols.

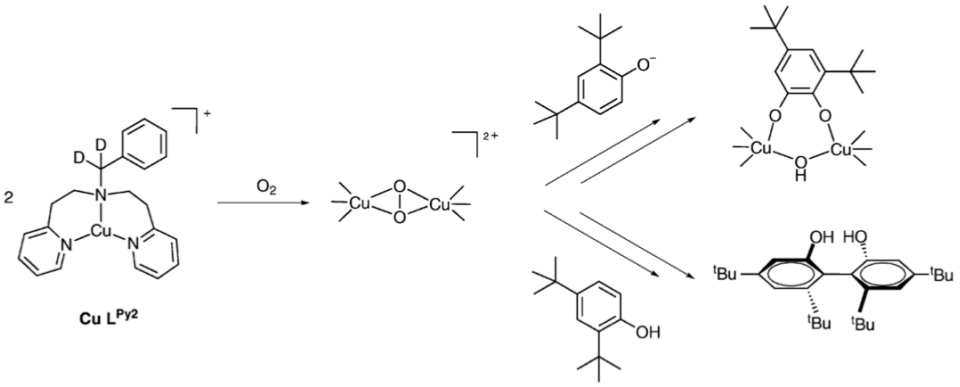

Scheme 1-10. Reactivity of the ^{S}**P** species supported by ligand L^{Py2}.[15, 31, 41]

From then on, various reactions of **O** species with external phenols and phenolates were attempted. In all examples, phenolates led to oxygenation products whereas phenols led to C−C and C−O coupling products. The consensus is that the closely packed **O** core is quite inaccessible and tends to induce via outer-sphere electron-transfer/H-atom abstraction reactions.[31, 41]

In seminal work, Stack et al [42-43] developed a Cu^{I}DBED system (DBED = *N,N'*-di-*tert*-buylethylenediamine) that was the first well-characterized monooxygenation of an external phenolate via an **O**-like species (Scheme 1-11). The reaction was performed at −120°C in 2-methyltetrahydrofuran (2-MeTHF). Once the DBED-Cu(I) precursor complex reacted with O_2 to form the ^{S}**P** species, O_2 was removed and the substrate sodium 2,4-DBPNa (2.5 equivalents with respect to ^{S}**P**) was added. A new species formed that was formulated as the phenolato-bis(μ-oxo)dicopper(III) **A**. Therefore, coordination of the phenolate (now believed to be two phenolates, actually) triggers isomerization of the ^{S}**P** core to an **O** core. In species **A**, the O atoms of the $Cu^{III}_2O_2$ core are electrophilic, and the electron-rich coordinated phenolate underwent an electrophilic aromatic substitution, characterized by an inverse kinetic isotope effect (KIE = 0.83). This provides a new mechanism scenario for the reactivity in tyrosinase because it indicated that the O−O bond on ^{S}**P** might be cleaved before the hydroxylation

occurs.[44] After an acidic workup, a 1:1 mixture of the corresponding catechol and 3,5-di-*tert*-butylquinone (DBQ) was isolated in 30% yield of each.

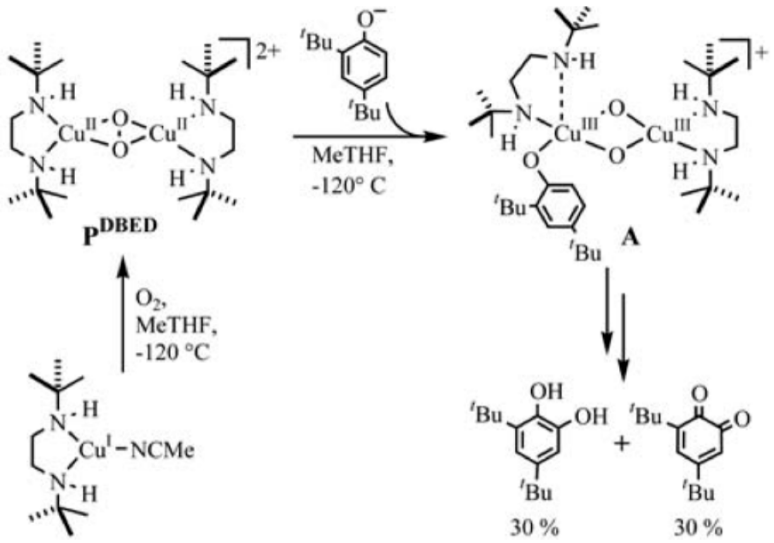

Scheme 1-11. Reactivity of the ^{S}**P** species with DBED ligand and 2,4-di-*tert*-butylphenolate at −120°C in 2-MeTHF, showing the intermediary of an **O**-like species, **A**.[44]

Therefore, the only way to mimic the tyrosinase−like reaction is a deprotonated phenolate coordinates to the Cu centre before aromatic oxygenation occurs, which ensures a selective oxygen-atom transfer (OAT) via an inner-sphere mechanism. If the intermediary of species **A** can be generalized to other ligands systems, one can take Scheme 1-12 as the general stoichiometric pathway going from a ^{S}**P** and a phenolate to the oxygenation product(s), catechol and/or *ortho*-quinone. After the LCu^{+} complex activates O_2 to make the ^{S}**P** core, phenolate binds to one Cu centre, inducing O−O bond cleavage to make the **O** core, at this stage. In the **O** core, the oxygen atoms are polarized by Cu(III) oxidation states and become electrophilic.[43] Therefore a natural S_EAr occurs between one of these O atoms and the electron-rich phenolate, generating catecholate species **C** (note the H^{+} transfer from the C−H bond to the distal O atom upon rearomatization) After acidic work-up oxygenated organics are obtained.

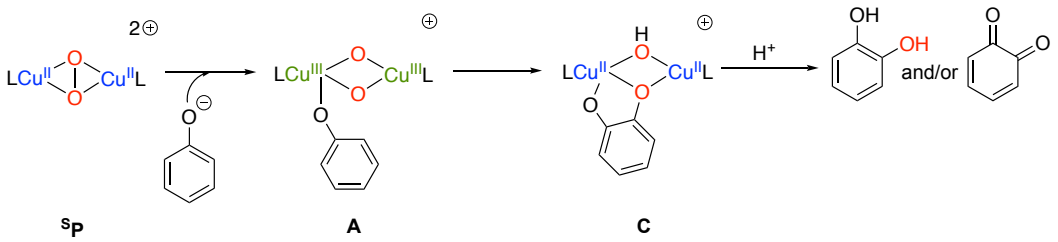

Scheme 1-12. Inner-sphere mechanism upon deprotonation.

For synthetic purposes, single-turnover stoichiometric reactions eliminate complexities such as side-reactions, concentration dependence and catalyst degradation, but they are not desired because they create large amounts of chemical waste (the remains of the Cu, ligands and/or base). Therefore, developing catalytic reactions becomes important, in line with green chemistry principles. Creating the phenolate in situ is not difficult pK_A-wise, but there is another condition that needs to be met for turnover: complex **C** has to be protonated in situ with an internal acid in order to release **SQ**, which can dissociate into the quinone product and a Cu(I) complex that shall re-enter the catalytic cycle. Therefore, the base used to deprotonate the phenol must make a conjugate acid strong enough to protonate **C** and form **SQ**.

Another important consideration is that phenolates are even more electron-rich than phenols and can thus undergo single-electron transfer at lower redox potentials. This thermodynamic drive would likely result in faster formation of phenoxyl radicals and unwanted products along an outer-sphere pathway. It is therefore essential that the phenolate binds to the active oxidant prior to the redox transfer, but this is something that is near-impossible to design successfully in a pre-catalyst.

1.4.4 Early catalytic model systems (with 2,4-DBP)

The biggest challenge in developing a good catalytic system is to achieve selectivity for *ortho*-oxygenation over radical-based pathways.

In 1955, Brackman and Havinga disclosed a catalytic oxygenation of unsubstituted phenol using Cu(I) salts and primary or secondary mono-amines.[45] The amine actually condenses with

the quinone to generate a stable product (Scheme 1-13). A few other examples followed to improve the model system by coordinating N-donor ligands (e.g. pyridine) to copper. However, all attempts showed a mixture of products, thus these conditions are far from being synthetically useful.

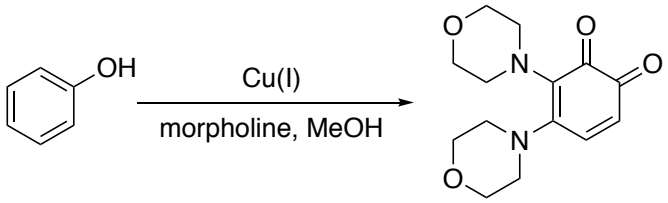

Scheme 1-13. Example of the oxygenation of unsubstituted phenol with morpholine to generate a stable product.[45]

2,4-di-*tert*-butylphenol (2,4-DBP) was the most used substrate for catalysis development, because it has only one position available for reactivity (C2) and its associated quinone, DBQ, is stable. Apart from a patent filed by Bulkowski,[46] there are only three examples reported.

1. The first model was designed by Réglier et al in 1990[35] using the binucleating tetradentate N-donor ligand BiPh(impy)$_2$ (Chart 1-3, left). This dinuclear Cu(I) precursor complex was able to mediate the catalytic conversion of 2,4-DBP to DBQ and/or 3,5-di-*tert*-butylcatechol in dry dichloromethane. The reaction, however, employs 2 equiv. of triethylamine (Et_3N), and is therefore not fully catalytic. Also, the conditions were not applied on other substrates. Interestingly, removing Et_3N led to C−C coupling products exclusively.

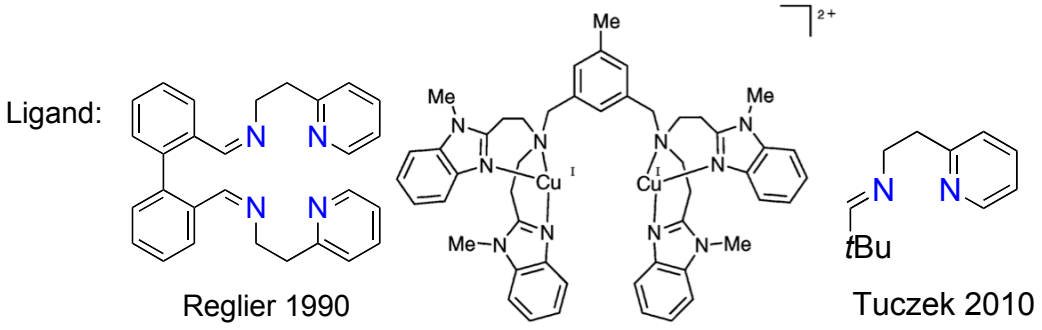

Chart 1-3. The structure of ligand BiPh(impy)$_2$ published by Réglier (binucleating, left) and Tuczek (mononucleating, right) and Cu(I)L66 reported by Casella (middle).

2. After this study, Casella et al described a binuclear Cu(I) complex supported by ligand L66 (Chart 1-3, middle) was able to convert the substrate 2,4-DBPNa to DBQ and/or catechol and yield of *ortho*-bisphenol (37%).[15]

3. Tuczek et al published a Cu(I) complex with mononucleating $BiPh(impy)_2$ model (Chart 1-3, right) which also catalytically converts 2,4-DBPNa to DBQ and/or catechol, with 50 equiv. substrate and 100 equiv. Et_3N.[15]

In summary, there are two issues in these three experiments: the selectivity and the superstoichiometric amount of Et_3N. In these investigations, a large excess of Et_3N is able to deprotonate phenol in situ, and the resulting triethylammonium can return the proton to the cycle leading the formation of water. As described below, water is deleterious to turnover and Et_3N alone can support turnover. Therefore, these systems, based on complicated, tailored ligands are not ideal.

1.4.5 Lumb's fully catalytic and selective catalytic system

1.4.5.1 Reaction conditions

In 2014, Lumb reported two catalytic systems one with Et_3N and one with DBED to adjust the pH of the reaction and ligates Cu salt.[47] He also addressed the selectivity issue by switching the model substrate to 4-*tert*-butylphenol (4-BP) instead of 2,4-DBP, which undergoes radical-based reactions exclusively.[47]

Lumb showed that 8 mol% Cu(I) and 50 mol% Et_3N alone could catalyze the oxygenation reaction, but the problem was to remove the by-product water from the mixture. Therefore, a desiccant (4 Å molecular sieves) was added into the reaction mixture to achieve high conversion and yield. In the absence of molecular sieves, the yield drops dramatically to 30-60%. Lumb postulates that water reacts with the quinone product to form a 2-hydroxy-*p*-quinone, which is a known poison to tyrosinase activity (Scheme 1-14).

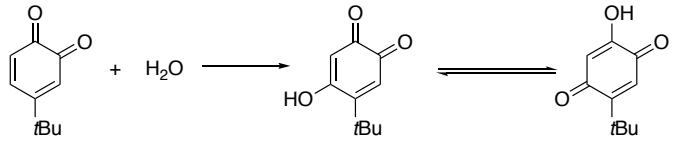

Scheme 1-14. Formation of 2-hydroxy-*p*-quinone, a poison to the catalyst.

Allan Hay showed that DBED as supporting ligand is not sensitive to water as by product in his Cu-catalyzed aerobic phenol polymerization.[48] Stack later used DBED to mimic a **^{S}P** as tyrosinase does, which makes it for a good stoichiometric phenolate oxygenation system.[49-50] Without any molecular sieves presented, 4 mol% Cu(I), 5 mol% DBED catalyzed the full conversion of 4-BP over 4 h at room temperature to obtain a greater 95% yield of a pure coupled quinone product, Q2 (Scheme 1-15). These conditions are homogeneous, selective and efficiency, which make the Lumb system ideal for mechanistic study of the oxygenation process by spectroscopy methods. These conditions have been now used on more than 70 phenols successfully (more examples in Chapter 2).[51]

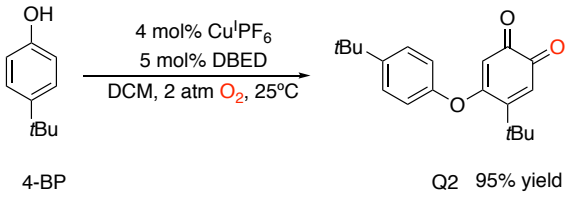

Scheme 1-15. Lumb reaction on 4-BP.

1.4.5.2 Mechanism studies at low temperature

The mechanism of the Lumb reaction on 4-BP was studied by one of our former group member, Mohammad Askari.[33] Using UV-Vis spectroscopy, a purple intermediate semiquinone complex, **SQ1**, forms rapidly and remained near steady-state concentration along phenol conversion and formation of coupled quinone Q2 (Scheme 1-16).

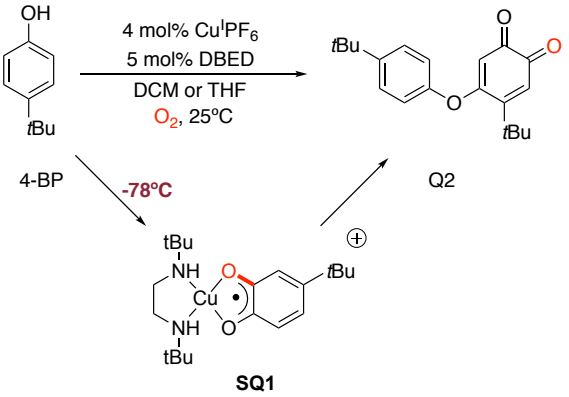

Scheme 1-16. Lumb reaction on 4-BP at low and room temperatures, with semiquinone complex intermediate.

By decreasing the temperature to −80°C, Mohammad was able to study the formation of **SQ1**, wherein *ortho*-oxygenation has occurred and the oxidative coupling is shut down. The mechanism at low temperature is provided in Scheme 1-17.[33]

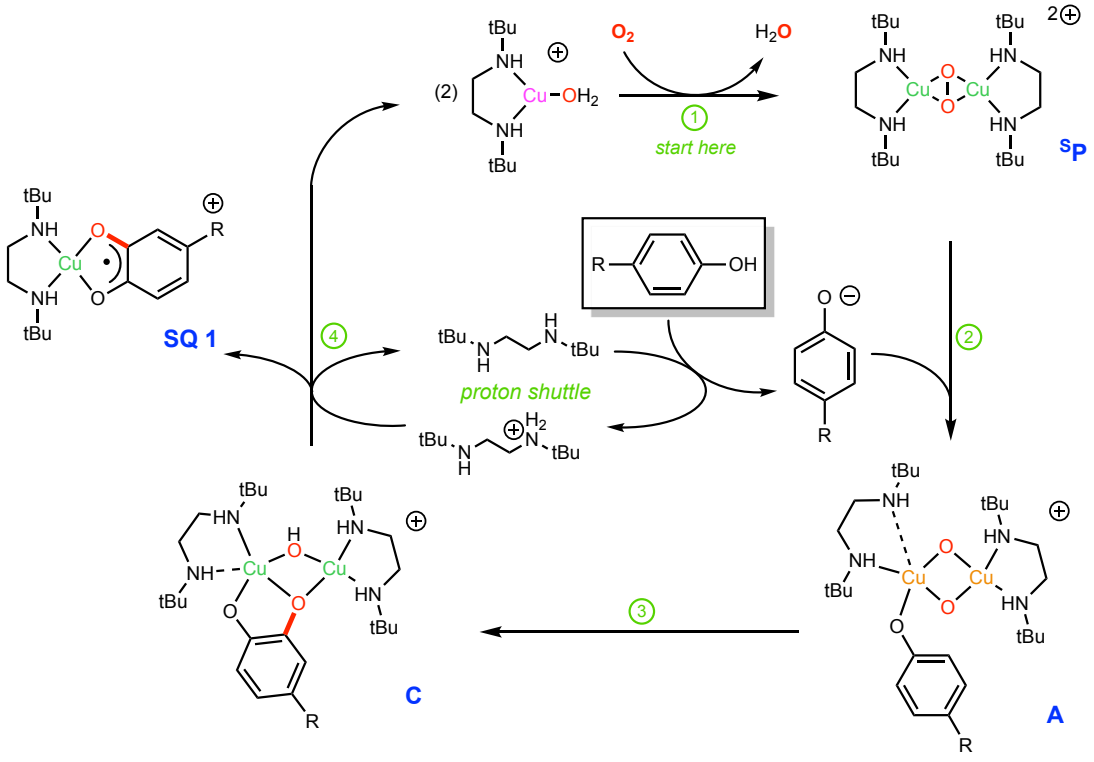

Scheme 1-17. Proposed mechanism for the oxygenation of 4-BP to **SQ1** at −80°C.[33]

In the first step, the DBED-Cu(I) complex actives O_2 to make the ^{S}**P** species (step ①). The small excess of DBED with respect to Cu acts as a base to deprotonate 4-BP into its phenolate that reacts with ^{S}**P** to generated postulated species **A** (step ②). The key step follows, an S_EAr from **A** to **C** that creates the C–O bond. Subsequent protonation of C releases **SQ1** and DBEDCu(I) that can re-enter the catalytic cycle.

At room temperature, the mechanistic study is thwarted by the involvement of the oxidative C–O coupling at position 4. This coupling is occurring with many other substrates (see 0). In search of ways to suppress the oxidative coupling, the Lumb group increased steric hindrance on the substrate. This led to the discovery of 3,5-di-*tert*-butylphenol, 3,5-DBP, as a substrate that only undergoes *ortho*-oxygenation. This substrate is the core for this thesis.

1.5 Thesis Objectives

Reaction of 3,5-di-*tert*-butylphenol (3,5-DBP) with O_2 (2 atm) using 8 mol% $Cu^{I}PF_6$ and 15 mol% DBED as catalyst in DCM for 4 h shows a greater than 96% NMR yield of 3,5-di-*tert*-butyl-*ortho*-quinone (DBQ) obtained with neither molecular sieves nor complicated work-up (Scheme 1-18).[52] Therefore, 3,5-DBP is an ideal substrate to study the *ortho*-oxygenation reaction at room temperature: the reaction is homogeneous, very high-yielding, and 100% selective.

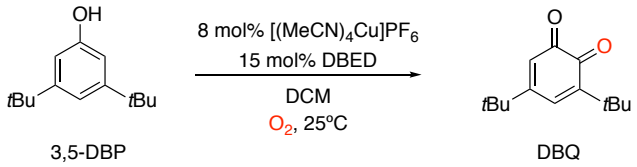

Scheme 1-18. *Ortho*-oxygenation reaction with 3,5-di-*tert*-butylphenol at room temperature.

The main **goal** of this thesis is to study the mechanism of the oxygenation reaction on 3,5-DBP in order to gain understanding of the inner-workings of the Cu^{I}/DBED conditions, especially at room temperature. The **specific objectives** are delineated in the three following chapters:

– Chapter 2 describes the oxidation of phenols by the DBED/Cu^{I} catalyst that led to the use of 3,5-DBP as ideal substrate. Mechanistic insight is also proposed that guides the next chapters.

− Chapter 3 describes the use of other diamine ligands than DBED. The purpose of this study is to probe the mechanism via structure-activity relationships (SAR), a key concept in organic methodology. While DBED remains the best amine to employ. This study allowed us to pinpoint at the source of the reaction selectivity (or lack therefore).

− Chapter 4 reports on the kinetic profiling of the DBED/Cu reaction on 3,5-DBP. The influence of the concentration of phenol, Cu and DBED highlight key steps of the mechanism. Kinetic isotope effect (KIE) measurements also confirm that oxygenation proceeds via S_EAr, as is the case in tyrosinase itself. This hallmarks the DBED/Cu mechanism as being bio-mimetic.

Chapter 2: DBED-Promoted Oxidations of Phenols

2.1 Introduction

In 2014, the Lumb group reported the most efficient method for the selective *ortho*−oxygenation of many phenols.[53] The typical reaction conditions employ 4 mol% of $[Cu^{I}(CH_3CN)_4](PF_6)$ (herein abbreviated $Cu^{I}PF_6$), 5 mol% of *N,N'*−di−*tert*−butylethylenediamine (DBED) in the stirring phenol solution (usually 0.1 M) in dichloromethane (DCM) at 25°C for 4 h under 2 atm O_2. These conditions are both selective and efficient, and work on a large array of phenols (see next section).

DBED was selected because it supports an **^{S}P** complex (like in oxytyrosinase) when its Cu(I) complex is oxygenated at −80 °C in THF (Scheme 2-1).[49-50] The Cu(I) species is formulated as $[(DBED)Cu(MeCN)]^+$ ($CuDBED^+$), in which the MeCN ligand stabilizes the Cu(I) oxidation state, but is labile enough for the reaction with O_2 to occur. The anion PF_6^- was chosen because of its non-coordinating properties and because $Cu^{I}PF_6$ is commercially available. The **^{S}P** species, $[(DBEDCu)]_2(O_2^{2-})]^{2+}$ is stable at low temperature for the analysis by spectroscopic techniques, with UV−Vis signature charge-transfer bands at 350 nm (ε = 36 000 M^{-1} cm^{-1}), 485 nm (ε = 1 200 M^{-1} cm^{-1}), and 605 nm (ε = 900 M^{-1} cm^{-1}).

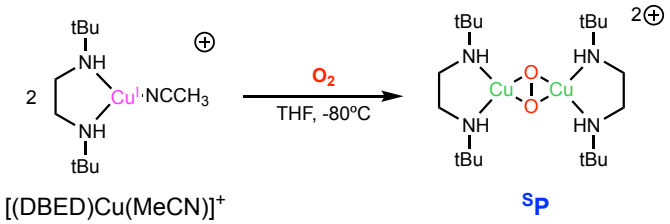

Scheme 2-1. **^{S}P** formation from $[(DBED)Cu(MeCN)]^+$ complex.[49]

Under the Lumb catalytic conditions, DBED is in slight excess to $Cu^{I}PF_6$ (5 mol% and 4 mol% to the phenol, respectively). The reason being 4 mol% DBED acts as a ligand to Cu, while the extra 1 mol% act as a base to deprotonate the phenol and generate the phenolate in situ.

As mentioned on section 1.3.3, ^{S}**P** and **O** can be equilibrium when varying the temperature and counterion. With DBED, no more than 5% of the **O** isomer was observed at low temperature, whatever the counterion used (PF_6^-, SbF_6^-, BF_4^-, ClO_4^-, TfO^-). Since higher temperatures will favour the ^{S}**P** isomer,[16] one can minimize the influence of an **O** isomer during turnover, at least when a phenolate is not bound to Cu.

The DBED system is therefore simple enough to start probing the mechanism of action of a selective oxygenation reaction. In this chapter, we will look at the influence of the substrate structure and the effect of using different Cu(I) and Cu(II) sources. The end-point is the selection of 3,5-di-*tert*-butylphenol as the best substrate for a deeper mechanistic analysis of the catalytic reaction.

2.2 Influence of the Substrate Structure

2.2.1 Mono-substituted phenols

Lumb and coworkers have screened the catalytic DBED conditions against *para*, *meta* and *ortho* mono-substituted phenols with a range of common functional groups including alcohol, amide, aldehyde, and nitrile functionalities. In all cases, the phenols underwent *ortho*-oxygenation and subsequent oxidative coupling(s) with the starting phenol, to afford so-called coupled products (Scheme 2-2).[53] Notably, in *meta*- or *ortho*-substrates, 4,5-disubstituted or 3,4,5-trisubstituted *ortho*-quinones are isolated, after one or two oxidative coupling steps, respectively. For the *para*-substituted phenols, the single product is the *ortho*-quinone coupled with phenol at C4 position.

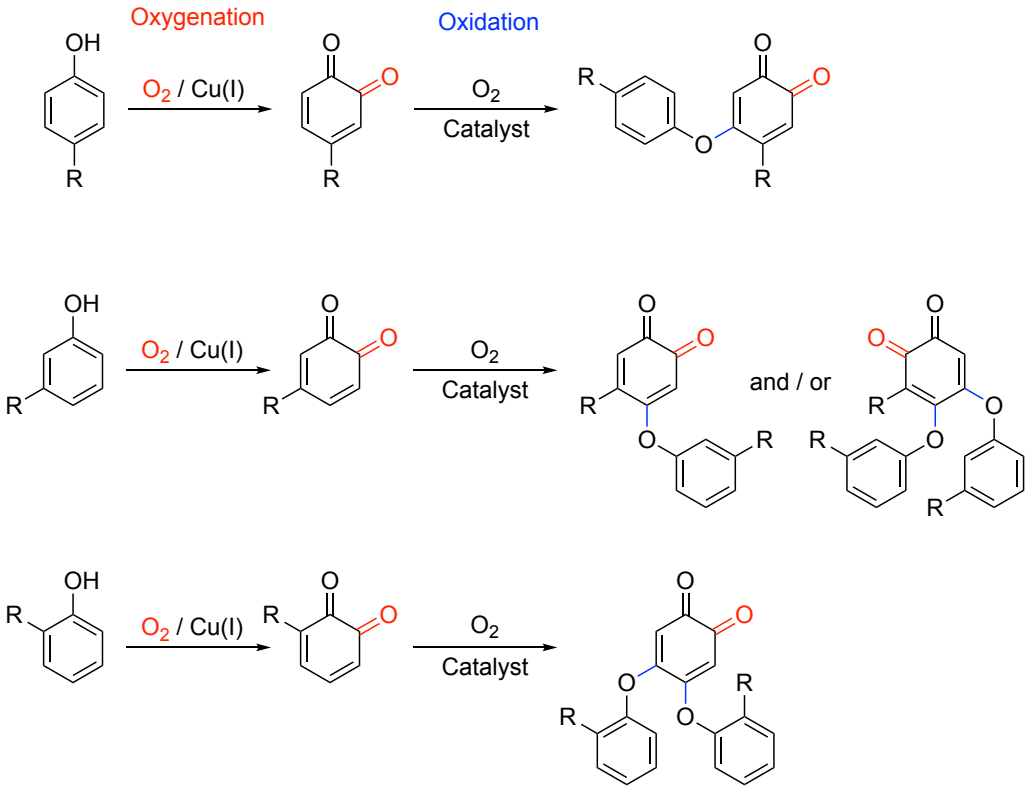

Scheme 2-2. Substrate scope under catalytic DBED conditions: phenol (1.0 mmol), O_2 (2 atm), $Cu^{I}PF_6$ (4 mol%), DBED (5 mol%), CH_2Cl_2 (0.1 – 0.5M) at 23°C for 4 hours.[53]

The mechanism of the reaction for the archetypal 4-BP substrate was studied by a former member of our group (see Introduction, section 1.4.5.2).[33] With this substrate, and very likely with all other substrates, the *ortho*-oxygenation occurs first and the oxidative coupling(s) occur next. When decreasing the temperature down to −80°C, the coupling is shut down kinetically, and only the oxygenation occurs, to yield the DBED-Cu(II)-semiquinone complex **SQ1**. If phenol is in excess, oxidative coupling turns on while warming-up to room temperature.

In order to get mechanistic insight at room temperature, at which the experimental catalysis proceeds, a substrate is desired that would completely thwart the oxidative coupling. Steric encumbering on the substrate was therefore used as a means to steer the reaction towards oxygenation without coupling pathways.

2.2.2 Disubstitution at positions 2,4

Identical reactions conditions were applied to 2,4-di-*tert*-butylphenol (2,4-DBP), with greater than 90% yield of benzoxepine **X** as the only product (Scheme 2-3).[47] The formation of benzoxepine is consistent with an oxidative dimerization of 2,4-DBP to bisphenol **BisP** via formation of a phenoxyl radical, followed by subsequent oxidation and isomerization. Stack and co-workers demonstrated the stoichiometric reaction of 2,4-DBPNa and the DBED-born ^{S}**P** at low temperature yielded oxygenated products (*ortho*-quinone and catechol), without bisphenol nor benzoxepine reported.[50] This complete change in selectivity from *ortho*-oxygenation to oxidative coupling highlights the divergence between stoichiometric and catalytic conditions.

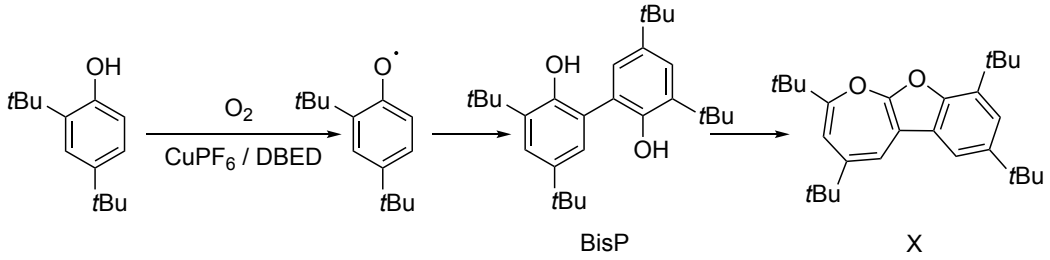

Scheme 2-3. Oxygenation of 2,4-DBP at room temperature.[47]

The reaction of 2,4-DBP (16 mM) with 4 mol% $Cu^{I}PF_6$ and 5 mol% DBED in CH_2Cl_2 under O_2 (2 atm) was monitored by UV-Vis at −75°C. Within a few minutes of reaction, an intense purple-coloured intermediate (ca. 600nm) forms (Figure 2-1). This known intermediate is the **SQ** complex.[54] Given the absorbance measured, it forms at 36% of the limiting Cu^{I} concentration. This is evidence that *ortho*-oxygenation can occur in the initial stages of the reaction. Whether this low-temperature experiment has valid repercussions on the room-temperature catalysis is, however, unknown. Because associative reactions are thermodynamically favoured at lower temperatures, the inner-sphere pathway becomes accessible in this case, while outer-sphere pathways would prevail at more elevated temperatures.

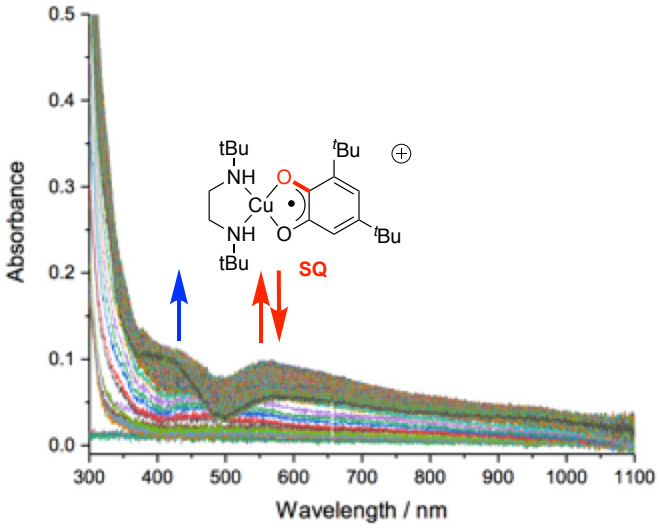

Figure 2-1. UV-Vis monitoring of the reaction of 2,4-DBP (16 mM), $Cu^{I}PF_6$ (5 mol%) and DBED (10 mol%) in DCM at −75°C when O_2 (1 atm) is introduced, for 4 hours, 36% SQ forms based on the absorbance measurement.

Both electronic and steric arguments are reasons to favour outer-sphere reaction pathways at room temperature. Thermodynamically, 2,4-DBP is more prone than 4-BP at a $1e^-$-oxidation, given its lower redox potential (E^o = 1.46 V vs. SCE) than 4-BP (E^o = 1.52 vs. SCE).[31] Kinetically, the steric interaction between the *tert*-butyl group located in C2 and the sterically encumbered DBED also disfavour inner-sphere oxygen atom transfer and promote the formation of free radicals.[47]

2.2.3 Disubstitution at positions 3,5

2.2.3.1 Reaction of 3,5-dimethoxyphenol

In order to avoid radical pathways caused by steric crowding at position 2, substitution at positions 3 and 5 was chosen as the next logical step. The first substrate tested was 3,5-dimethoxyphenol because it is commercially available. The two methoxy groups block positions C3 and C5, while the *ortho* (C2, C4) positions are accessible for oxygenation. Position C4 could, however, be accessible for oxidative coupling (see the *meta* derivatives of 2.2.1).

Experimentally, aerobic catalytic reaction of 3,5-dimethoxyphenol with 5 mol% $Cu^{I}PF_6$ and 10 mol% DBED (2 atm O_2 in DCM for 4 h) gives a mixture of two red products that were separated by column chromatography (Scheme 2-4).

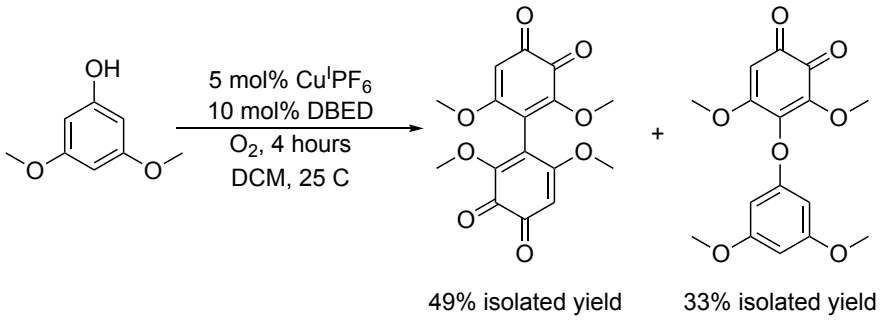

Scheme 2-4. Oxygenation of 3,5-di-methoxyphenol under Lumb's conditions.

The deep-red product of the first fraction crystallized by slow layered diffusion at −30°C of hexanes in a DCM solution. The X-ray structure unequivocally shows this fraction to be the C4-C4' coupling product of two quinones, i.e. 3,5-dimethoxyphenol underwent *ortho*-oxygenation at position C2, and the oxidative catalytic medium performed an oxygenation coupling of two molecules of this quinone. The ^{1}H-NMR of this compound is consistent with this bis-quinone formulation: it shows only one quinone-type signal, at 5.7 ppm (Figure 2-2).

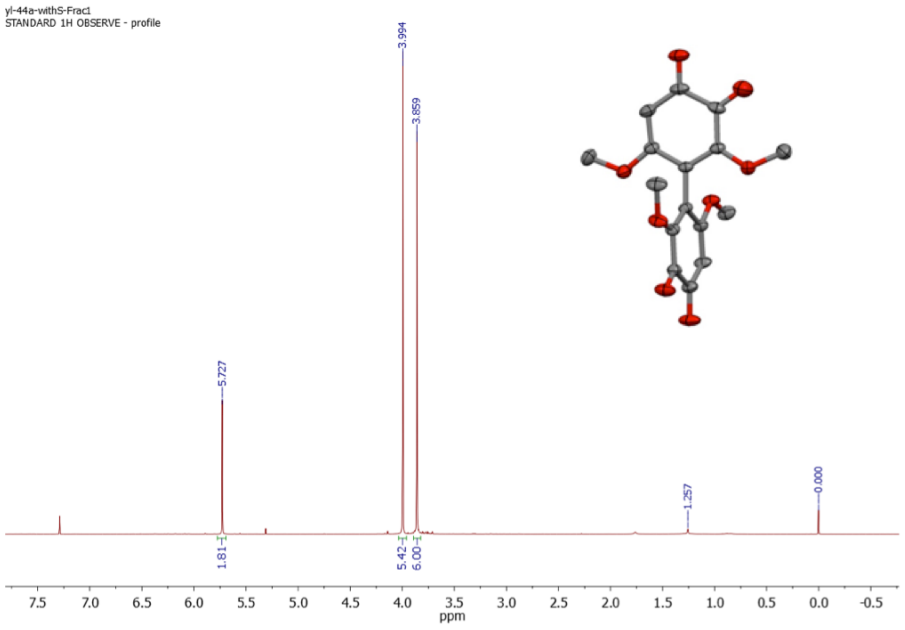

Figure 2-2. ^{1}H-NMR spectrum of the first fraction of the oxidation of 3,5-dimethoxyphenol ($CDCl_3$, 500 MHz, 25°C): δ 3.86 (s, 6H), δ 3.99 (s, 6H), δ 5.73 (s, 2H). ORTEP at 50% ellipsoid probability of the structure of the first fraction of by−products of oxygenate 3,5−di−methoxyphenol. Hydrogen atoms were omitted for clarity.

No crystals were obtained for the second fraction. The possible formulation is proposed based on the ^{1}H-NMR spectrum (Figure 2-3). The spectrum shows three signals at 3.7 (s, 12H), 5.7 (s, 1H) and 6.2 (s, 2H) ppm. The signal at 5.7 ppm is consistent with quinone-type proton, while that at 6.2 would be characteristic of a phenoxy residue.[53] We therefore propose that this product is the coupled quinone resulting from *ortho*-oxygenation and C4−O coupling.

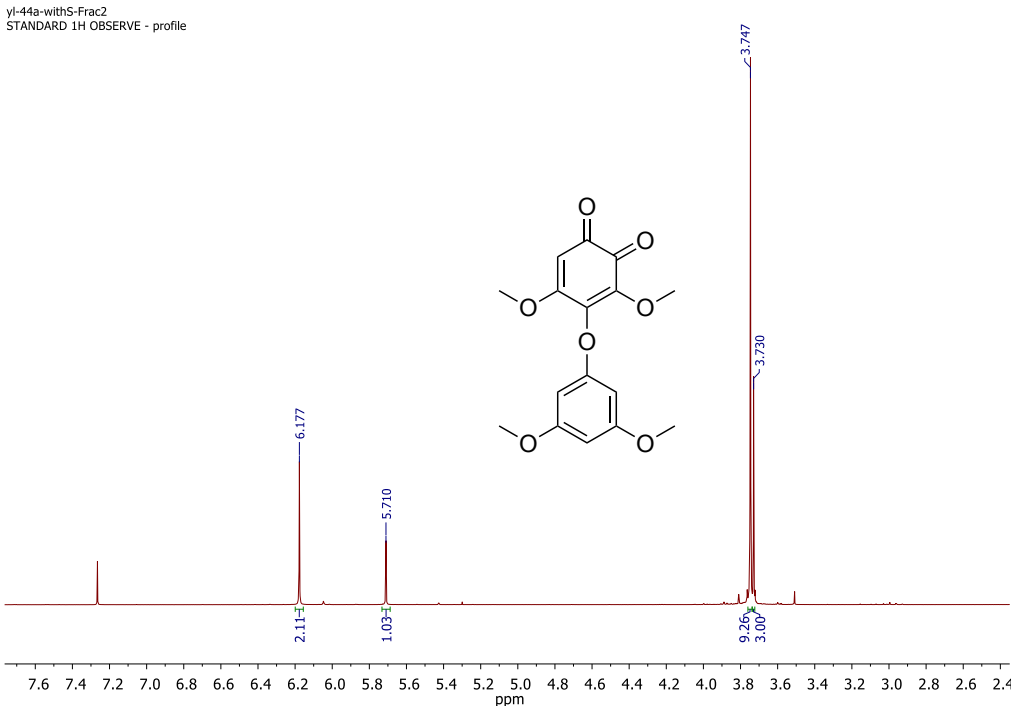

Figure 2-3. ^{1}H-NMR spectrum of the second fraction of the oxidation of 3,5-dimethoxyphenol ($CDCl_3$, 500 MHz, 25°C): δ 3.73 (s, 3H) δ 3.75 (s, 9H), δ 5.71 (s, 1H), δ 6.18 (s, 2H).

To conclude, 3,5-dimethoxyphenol is not a good substrate because it undergoes C–C and C–O couplings that cause a lack of selectivity. This substrate is not sterically crowded enough to prevent reactivity at position C4, and the electron-richness of the methoxy substituent would also favour radical-based pathways.

2.2.3.2 Reaction of 3,5-di-*tert*-butylphenol is optimal

In order to increase the steric crowding surrounding position C4, the Lumb and Ottenwaelder labs reengineered the synthesis of 3,5-di-*tert*-butylphenol, 3,5-DBP.[52] For our mechanistic analysis purpose (see below), it is essential to obtain this substrate in large quantities and the best synthetic protocol is reported on Scheme 2-5. The synthesis starts with 1-bromo-3,5-di-*tert*-butylbenzene, which can be prepared by adapting procedures for the bromination of 1,3,5-tri-*tert*-butylbenzene[52] using $SbCl_5$ as catalyst. 1,3,5-tri-*tert*-butylbenzene is then converted into

its Grignard, followed by borylation with $B(OMe)_3$ and oxidation with Oxone® to yield 3,5-DBP in 80% yield on decagram scale.

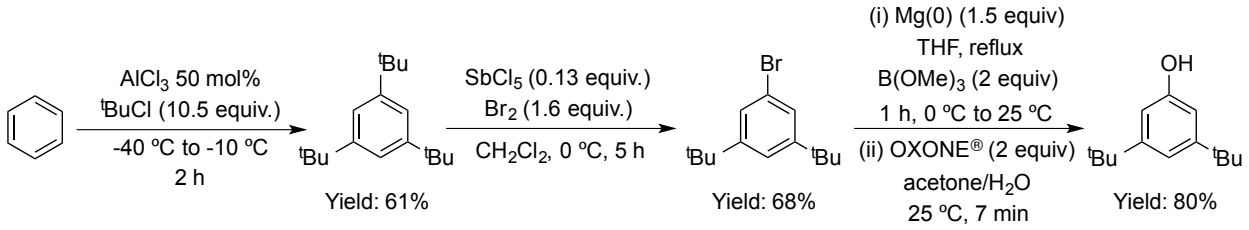

Scheme 2-5. Synthesis of 3,5-di-*tert*-butylphenol, 3,5-DBP.[52]

After optimization, the reaction of 3,5-DBP (10 mM) with 8 mol% $Cu^{I}PF_6$ and 15 mol% DBED under O_2 (2 atm) in DCM at 25°C shows a greater than 96% NMR yield of DBQ (Scheme 2-6). The optimal conditions require a higher loading of $Cu^{I}PF_6$ and a larger DBED/Cu^{I} ratio than the conditions used with mono-substituted phenols (4 mol% $Cu^{I}PF_6$, 5 mol% DBED, which yield 76% at 84% conversion when applied to 3,5-DBP). It is yet unclear why this particular substrate requires such higher loadings, but given the simplicity, low-price and low-toxicity of the catalyst components, this is not detrimental to the applicability of the reaction.

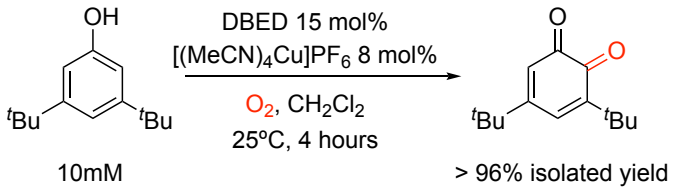

Scheme 2-6. Reaction of 3,5-DBP in bulk, optimized conditions.

The reaction is very clean throughout its conversion. An ^{1}H-NMR spectrum taken at mid-course (Figure 2-4) only shows the starting 3,5-DBP and the product DBQ (plus the hexamethylbenzene standard and residual solvent peaks). Therefore, the reaction is ideal for mechanistic studies as no side-product is detected, the reaction is 100% selective, with excellent yield, is fully homogeneous and proceeds within 4 h.

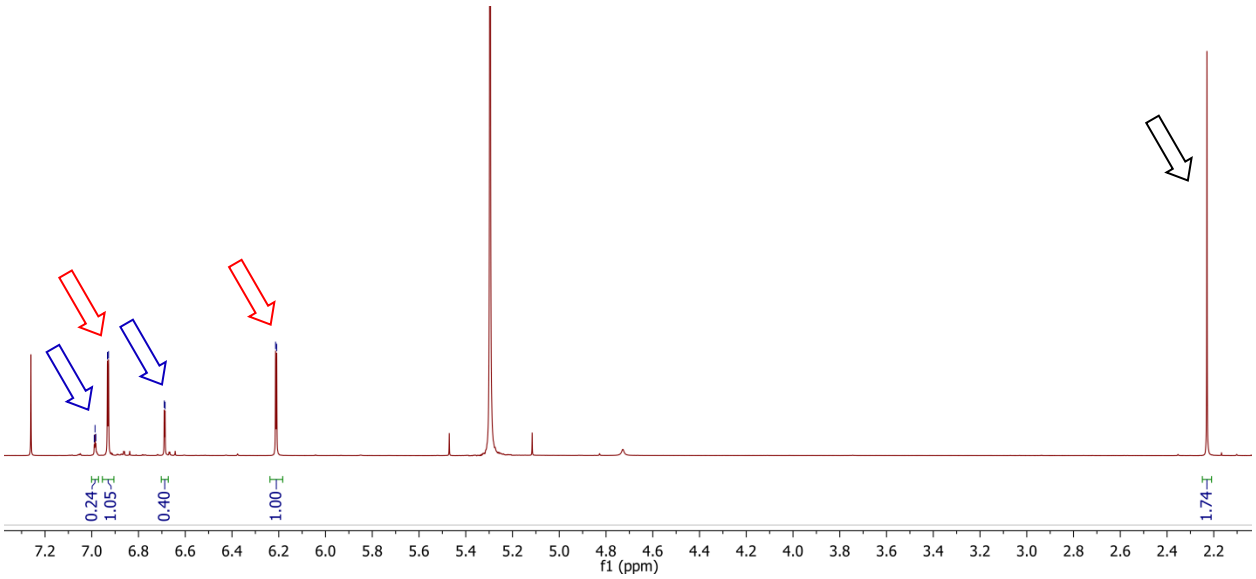

Figure 2-4. Crude ^{1}H-NMR (^{t}Bu region now shown) of a representative reaction at 84% conversion showing DBQ (red arrows, 76%) and 3,5-DBP (blue arrows, 16%). Conditions: 3,5-DBP (206.3 mg, 1 mmol), $Cu^{I}PF_6$ (14.9 mg, 4 mol%), DBED (10.8 µL, 5 mol%), CH_2Cl_2 (0.1 M), O_2 (2 atm), 1 h, hexamethylbenzene (internal standard, black arrow, 11.9 mg, 0.073 equiv.). ^{1}H−NMR of DBQ: δ (500 MHz, $CDCl_3$): 1.27 (s, 9H), 1.23 (s, 9H), 6.21 (s, 1H), 6.94 (s, 1H).[52]

2.3 Screening of Cu Precursors in the Reaction of 3,5-DBP

Other Cu precursors beside $Cu^{I}PF_6$ have been used successfully in the catalytic oxidation of 4-*tert*-butylphenol, including Cu(0) metal and air-stable Cu(II) salts (Table 2-1).[55] The precatalytic DBED-$Cu^{I}PF_6$ mixture is itself sensitive to O_2 and after complete conversion is recovered as the $[DBEDCu^{II}(\mu{-}OH)_2Cu^{II}DBED](PF_6)_2$ (**bisOH**) complex, as confirmed by IR spectroscopy and crystallization. The air−stable **bisOH**, prepared independently by exposing a 1:1 mixture of DBED:$Cu^{I}PF_6$ to O_2, is able to re-enter the catalytic cycle which implies in-situ reduction from Cu(II) to Cu(I) prior to *ortho*-oxygenation turnover. From a practical viewpoint, $Cu^{I}PF_6$ are not an ideal pre-catalyst due its relatively low solubility and its high O_2-sensitivity in the presence of DBED (glovebox work or careful N_2 blanketing are required). This prompted us to investigate other Cu salts with a range of oxidation states from 1 to 2. This screening study will also inform on the sensitivity of the reaction conditions to changes in counteranion and Cu precursor solubility.

In order to optimize the DBED-Cu complexes, a series of Cu sources have been investigated. In the glovebox, Cu complexes were made by mixing 8 mol% Cu source and 15 mol% DBED with 3,5-DBP in DCM. O_2 exposure was carried out for 4 hours for most of the Cu(I) cases, except the insoluble Cu_2O which required 4 days, and 24 hours for some Cu(II) cases. Most reactions were also tested in the presence of 4 Å molecular sieves, as it was shown before that a desiccant can improve turnover.[47, 53]

Table 2-1. Oxygenation of 3,5-DBP with various Cu(I) and Cu(II) sources.

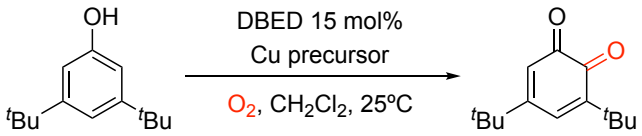

Entry	Cu Species	Time (h)	Conversion [yield] (%) [a]	
			No MS [b]	+ MS [b]
Cu(I) Species				
1	$[Cu(CH_3CN)_4](PF_6)$	4	96 [96]	100 [100]
2	$[Cu(CH_3CN)_4](TfO)$	4	100 [93]	100 [91]
3	CuCl	4	85 [19]	88 [24]
4	CuBr	4	94 [30]	94 [33]
5	CuI	4	96 [36]	92 [22]
6	Cu_2O	72	11 [3]	74 [32]
Cu(II) Species				
7	$Cu(OAc)_2{\cdot}H_2O$	24	11 [3]	
8	$Cu(OTf)_2$	4	92 [26]	86 [17]
9	$Cu(OTf)_2{\cdot}4H_2O$	4	91 [36]	44 [22]

[a] 0.25mmol of 3,5-DBP, 8 mol% Cu precursor and 15 mol% DBED, NMR yields determined with HMB as internal standard. [b] MS = 4 Å molecular sieves (100 mg).

Among the Cu(I) species that were probed (see Table 3-1), weakly coordination anions such as PF_6^- or TfO^- show the best catalytic activity and selectivity. Insoluble pre-catalysts (CuCl, CuBr, CuI, and Cu_2O) lead to low selectivity either with or without molecular sieves. Interestingly, Cu_2O required an induction period of three days, and at one point the catalysis begins and

complete conversion is achieved within a few hours. This suggests that turnover requires a soluble catalyst.

None of the Cu(II) salts tested led to efficient *ortho*-oxygenation catalysis. Commercial $Cu^{II}(OAc)_2 \cdot H_2O$ is a good candidate due to its high conversion and yield (97%) when 4-BP is used as substrate.[55] However, with 3,5-DBP, no significant conversion was achieved. Cu(II) triflate salts, which hydrated form $Cu^{II}(TfO)_2 \cdot 4H_2O$ was efficient with 4-BP (84% yield), are both inefficient with 3,5-DBP, but high conversion indicate uncontrolled radical pathways. The Cu(II) oxidation state is therefore detrimental when 3,5-DBP is used as substrate. This result is surprising since the oxidation potential of 3,5-DBP (1.62 V vs. SCE)[52] is higher than that of 4-BP (1.52 V vs. SCE)[56] and should therefore hamper single-electron transfer to form a phenoxyl radical. We therefore surmise that the deprotonation of the phenol may have a role, but pK_A values were not measured. Also, the missing insight into the initial in-situ reduction from Cu(II) to Cu(I) would require studies by another student.

In summary, $Cu^{I}PF_6$ remains the optimal Cu source for studying the reaction optimization and probing the mechanism of catalytic aerobic *ortho*-oxygenation of 3,5-DBP.

2.4 Mechanistic Profiling of the DBED-$Cu^{I}PF_6$-Catalyzed Reaction of 3,5-DBP

2.4.1 A semiquinone complex as reaction intermediate

The reaction of 3,5-DBP with 8 mol% $Cu^{I}PF_6$, 15 mol% DBED under O_2 (1 atm) was monitored via UV-Vis for 4 hours (Figure 2-5). An intense purple colour develops right after O_2 injection, then the solution slowly turns brown-orange inasmuch as the quinone product forms (absorption at 403 nm). This is the same behaviour as in previous studies with 4-BP.[38] The purple intermediate, with a maximum absorption at 578 nm, is easily recognized as the DBED-Cu^{II}-semiquinone complex, herein abbreviated **SQ** (Figure 2-5).

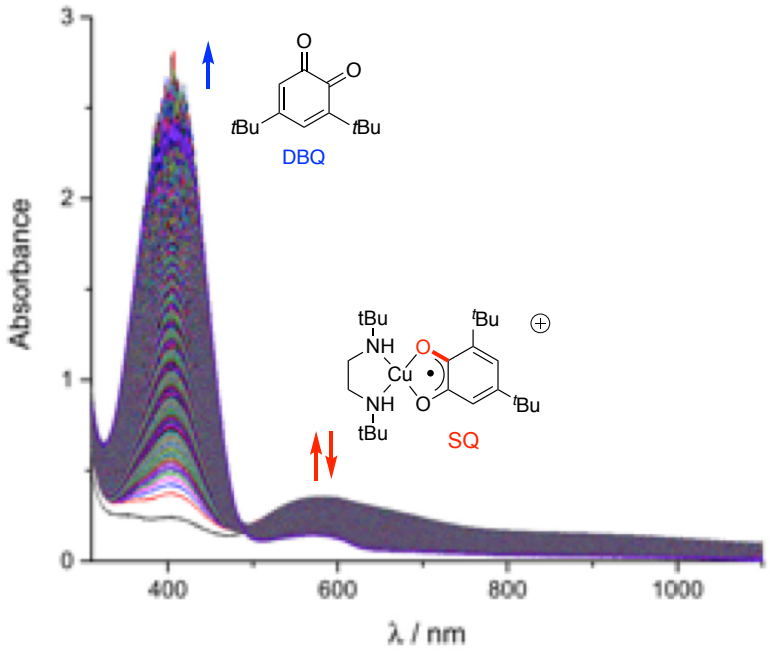

Figure 2-5. UV-Vis monitoring of the reaction of 3,5-DBP (13.0 mM), $Cu^{I}PF_6$ (8 mol%) and DBED (15 mol%) in CH_2Cl_2 at 25°C when O_2 (1 atm) is introduced, for 4 h, 100% SQ forms based on the absorbance measurement (left), and the time profile of formation of Q (blue) and SQ (red) with its decay (right).

This **SQ** intermediate compound was made independently by mixing equimolar amounts of DBED, $Cu^{I}PF_6$ and DBQ in THF (Scheme 2-7) and isolated by layered crystallization with pentane/ether in the glovebox at −30°C for two days. The solid-state molecular structure of **SQ** (Figure 2-6) is very similar to that reported by Stack and coworkers, notwithstanding the presence of a solvent molecule in their unit cell.[54] The most striking structural feature in this complex is the pronounced twist between the CuN_2 and the CuO_2 planes: 48.49° in our case and 51° in Stack's case. We will come back to this important point in the next chapter.

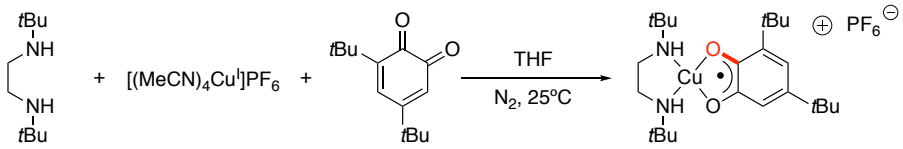

Scheme 2-7. Formation of semiquinone with equimolar $Cu^{I}PF_6$, DBED and DBQ.

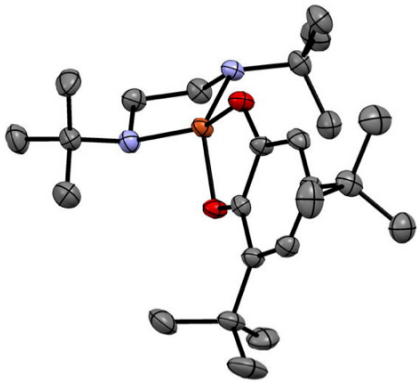

Figure 2-6. ORTEP at 50% ellipsoid probability of the cation in **SQ**(PF_6). Hydrogen atoms and PF_6^- anion were omitted for clarity.

At any given time point of the reaction, the UV-Vis spectrum of the reaction can be modeled as the overlay of the spectra of 3,5-DBQ and **SQ** only (Figure 2-7). The final yield of the reaction, after acidic work-up, is consistently 96%, denoting the high selectivity of the reaction even at the lower concentration (10 mM) required for UV-Vis characterization.

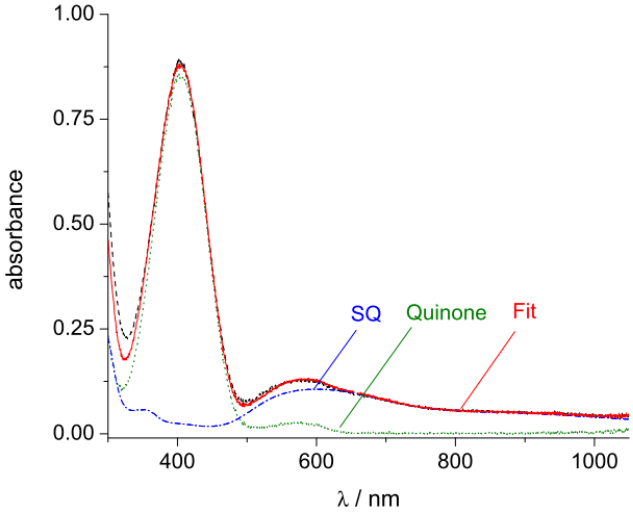

Figure 2-7. Deconvolution of the UV-Vis spectrum after 17 minutes of reaction. Conditions: 3,5-DBP (18.18 mM), $Cu^{I}PF_6$ (5 mol%, 0.91 mM), DBED (10 mol%, 1.82 mM), O_2 (2 atm), DCM, 25°C, pathlength 1.0 mm.

2.4.2 Time profiling of the reaction

The time profiles of the absorbance of the **SQ** intermediate and DBQ product are given in Figure 2-8, left. The *ortho*-oxygenation step to form **SQ** is fast and product release is slow. This product release is the reverse step of the formation of complex **SQ** (Scheme 2-8), for which a dissociation constant of $10^{-3.8}$ was measured.

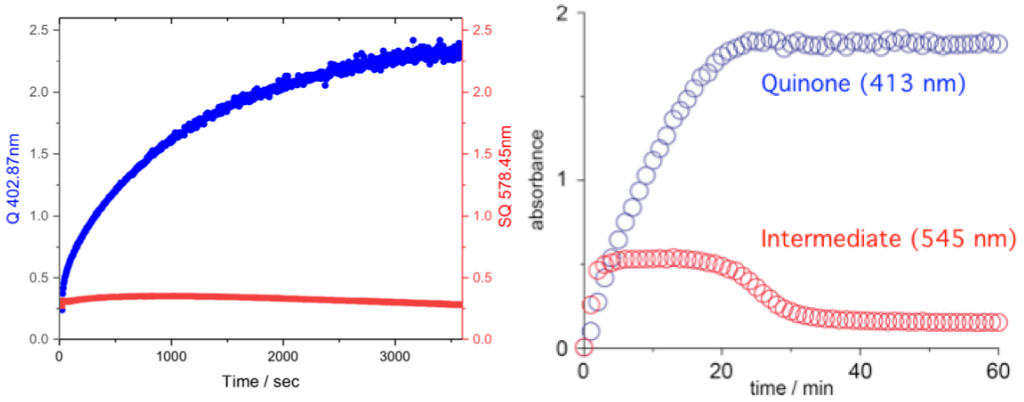

Figure 2-8. Time profiles of the reaction of 3,5-DBP (left) and 4-BP[33] (right).

The oxidation reaction of 4-BP under very similar $Cu^{I}PF_6$/DBED conditions was studied by Mohammed in our lab (see Introduction, section 1.4.5.1).[33] While 4-BP leads to a coupled quinone (Q2), the purple intermediate that forms fast is the semiquinone complex of the *uncoupled* quinone, i.e. of 4-*tert*-butyl-*o*-quinone (Scheme 2-8, top). Therefore, *ortho*-oxygenation occurs fast to generate the semiquinone complex, and the oxidative coupling is subsequent and slow.[33] These results are summarized in Scheme 2-8.

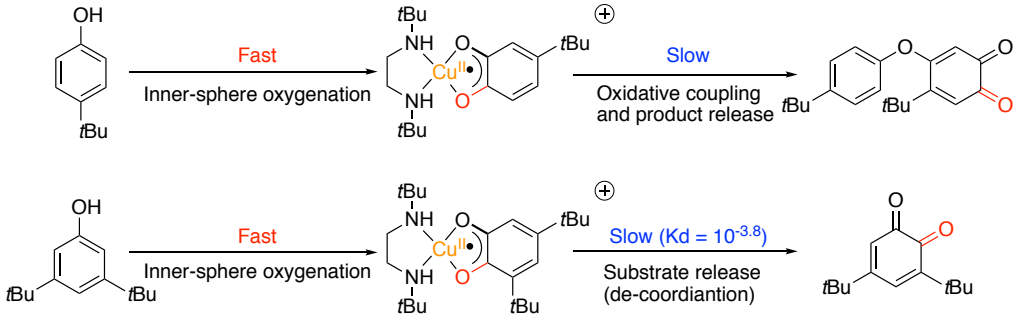

Scheme 2-8. Stepwise substrate conversion in the reaction of 4-BP (top) and 3,5-DBP (bottom).

Interestingly, the time profile of the semiquinone intermediate concentration is not the same in the reactions of 4-BP and 3,5-DBP. With 4-BP, the semiquinone intermediate is at a steady-state concentration throughout full conversion, whereas **SQ** decays before full conversion is reached in the case of 3,5-DBP (Figure 2-8). The decomposition of the coloured intermediate is due to the fact that the DBED-Cu(I) complex is O_2-sensitive and decomposes to the bis-hydroxo complex **bisOH** described above (Scheme 1-17). Therefore, while the substrate is present, the Cu species remains active in turnover, but starts to fall out of turnover when the substrate becomes less available at high conversion.

2.4.3 Simplified mechanism

These results above allow us to propose a very simple mechanism of the reaction at room temperature (Scheme 2-9). In step 1, after the DBED-Cu^{I} complex activates O_2 to make the oxidant (^{S}**P**, not shown here), the substrate 3,5-DBP gets *ortho*-oxygenated (via in situ deprotonation by the excess DBED with respect to Cu), to yield the **SQ** intermediate. In step 2, **SQ** can dissociate into DBQ and the DBED-Cu^{I} species in a reversible manner, at which stage the DBED-Cu(I) species can re-enter the catalytic cycle via step 1. In step 3, the Cu species decompose to the bis−hydroxo complex. The fork between step 1 and 3 probably occurs after the ^{S}**P** species is formed (see Chapter 4). Step 1 is fast as long as the phenol concentration is high, i.e. at the initial stages of the reaction. At higher substrate conversion, step 3 becomes increasingly prevalent, which diminishes the turnover frequency.

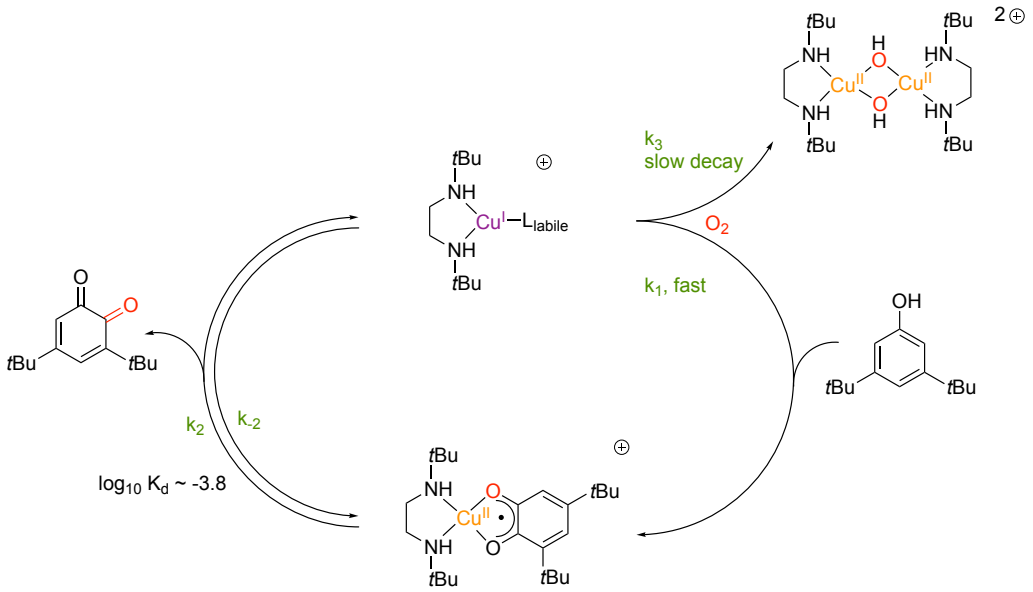

Scheme 2-9. Simple mechanism of the *ortho*-oxygenation of 3,5-DBP at room temperature.

2.5 Conclusion

The DBED/$Cu^{I}PF_6$/O_2 catalytic system is able to convert more than 70 phenols to *ortho*-quinones.[53] However, oxidative coupling and/or subsequent oxidations occur as well for almost all substrates. This suggests that a catalyst able to perform the oxygenation (i.e. addition of an O atom) is oxidatively strong enough to carry out oxidations (i.e. removal of two H atoms). In addition, the difference between 2,4 and 3,5 substitution patterns on the phenol is striking, with the former undergoing radical-based oxidations only, while the latter undergo oxygenation first. This indicates that the reaction outcome is highly dependent on the substrate, which is not surprising given that Cu catalysts are very labile and therefore able to accommodate many reaction pathways. Currently, the only way used to shut down the oxidative coupling is by increasing the steric demands on the substrate around the position where the coupling would occur, as in 3,5-DBP. This is an artificial way to isolate the oxygenation reactivity because it is limited to one substrate. However, it provides ideal circumstances to develop a mechanism for the oxygenation step that should be applicable to all phenols.

The simplified mechanism above (Scheme 2-9) shall be used as a preliminary canvas to understand the next chapters. In Chapter 3, varying ligands will modify the nature and structure of the oxidant (^{S}**P**/**O**) and naturally will affect steps 1 and 3. Changes in ligand will also influence step 2 via the structure of the semiquinone intermediate. Chapter 4 will deal with more detailed mechanistic studies, notably how to kinetically model this simplified mechanism (and show that it is actually not simple), as well as study the intermediates preceding DBSQ in step 2.

Chapter 3: Ligand Screening

3.1 Introduction

The two key intermediates in phenol oxygenation are the oxidant (an ^{S}**P** species with DBED, but can be its isomer **O**), and **SQ**.[57] According to previous stoichiometric studies, it is believed that only ^{S}**P** species can undergo *ortho*-oxygenation processes whereas **O** species prefer following radical pathways. As the DBQ product is released from **SQ** in the last step of the catalysis (Scheme 2-9), understanding the electronic structure of **SQ** species is also important to inspect.

As every case of valence isomerism, a certain number of electrons are located differently in ^{S}**P** and **O** where the metal is more oxidized to make stronger bonds and more compact thus it more stable by enthalpy. Compared with **O**, ^{S}**P** has a more elongated Cu_2O_2 core and weaker Cu−O bonds that makes it entropically favoured and enthalpically unfavoured compared with **O**.[58] Thus more ^{S}**P** forms when temperature increases. At parity of temperature, changing the supporting ligand also could change the equilibrium position because more donor ligands will favour the Cu^{III} oxidation state of **O** and increasing steric demands of the ligand will favour ^{S}**P**.

In this chapter, both secondary and tertiary amine ligands are used to carry out the 3,5-DBP oxygenation in bulk conditions. The yields of these reactions are then linked to the nature of the oxidant (^{S}**P**/**O**), the structure of the **SQ** intermediate (if there is one indeed) and other physico-chemical parameters. The ligand candidates are DBED, DBPD, DiBED, IMED, DAdED, DtOED, DTrED, TMED, BMED, TMPD, TEPD, and BMPD (chemical structures in Table 3-2).

3.2 Ligand Screening Experiments in Bulk

The assay reaction is performed in Radley tubes loaded with 3,5-DBP (0.1 M), 8 mol% $Cu^{I}PF_6$ and 15 mol% ligand in DCM under N_2 atmosphere, then stirred and exposed to O_2 (2 atm) for 4 h, except BMED and DBPD which require 24 h to achieve decent conversions. The reactions were also performed in the presence of molecular sieves (MS), because desiccants have been shown to improve yields in some cases.[53] After acidic workup, the ^{1}H-NMR conversion and yield are calculated using HMB as internal standard.

Reactions with common monodentate amines are summarized in Table 3-1. Most are inefficient at performing the oxygenation. In some cases, substrate conversion was observed but with very poor selectivity for the quinone product, even in the presence of molecular sieves. Reactions tested with tri- and tetradentate nitrogen-based ligands (not shown) were also unsuccessful, with very low conversions. One of the reasons is that the Cu(I) complexes of the more donor ligands are known to abstract a Cl atom from DCM, forming the catalytically inactive L-Cu^{II}-Cl species.[55] Sterics could also play a role, as could electronic arguments. In particular, tridentate ligands tend to favour **O** species while tetradentate ligands support the end-on peroxodicopper(II) species, both of which are not suitable for inner-sphere oxygenations.

Table 3-1. Oxygenation of 3,5-DPB with different L/$Cu^{I}PF_6$ conditions, with monodentate L.

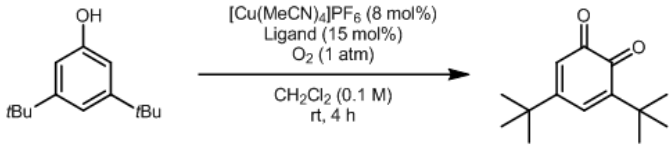

Entry	Ligand	Conversion [yield] (%) [a]		Entry	Ligand	Conversion [yield] (%) [a]	
		No MS [b]	+ MS [b]			No MS [b]	+ MS [b]
1	 Et_3N	15 [7]	82 [42]	4	 Im	NR [c]	NR [c]
2	 DIEA	4 [3]	12 [8]	5	 MeIm	67 [8]	97 [15]
3	 py	15 [<1]	56 [27]				

[a] NMR yields determined with HMB as internal standard. [b] MS = 4 Å molecular sieves (100 mg). [c] NR: no reaction.

By far, the ligand subset that worked best at catalyzing the oxygenation reaction are bidentate aliphatic diamine ligands (Table 3-2). Aromatic nitrogen-containing ligands (with pyridine derivatives) did not work as well and were abandoned because of lengthy procedures to synthesize them. Most of the ligands of Table 3-2 are commercially available or easily prepared.

Table 3-2. Oxygenation of 3,5-DPB with different L/$Cu^{I}PF_6$ conditions, with bidentate L.

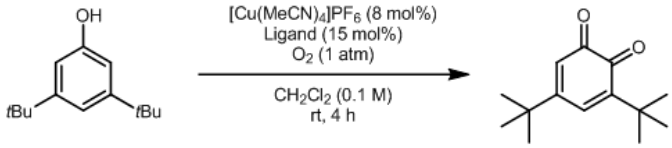

Entry	Ligand	SQ [a]	Conversion [yield] (%) [b]	
			No MS [c]	+ MS [c]
Secondary ED				
1	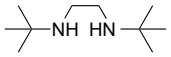 DBED	Yes	100 [96]	100 [98]
2	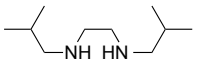 DiBED		4 [2]	6 [2]
3	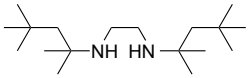 DtOED	Yes	85 [79]	100 [83]
4	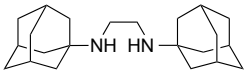 DAdED	Yes	90 [59]	77 [51]
5	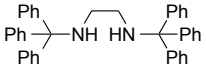 DTrED		8 [0]	2 [0]

Entry	Ligand	SQ [a]	Conversion [yield] (%) [b]	
			No MS [c]	+ MS [c]
Secondary PD				
6	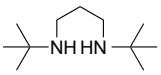 DBPD	Yes	37 [28] 28 [25][e] 60 [36][de]	99 [66]

(to be continued on next page)

Table 3-2 (continued).

Entry	Ligand	SQ [a]	Conversion [yield] (%) [b]		Entry	Ligand	SQ [a]	Conversion [yield] (%) [b]	
			No MS [c]	+ MS [c]				No MS [c]	+ MS [c]
Tertiary ED					**Tertiary PD**				
7	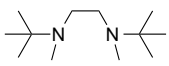 BMED	Yes	30 [20] 50 [40][d]	70 [46] 93 [78][d]	11	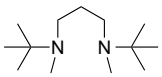 BMPD		5 [5]	35 [19]
8	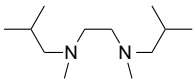 IMED		25 [4]	35 [9]					
9	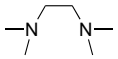 TMED		5 [4]	42 [22]	12	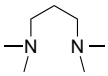 TMPD		87 [12]	94 [18]
10	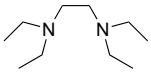 TEED		56 [13]	92 [8]	13	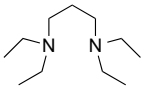 TEPD		17 [4]	94 [12]

[a] Presence of a semiquinone intermediate observed during turnover (see below). [b] NMR yields determined with HMB as internal standard. [c] MS = 4 Å molecular sieves (100 mg). [d] Reaction performed for 24h. [e] Reaction carried out in the UV-Vis spectrometer with [3,5-DBP] = 12.1 mM.

The ligands studied are divided into secondary and tertiary diamines, with either ethylene (ED) or propylene (PD) backbone. DBED is the best ligand of all, a feature that was already recognized in the Hay phenol polymerization for the insensitivity of the DBED-Cu(I) system to the water by-product. Changing the isomerization of the *tert*-butyl in DBED to *iso*-butyl groups in DiBED (entry 2) proves to be inefficient, likely because of the high oxidative sensitivity of C–H bonds α to amines.[16, 58] Increasing the sterics in DBED analogues leads to some efficient (entry 3 & 4) or completely inefficient reactions (entry 5). The slow-down of the oxygenation catalysis by steric effects opens up side-paths and makes the reaction less selective or completely shuts down the process. The PD analogue of DBED, DBPD (entry 6), is more sterically encumbered because of 90° bite-angle of PD ligands (vs. 105° of ED) that projects the substituents closer to the metal.[16] Therefore, DBPD (entry 6) works but more slowly, requiring 24 h for decent

conversion, and is less selective. With tertiary diamines, the steric argument is also valid. Methylating DBED to BMED (entry 7) leads to slow but relatively selective catalysis. Its PD analogue, BMPD (entry 11), however, is too crowded and the reaction does not turn over well. Interestingly, the reactions with less sterically encumbered ligands such as IMED, TMED, TEED, TMPD or TEPD (entries 8-13) do turnover but are poorly selective for oxygenation. This could be because of the oxidative sensitivity of the α C−H bonds.

Based on the reaction yields shown in Table 3-2, a subset of diamine ligands was selected for mechanistic characterization and divided into three families by decreasing reaction efficiency (Table 3-3). For the sake of simplifying the discussion, we have selected five representative ligands from these families to elucidate the structure-activity relationships underlying the mechanism(s). Most of the following discussion will focus on these five ligands.

Table 3-3. Family of ligands and selected ligands

Family	Category	Ligands	Representative ligands
A	Excellent yields and selectivity	DBED, DtOED	DBED
B	Moderate yields and selectivity (slow reactions)	DAdED, BMED, DBPD	BMED, DBPD
C	Low yield and/or poor selectivity	All others	TEED, TMPD

3.3 Nature and Low-Temperature Stability of the Oxidants (^{S}P/O)

Different ligands support different Cu/O_2 chemistry.[58,16] Referring back to the DBED-based mechanism of the reaction with 4-BP (section 1.4.5.2), a ^{S}**P** species was identified as the oxidant. This species can be prepared independently by reacting a DBED-Cu(I) mixture with O_2 at −75°C.[31,59] The other ligands support ^{S}**P**, **O** cores or a mixture of both. We determined/confirmed the nature of these Cu/O_2 species by UV-Vis spectroscopy (see sections 1.3.2 and 1.3.3 for ^{S}**P** And **O** signatures). This UV-Vis monitoring also provided an appreciation of the decay rate of the Cu/O_2 species. The reason we are looking at decay is because the stability of the oxidant is essential for turnover, as indicated in the simplified Scheme 2-9, a point that

will be described further in Chapter 4. Thus, 1:1 L-$Cu^{I}PF_6$ solutions prepared in the glovebox were cooled to −75°C in the UV-Vis cell, then O_2 (1 atm) was injected. Typical experiments are reported in Figure 3-1 and the nature of the species and their stability gathered in Table 3-4.

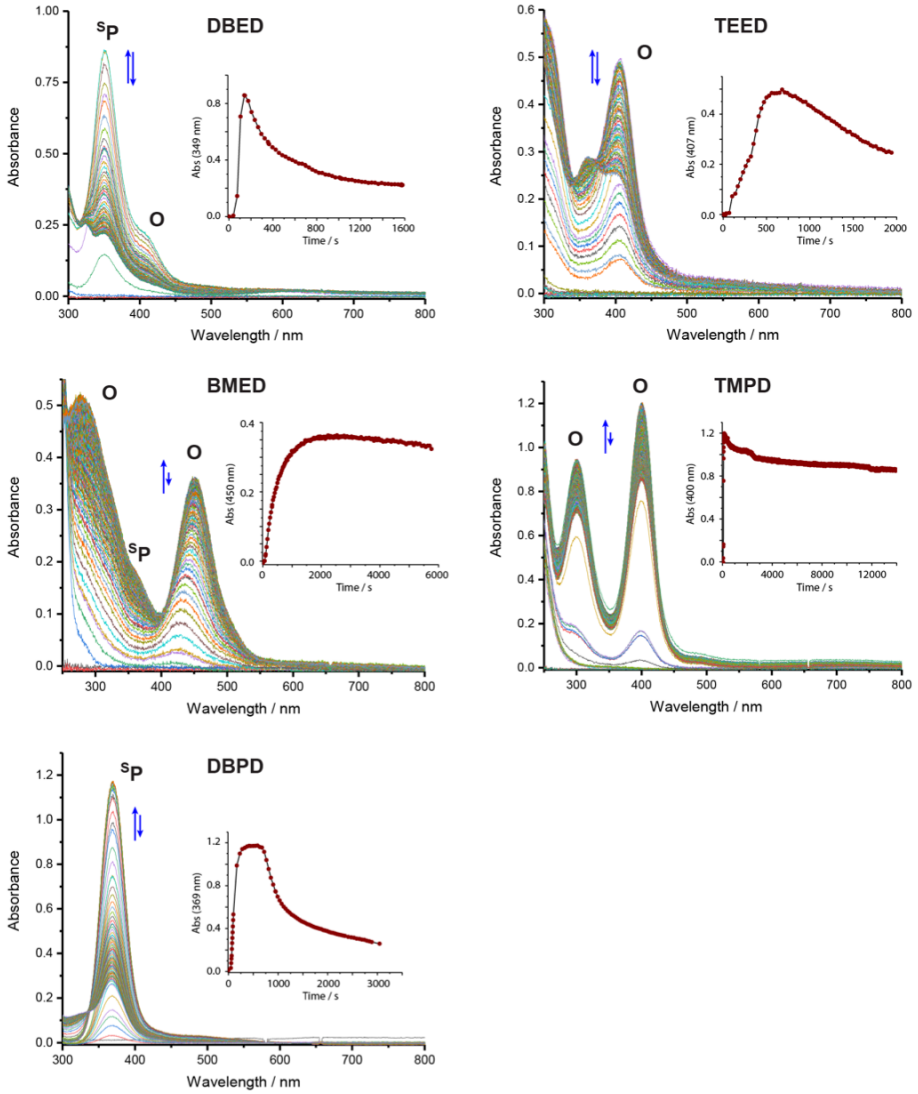

Figure 3-1. Formation and decay of **^{S}P** and/or **O** complexes at −75°C in DCM monitored by UV-Vis spectroscopy. Complexes were formed by adding O_2 (1 am) to a 1:1 mixture of L and $Cu^{I}PF_6$ in 1.33 mM concentration.

Table 3-4. Nature of the Cu/O_2 species at −75°C in DCM.

Family A/B	Cu/O_2 species	$t_{½}$ decay (s) [a]	Family C	Cu/O_2 species	$t_{½}$ decay (s) [a]
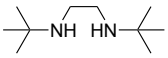 DBED	^{S}**P** + <10% **O**	220	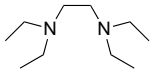 TEED	**O**	400
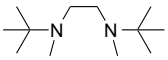 BMED	**O** + ^{S}**P**	28 000	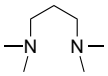 TMPD	**O** + <5% ^{S}**P**	>20 000
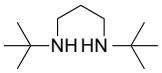 DBPD	^{S}**P** + <5% **O**	500			

[a] Approximate time to go from the maximum absorbance of the Cu/O_2 species to 50% of this value (corrected from absorbance of the decay product).

The ligands DBED and DBPD stabilize a ^{S}**P** species, but a very small amount of **O** isomer can be seen as a shoulder near 400 nm in the case of DBED.[10] BMED leads to a near-equimolar mixture of ^{S}**P** and **O**, the ratio of which depends on the solvent and the counteranion. With PF_6^-, more **O** is observed. With TEED, an **O** core forms and the ^{S}**P** isomer is thought to be much too high in energy to be observable. With TMPD, an **O** forms, but the ^{S}**P** isomer is not far in energy and can be revealed by increasing the coordinating ability of the counteranion (Dr. X private communication). These observations are in line with the increasing steric demands of a PD backbone destabilizing the **O** core. In summary, the five ligands approximately span 3 kcal/mol in favour of ^{S}**P** (DBPD) to more than 5 kcal/mol in favour of **O** (TEED), but there is no clear correlation between the nature of the Cu/O_2 species at −75°C and the turnover efficiency at 25°C. In addition, the facile equilibrium in between ^{S}**P** and **O** (sections 1.3.3 and 3.1), which also favours ^{S}**P** at raised temperatures, would level this isomer discrimination, except perhaps in the case of TEED.

The stability of the Cu/O_2 species in DCM solution was measured as the time $t_{½}$ to reach 50% of the absorbance maximum (minus the final absorbance of the decomposition product), which means the shorter the half time is, the more unstable the structure is. Most of the species are in

the same range (200-400 s) except for the BMED and TMPD mixture (>20 000 s). With BMED, ^{S}**P/O** mixture is much more stable because the *tert*-butyl and methyl substituents make it a more sterically protected oxidant. This steric shielding also causes the turnover to become slower.

3.4 Reaction Profiling at Room Temperature

3.4.1 UV-Vis monitoring of the reactions

As discussed in section 2.4.1, monitoring the DBED-catalyzed reaction by in-situ UV-Vis spectroscopy reveals the presence of a fast-forming purple **SQ** intermediate (Figure 3-2). The same in-situ monitoring was carried out on reactions with ligands L = DBPD, BMED, DAdED, DtOED, DTrED, TMED, TEED, TEPD, TMPD and BMPD. Only with L = BMED (Figure 3-3), DBPD (Figure 3-4), DtOED, and DAdED are **SQ** complexes evident, i.e. members of families A and B, denoting a clear correlation between the yield of the reaction and the presence of the **SQ** complexes, which we will abbreviate as **L-SQ**, keeping "**SQ**" for the general description of a this type of species.

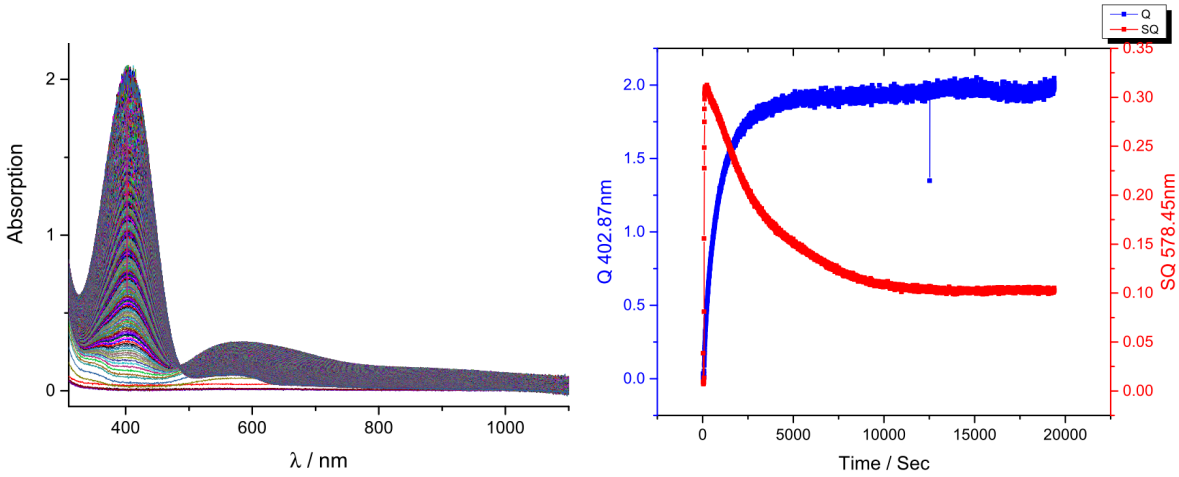

Figure 3-2. (Left) UV-Vis spectra during the reaction of 3,5-DBP (12.98 mM) with $Cu^{I}PF_6$ (8 mol%), DBED (15 mol%) and O_2 (1 atm) in DCM at 25°C for 4 h (pathlength 1.0 mm). (Right) time profile of the absorbances where the DBQ (blue) and the **SQ** intermediate (red) absorb.

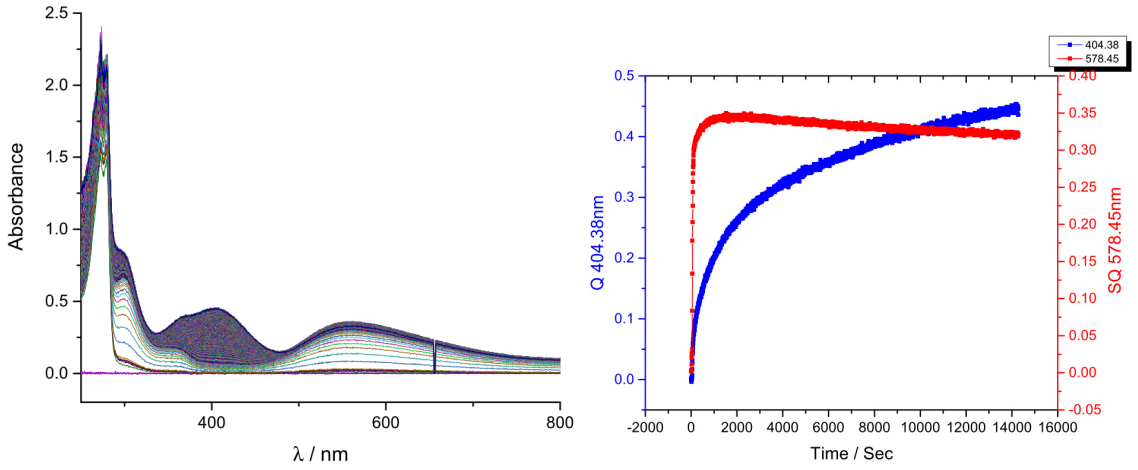

Figure 3-3. (Left) UV-Vis spectra during the reaction of 3,5-DBP (9.37 mM) with $Cu^{I}PF_6$ (8 mol%), BMED (15 mol%) and O_2 (1 atm) in DCM at 25°C for 4 h (pathlength 1.0 mm). (Right) time profile of the absorbances where the DBQ (blue) and the **SQ** intermediate (red) absorb.

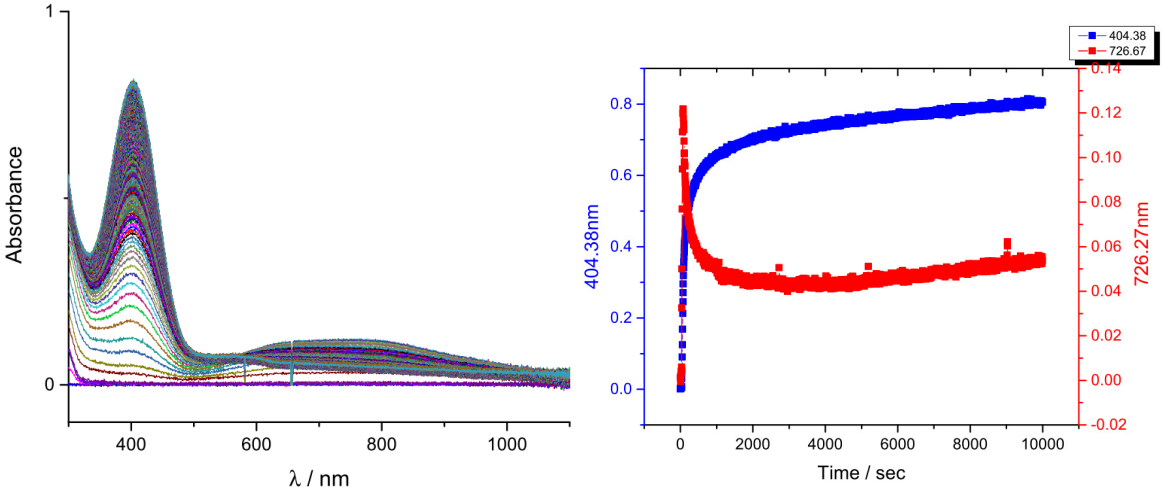

Figure 3-4. (Left) UV-Vis spectra during the reaction of 3,5-DBP (12.06 mM) with $Cu^{I}PF_6$ (8 mol%), DBPD (15 mol%) and O_2 (1 atm) in DCM at 25°C for 4 h (pathlength 1.0 mm). (Right) time profile of the absorbances where the DBQ (blue) and the **SQ** intermediate (red) absorb.

3.4.2 UV-Vis signature and formation constant of the SQ intermediates

To confirm that the intermediates observed are indeed **SQ** complexes, we prepared the **L-SQ** species independently and characterized in more detail. Reaction of LCu^+ with DBQ in O_2-free THF led to the immediate formation of a deeply coloured solution of the relevant **L-SQ** species. Titration of LCu^+ with 2 equivalent DBQ shows the rise of intense features in the visible range, as exemplified with DBED (Figure 3-5).

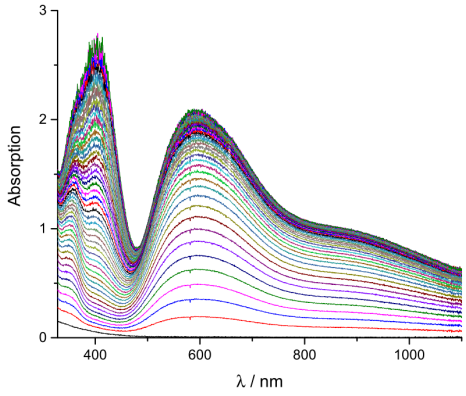

Figure 3-5. Titration of a 1:1 mixture of Cu^IPF_6 and DBED (0.192 mM) with 0-2 equiv. DBQ (5 µL increments of a 7.7 mM solution) in DCM at 25°C under N_2 (1.0 cm pathlength).

The spectral data was analyzed with ReactLab™ Equilibria using a A + B = C multivariate fitting (A = colorless LCu^+, B = known DBQ and C = **SQ** to fit, Eqn 3-1). Multivariate fitting using this 1:1 stoichiometry led to excellent fits, wherefrom the spectra of the $LCuSQ^+$ adducts can be extracted, in molar absorptivity units (Figure 3-6, bottom left), as well as the formation constant of the complex (Eqn 3-1). Low residuals (Figure 3-6, top right) ascertain of the quality of the fit.

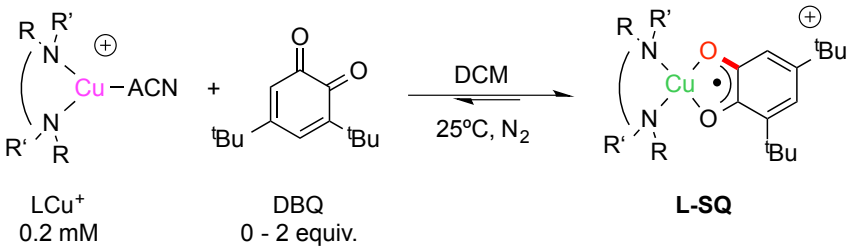

$$K_f = \frac{[\textbf{L-SQ}]}{[LCu^+]\,[DBQ]}$$

Eqn 3-1. Formation of the **L-SQ** complexes and formation constant.

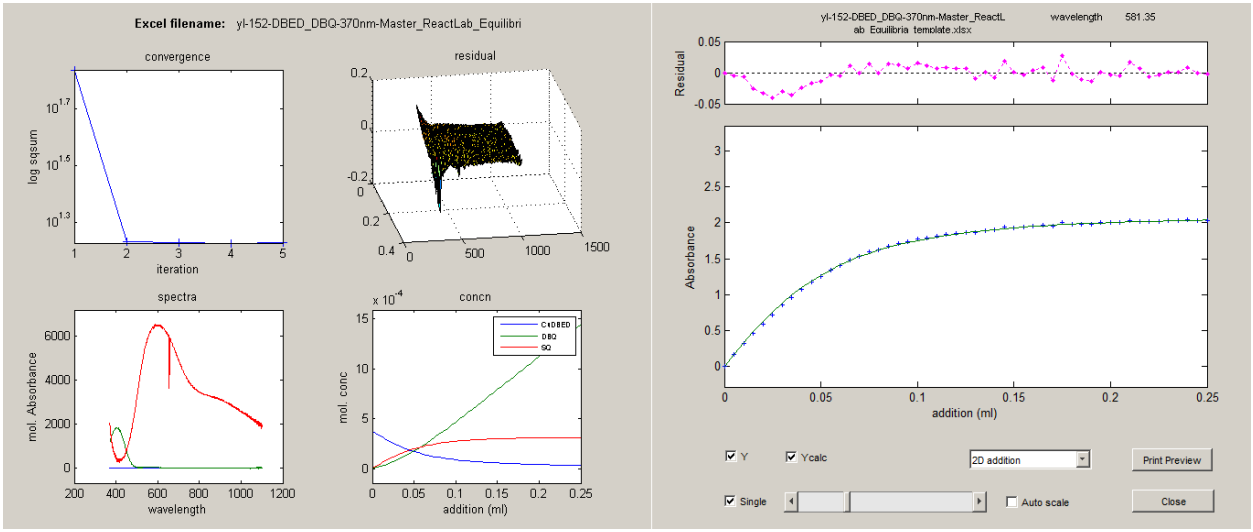

Figure 3-6. Screenshot of the fitting process with ReactLab™ Equilibria for DBED/Cu/DBQ model from Figure 3-5.

L-SQ formation constants extracted in this manner range between 4-5 $\log_{10}$ units, with BMEDCuSQ$^+$ showing the strongest thermodynamic stability (Table 3-5). Noteworthy to remember is the presence of 4 equivalents of CH_3CN molecules per Cu in these experiments because of the $Cu^{I}PF_6$ starting material. Acetonitrile being a good ligand to Cu(I) enables the dissociation of LCuSQ$^+$ into its components, DBQ and LCu$^+$, usually considered to have the $LCu(CH_3CN)_{1-2}^+$ formula in solution.

Table 3-5. Formation constants of the **L-SQ** species.

Entry [a]	Ligand		$\log_{10} K_f$	Entry [a]	Ligand		$\log_{10} K_f$
Secondary ED				**Secondary PD**			
1	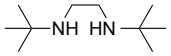	DBED	3.818	6	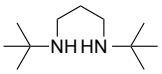	DBPD	3.843
3	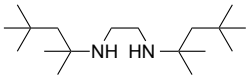	DtOED	4.468				
4	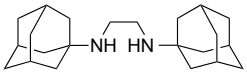	DAdED	4.736				
5	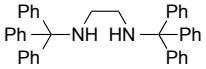	DTrED	2.865				
Tertiary ED				**Tertiary PD**			
7	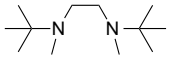	BMED	5.280	11	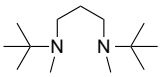	BMPD	weak binding
9	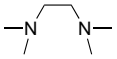	TMED	5.374	12	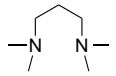	TMPD	n/a [b]
10	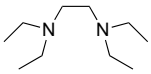	TEED	5.704	13	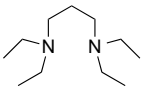	TEPD	4.852

[a] Entry numbers refer to Table 3-2. [b] Experiment with TMPD was performed 4 times, including under different conditions, yet no fit was satisfactory.

All the binding constant are in the same range from family A to C. Compared with TEED and TEPD, the **L-SQ** becomes less stable one order of magnitude by increasing the steric demand. However, the binding constant keeps the same in the case of DBED vs. DBPD. Therefore, based on the experiments, there is no correlation between the binding constant and the reactivity, we have not found the proper structure parameter to use for the correlation with the binding constant.

3.4.3 Fitting of the UV-Vis spectra

Another information provided from the titration is the **L-SQ** spectra, that could be used for fitting the reaction spectral evolution (presented in Figure 3-7).

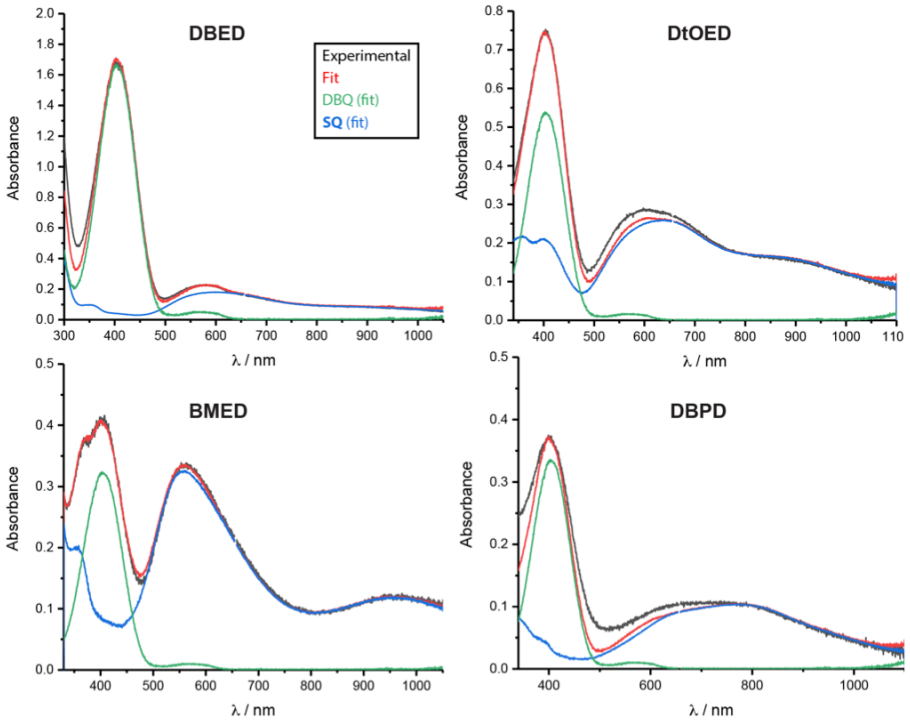

Figure 3-7. Deconvolution of the spectra in section 3.4.1 with DBED (33 min of reaction), DtOED (10 min), BMED (2.75 h), and DBPD (2 min). Black: experimental trace, red: fit via linear combination of known spectra of **SQ** and DBQ with appropriate ratios. At this stage, the quantity of **SQ** corresponds to 100% of the Cu present in solution.

In the case of DBED, BMED, the experimental spectra fit perfectly with known **L-SQ** and DBQ species, which means there is no other intermediate observed during the reaction at room temperature. The deconvolution of DtOED and DBPD spectra are not perfect and suggest that another species is involved during the reaction. With an absorption around 500 nm, one possible candidate would be the L-Cu^{II}-catecholato complex (i.e. the $1e^-$-reduced form of **SQ**),[54] while the **bis-OH** complex absorbs around 700nm (Chart 3-1).[57]

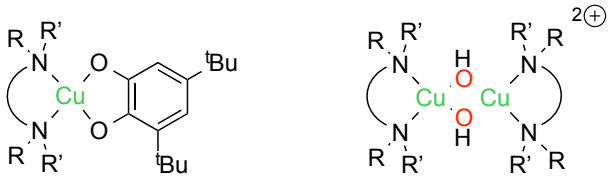

Chart 3-1. Structures of the L-Cu^{II}-catecholato (left) and **bisOH** (right) complexes.

3.5 Structure and Spin State of the Semiquinone Intermediates

3.5.1 Synthesis of the SQ species

In order to further prove the nature of the **L-SQ** intermediates, samples of **L-SQ** complexes were made independently under N_2 atmosphere (Scheme 3-1). The **L-SQ** complexes were made as described before by mixing equimolar amounts of L, $CuPF_6$ and DBQ in glovebox, the deeply coloured solution was then layered with pentane/ether to remove acetonitrile and prevent dissociation of the **SQ** complex, stored in the glovebox −30°C freezer until the crystal formed. The crystals were successfully obtained for the **SQ** complexes with following supporting ligands: DBED, BMED, DBPD, TMED, TEED and DiBED.

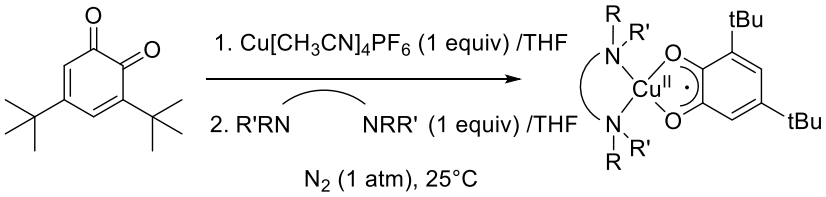

Scheme 3-1. Synthesis of **L-SQ** species with different ligands L.

3.5.2 Crystal structures of the L-SQ species

Slow recrystallization of the **L-SQ** compounds afforded single crystals amenable for X−ray diffraction analysis. Peter Gillich and I were able to collect structural data for **L-SQ** species with L = DBED, DiBED, BMED, TEED, TMED, DBPD. For TMPD-DBSQ, due to the failure and maintenance of the X-ray diffractometer, we instead report the structure of the complex with the 4-*tert*-butylsemiquinone moiety (obtained by mixing equimolar amounts of TMPD, Cu$^{I}PF_6$ and 4-BP).

The crystal structures of the **L-SQ** species all contain a cationic $LCuSQ^+$ moiety, a PF_6^- anion and, for some, solvent molecules. The molecular structures of the $LCuSQ^+$ complexes with the five selected ligands are given in Figure 3-8. The structures with TMED and DiBED (Figure 6-8 in the experimental section) are similar to that of TEED (flat coordination, see below).

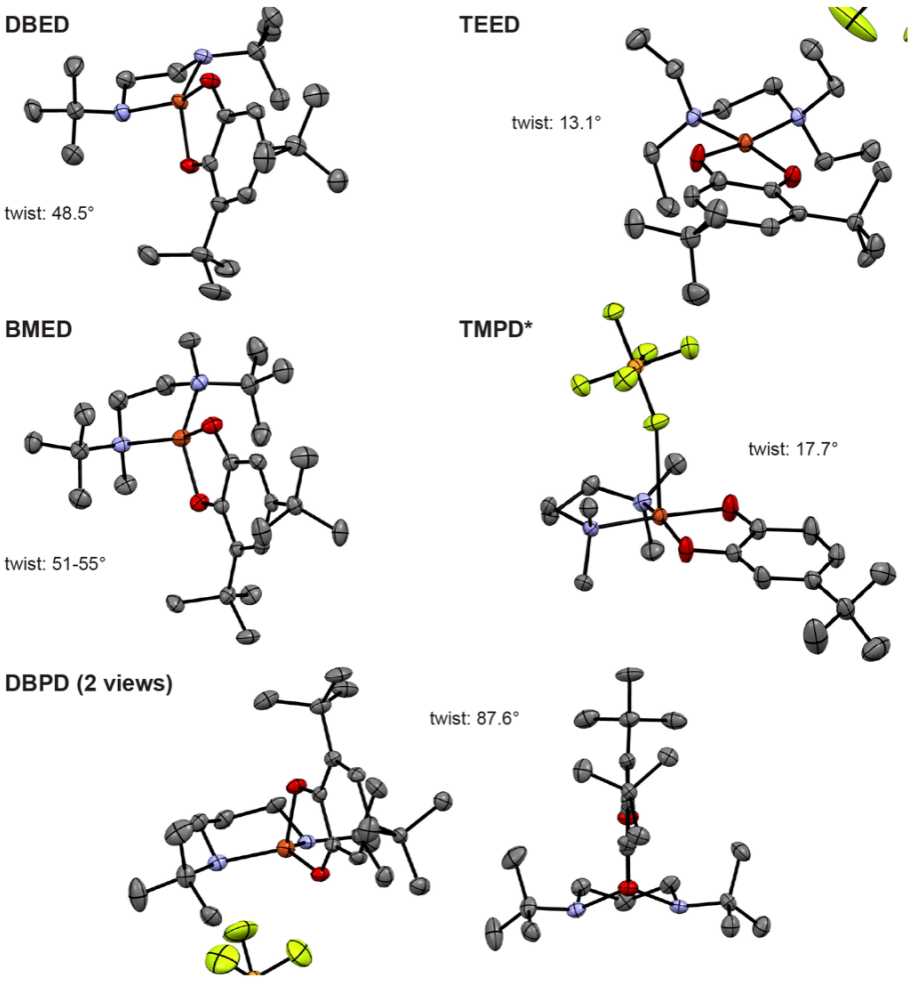

Figure 3-8. ORTEP at 50% ellipsoid probability of the **L-SQ** cations in the structures of the L-Cu-DBSQ(PF_6) compounds, except * for the TMPD complex made from the 4-*tert*-butyl-*o*-quinone. Hydrogen atoms were omitted for clarity. PF_6^- anions not necessarily shown.

The most striking feature in these structures is the molecular geometry of the $LCuSQ^+$ complexes, which is highly dependent on the steric demands of the ligand. A rhombic distortion about Cu is observed in most cases and reported as the twist angle between the N_1–Cu–N_2 and

O_1−Cu−O_2 planes (Scheme 3-2).[54] With DBED and BMED, this angle is close to 50°. With DBPD and its sterically demanding PD bite-angle, the twist is close to 90° and the Cu coordination geometry is intermediate between trigonal-pyramidal and tetrahedral. With ligands that do not possess *t*Bu substituents, the structures are all flat, with twist angles not exceeding 18° (including 12.5° for DiBED and 11.5° for TMED).

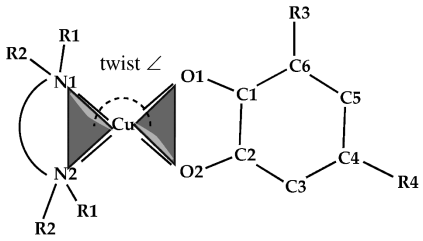

Scheme 3-2. Twist angle between the CuN_2 and CuO_2 coordination planes.[54]

It is the diamine ligand that controls the coordination twist. Firstly, the 3-*t*Bu substituent on the semiquinone moiety has no influence on the twist. With DBED and 4-DBQ, a 52.16° twist is observed,[33] close to the 48.5° and 51° observed with the DBQ moiety.[54] Therefore, the coordination in the **TMPD-SQ** (with the DBQ moiety) should also be close to planarity. Secondly, the **DiBED-SQ** complex, with *iso*-butyl substituents, displays a coordination close to planarity (12.5° twist). In the structure, the *i*Bu groups are projected "backwards", away from the semiquinone moiety and therefore do not provide any significant steric hindrance. In contrast, the large and spherical *t*Bu groups cannot find a position away from steric contacts. In brief, the *t*Bu substituents on DBED, and by extension BMED and DBPD, are the prime factor to engage Cu in a coordination twist. We could not obtain the structures with the even larger DtOED, DAdED and DTrED ligands, but it is sensible to think that the same twist will be observed in these structures.

In summary, there is a correlation between structure of these intermediates and activity. In Families A and B, **SQ** species observed during turnover and they have twisted structures. In contrast, family C ligands lead to inefficient catalysis and planar **SQ** species (but these complexes are not observed during turnover). While one could argue of the importance of the

SQ species in catalysis, however, one must remember that the turnover is controlled uphill by the ligand, not by **SQ**. We will therefore only use the **SQ** structural features to guide further probing of the mechanism.

3.5.3 Spin-state of the SQ species

The geometry of the **SQ** species directly influences their electronic structure and in particular, their spin state. In the $LCuSQ^+$ structure, Cu(II) has a spin ½, and another spin ½ located on the radical (Figure 3-9). Therefore, there are two alignment possibilities, the planar have either a spin 0 or a spin 1 ground state that correlate the coupling antiferro− or ferro−magnetic that will be stabilize the singlet or the triplet ground state. Stack[54] suggested that the triplet electronic state is energetically preferred for a planar structure, with increasing the rhombic distortion where the intersection angle between N_1−Cu−N_2 and O_1−Cu−O_2 increases, the triplet state destabilized and the singlet state becomes energetically favoured.

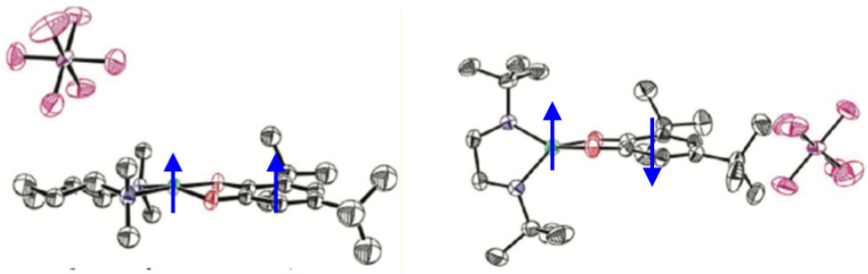

Figure 3-9. The two possible spin states of $LCuSQ^+$ complexes, a planer ferromagnetic (left) and a twisted diamagnetic (right) structure.[54]

In the case of the magnetic orbital of the planar structure, d_{x2-y2} of the Cu and π* of the ligand are orthogonal with no overlap between them. The ferromagnetic is known as soon as the twist exists then there's an overlap between the magnetic orbitals conduces strong anti−ferromagnetic components of the exchange, therefore a singlet ground state taking place. Therefore, the characterization of the $DBEDCuSQ^+$ is an antiferromagnetic ground state, and a twisted coordination with a singlet ground state is energetically favoured.

Another component influences the structure is the steric clash between substituents of the ligand and oxygen atoms of the $LCuSQ^{+}$ complexes[54]. A planar coordination with a triplet ground state is energetically favoured with limited steric bulk diamine ligands. With increasing the steric demands of the diamine ligands, a twist angle between in the coordination sphere will be occur which leads the changing of the magnetic properties.

3.5.4 Redox properties of the SQ complexes

The redox properties of the **SQ** complexes were measured by a visiting PhD student, Federica Gennarini (Table 3-6). Most **SQ** complexes display one reversible $1e^{-}$-reduction wave at E^{0}_{red} (to the Cu^{II}-catecholato complex) and one irreversible oxidation wave at E^{pa}_{ox} (presumably to the unstable Cu^{II}-quinone complex), with the exception of the **DBPD-SQ**, for which no oxidation wave was observed.

Table 3-6. Redox potentials of the **SQ** species. [a]

Family A/B	E^{0}_{red} (mV) [b]	E^{pa}_{ox} (mV) [c]	Family C	E^{0}_{red} (mV) [b]	E^{pa}_{ox} (mV) [c]
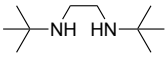 DBED	-535 [110]	550	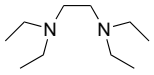 TEED	-507 [144]	478
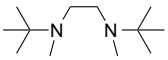 BMED	-492 [62]	120	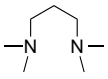 TMPD	-528 [139]	414
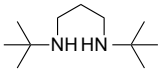 DBPD	-721 [243] -1073 (E^{pc}) [d]	n/a			

[a] Measured by cyclic voltammetry in DCM with 0.1 nBu$_4$PF$_6$ as supporting electrolyte on 1 mM concentrations of analyte. Working electrode: Pt, reference electrode AgCl/Ag, scan rate 100 mV/s, 25°C. Potentials are referenced to the $Fc^{+/0}$ couple measured in situ after the experiments. [b] Peak-to peak (E^{pa}-E^{pc}) separation given in square brakets. [c] E^{pa} = anodic peak potential. [c] E^{pc} =cathodic anodic peak potential.

If the **SQ** complexes were engaged in oxidation of a phenol(ate), their reduction potential is the parameter to consider. There is, however, little difference between the E^{0}_{red} values for DBED

(family A) and TEED/TMPD (family C), or even BMED (family B), despite their different structures (twisted vs. planar). Therefore, it is unlikely that an **SQ**-mediated oxidation is responsible for the lack of selectivity of the reactions. In addition, the reduction potential of 3,5-DBP is 1.15 V vs. $Fc^{+/0}$, therefore these **SQ** specie are thermodynamically unable to form the phenoxyl radical from a phenol (at least 1.6 V difference uphill). Redox data for the phenolate is unknown.

Interestingly, the **DBPD-SQ** species shows a wider range of redox stability (from -721 to more than 800 mV vs. $Fc^{+/0}$). Indicating that it is both harder to reduce to the Cu^{II}-catecholate species and oxidize to the putative Cu^{II}-quinone species. This is in line with the large twist in this species, which would stabilize the Cu(I) oxidation state and destabilize the Cu(II) oxidation state. Thus, reduction creates more steric clash because of Cu^{II}-O bonds shortening, which is prevented by the large steric demands of DBPD with its PD backbone. As for oxidation, the **SQ** can be seen as a Cu(I)-quinone valence isomer, therefore oxidation to Cu(II) is more difficult with a more stable Cu(I) in a pseudo-tetrahedral geometry.

3.5.5 ^{1}H-NMR of L-SQ species

Another way to assess the magnetic properties of the **L-SQ** species is via ^{1}H-NMR. A typical example in family A is **DBED-SQ**, which has been reported by Stack.[54] All of the peaks for **DBED-SQ** appear between −2 to +10 ppm (Figure 3-10), with no strongly paramagnetically shifted resonances with broad linewidths. By contrast, NMR spectra of ligands from family C (Figure 3-11 and Figure 3-12 for TEED and TMPD, respectively) spread over a very wide ppm range, with very broad signals. This is a key signature of paramagnetic behaviour, as was reported by Stack for another S = 1 semiquinone complex.[54]

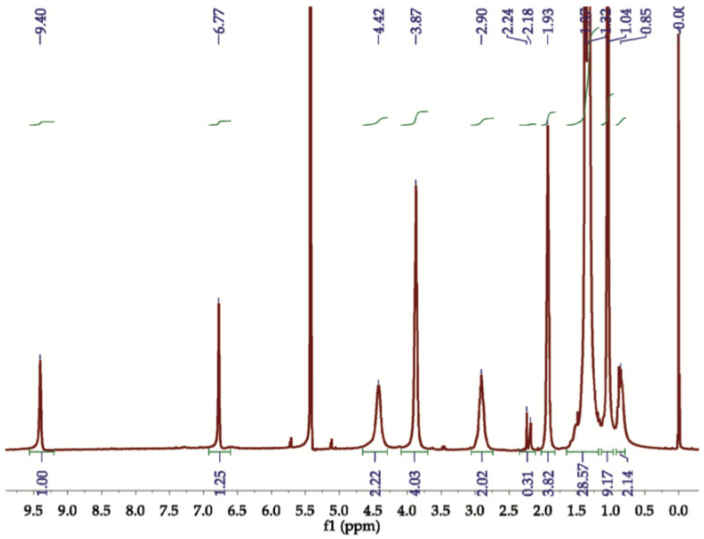

Figure 3-10: ^{1}H-NMR of **DBED-SQ** reported by Stack (CD_2Cl_2, 12 mM, 300 MHz, 193 K).[54]

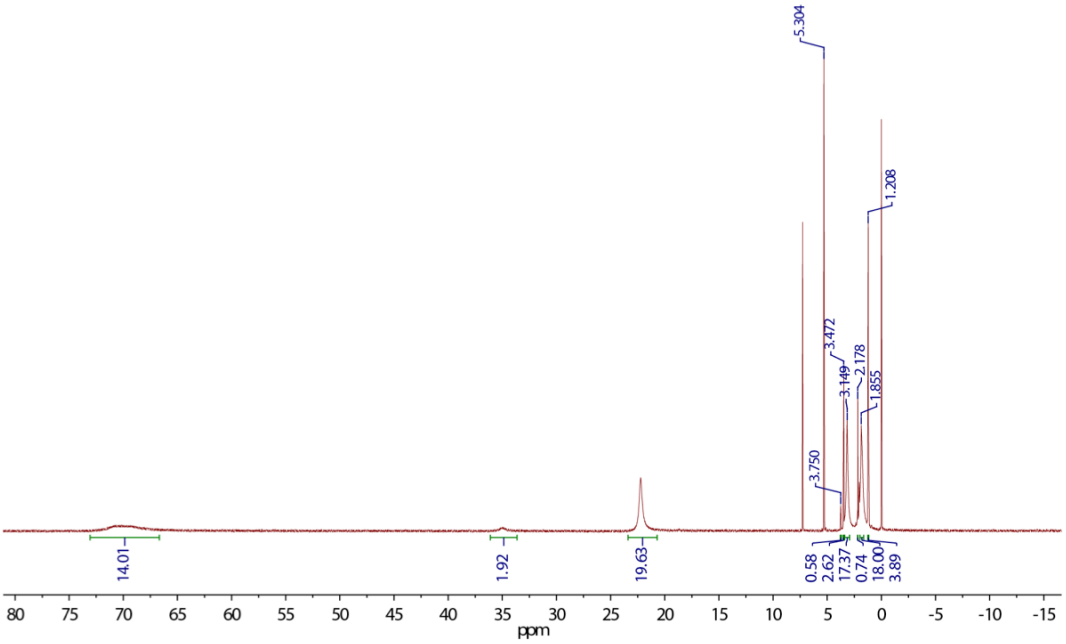

Figure 3-11. ^{1}H-NMR of **TEED-SQ** ($CDCl_3$, 500 MHz, 25°C).

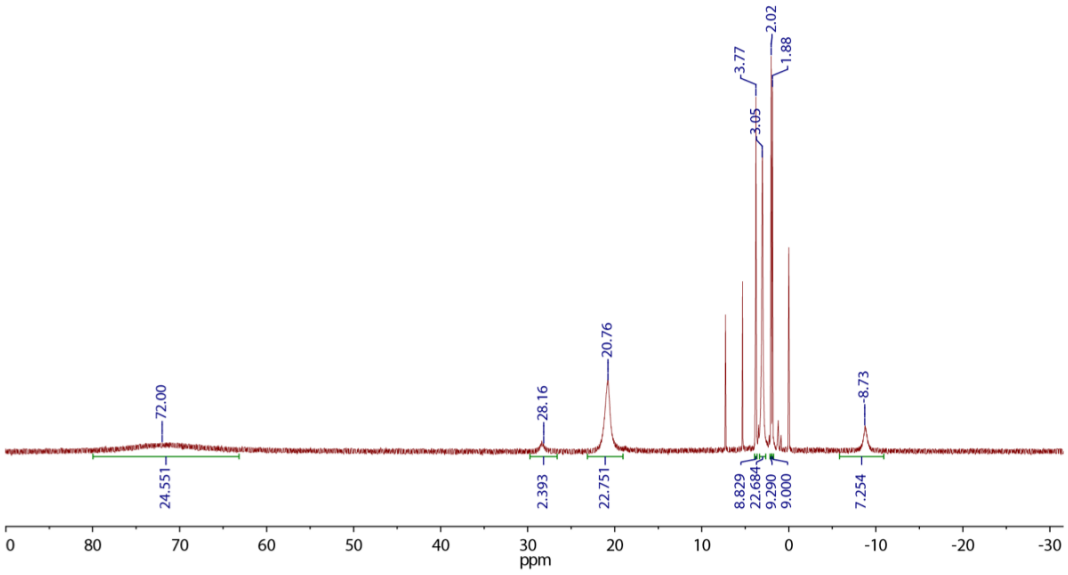

Figure 3-12. ^{1}H-NMR of **TMPD-SQ** ($CDCl_3$, 500 MHz, 25°C).

3.6 Conclusion

In conclusion, the only ligands supporting oxygenation catalysis are forming a significant quantity of ^{S}**P**-type oxidant at low temperature. With these ligands, a **SQ** intermediate is observed upon turnover, for which a diamagnetic ground state was confirmed. The intermediary of **SQ** is natural in these cases because, once DBQ is formed after a few turnovers, it will strongly coordinate to L-Cu(I), as per the **SQ** formation constants around 10^{+4} to 10^{+5} (Table 3-5). Nearly all the Cu in solution during turnover is in the form of the **SQ** species, with the exception of the **bisOH** decomposition product. LCu(I) only forms transiently by dissociation of **SQ** and it reacts very fast with O_2 and the phenol(ate) to regenerate **SQ**. The rate-determining step of the reaction is likely the dissociation of **SQ**. In fine, **SQ** acts as a reservoir of Cu(I), releasing it only when needed, and thus preventing uncontrolled decomposition to **bisOH**.

The reactions that were not selective all use a ligand that supports an **O** species at low temperature. The Cu_2O_2 core in **O** is much less accessible than in ^{S}**P**, thereby privileging outer-sphere reactions. In these cases, DBQ does not form efficiently in the first stages of turnover and the absent **SQ** cannot take its protective reservoir role. In addition, the involvement of

radical-chain propagation events would make a radical pathway uncontrollable once phenoxyl radical are formed. The first turnover is crucial in determining the fate of the reaction.

The reaction between the ^{S}**P**/**O** oxidant and the phenolate is the key step in charge of the efficiency and selectivity. In this repect, stoichiometric reactions are illuminating (Scheme 3-3). Stack showed that the DBED-^{S}**P** reacts with 2,4-DBPNa to form oxygenation products only,[50] in accordance with Itoh's original observations.[41] The same behaviour was observed by our lab with 4-BPNa.[33] In stark contrast, the reaction of TMPD-**O** with 2,4-DBPNa yield the bisphenol product, as reported by Herres-Pawlis and Stack.[60] These results are consistent with the more crowded **O** species favouring radical pathways, even with a coordinating phenolate substrate (this substrate is also more electron-rich and thus more prone to being reduced to a phenoxyl radical).

We attempted to repeat and extend these reactions from DBED-^{S}**P** and TMPD-**O** with 2,4-DBPNa, 4-BPNa and sodium 4-methoxyphenolate. As a note, we were not able to prepare the 3,5-DBPNa salt, because the *tert*-butyl groups seemed to re-arrange on the ring. After a few trials, these experiments were not conclusive. In some cases, no conversion was observed and the phenol was recovered after acidic work-up despite an immediate colour change when adding the phenolate. In other cases, the NMR indicated a mass loss, probably because radical pathways led to polymers (two *ortho* positions available). Further experimentations and expansion of the ligand set are warranted, but this could be the key to answer the selectivity question.

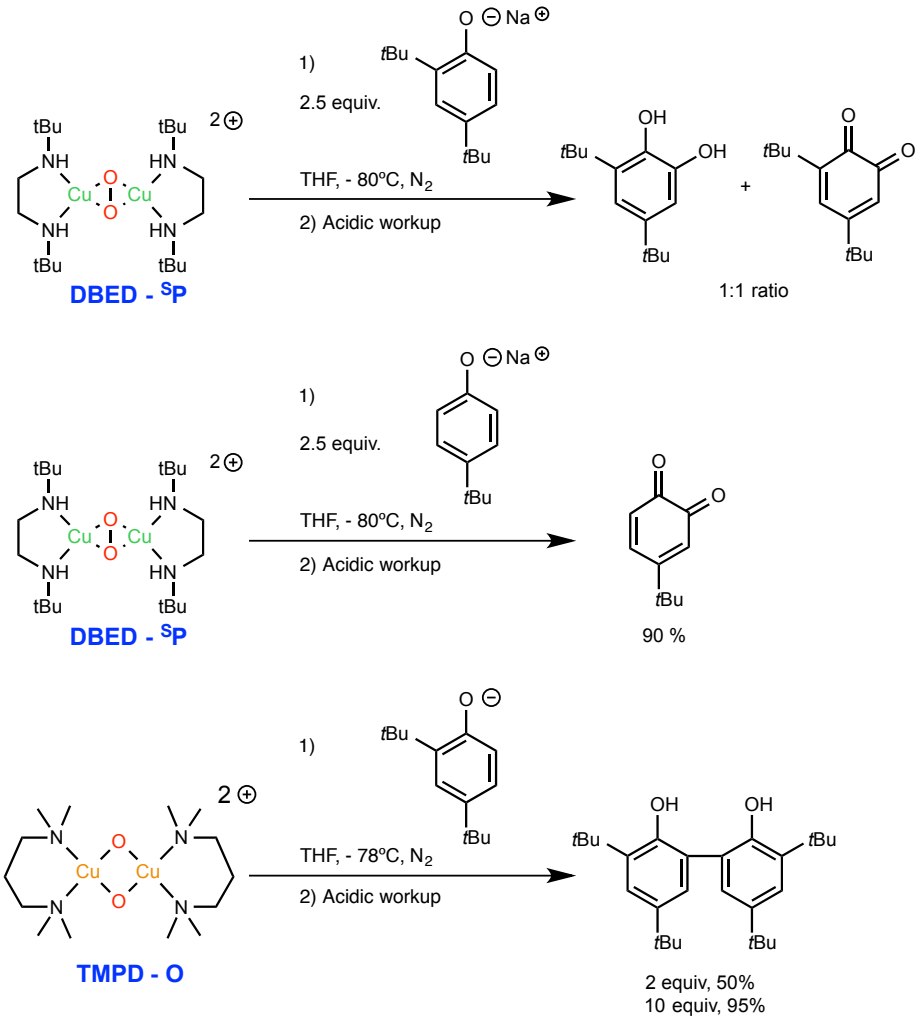

Scheme 3-3. Reactivity of DBED-^{S}**P** and TMPD-**O** species with phenolates.

Chapter 4: Kinetic Studies of the DBED-Catalyzed Reaction of 3,5-DBP

4.1 Introduction: Mechanistic Proposal

As discussed in previous sections, the *ortho*-oxygenation must proceed through the phenolate and underscores the importance of a slight excess of DBED per Cu for turnover, because the reaction does not proceed at or below stoichiometry of DBED with respect to $Cu^{I}PF_6$. The mechanistic proposal (Scheme 4-1) combines the simplified mechanism of Scheme 2-9, and the low-temperature mechanism established for the 4-BP substrate (Scheme 1-17).[33] It starts with by self-assembly of ^{S}**P** from DBED-Cu(I) and O_2 (step ①). ^{S}**P** is in equilibrium with a small amount to its **O** isomer. At this stage, a fork occurs in the mechanism. Either this ^{S}**P** species decomposes to the **BisOH** species that lies outside the turnover cycle (step ⑥), or it reacts with the in-situ-generated phenolate to form phenolatobis(μ-oxo) species **A** (step ②). Intramolecular electrophilic aromatic substitution generates catecholate complex **C** (Step ③). Protonation of binuclear **C** by $DBEDH^+$ (step ④) causes **SQ** release and the regenerates DBED-Cu(I). Last, **SQ** reversibly releases DBQ and DBED-Cu(I) (step ⑤) as the reverse of titration experiments (section 3.4.2).

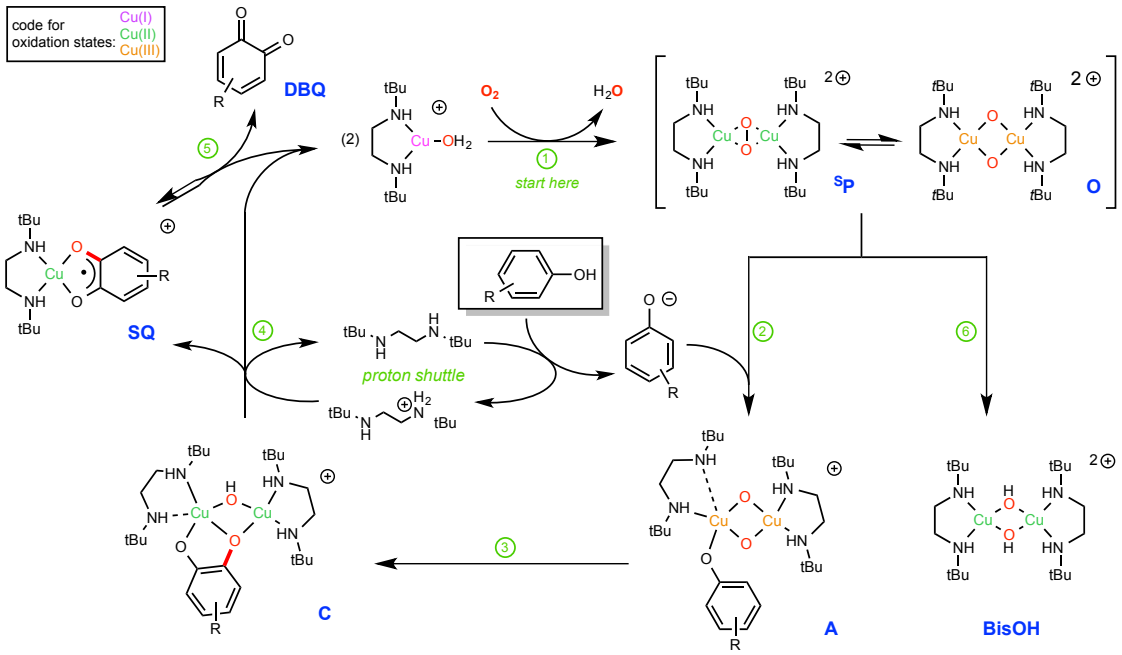

Scheme 4-1. Proposed mechanism for the *ortho*-oxygenation of 3,5-DBP. R = 3,5-di-*tert*-butyl substitution.

This chapter will focus on the formation of intermediates and products at three temperatures: 25°C, –35°C and –80°C. In particular, conditions will be changed in each experiment so as to probe the influence of each component over the kinetic of the system. The trends will then be discussed in light of Scheme 4-1 in order to validate our mechanistic proposal.

Because of the characteristic electronic absorptions of ^{S}**P** (355 nm), **A** (418 nm), **SQ** (590 nm) and the DBQ product (405 nm), UV-Vis spectroscopy is the method of choice to probe these trends (note: DBED-Cu(I), **C** and **BisOH** are quite featureless over the 300-1100 nm wavelength range). From the previous discussions, it is implied that ^{S}**P** and **A** can only be observed at low temperatures (e.g. species **A** made from 2,4-DBP was only observed only between –125°C and –85°C)[42-43] whereas **SQ** and DBQ can be observed over the whole temperature range (albeit dissociation of DBQ from SQ is unlikely at –80°C).

Two mixing methods were used in this chapter. One is conventional syringe injection into our UV-Vis set-up (Schlenk flask with an optical quartz dip-probe), wherein homogenization of the solution is slow. The second method is stopped-flow, whereby two syringes are mixed in a Y-junction right before entering a UV-Vis cuvette that is immersed in a bath at the desired temperature. This method allows for very fast mixing and is perfect to study rapid reactions. Typically, one syringe contains $Cu^{I}PF_6$, DBED and 3,5-DBP in DCM (prepared in the glovebox), the other contains O_2-saturated DCM. The concentrations given below are the final concentrations after mixing.

4.2 Component Effects at 25°C and –35°C

4.2.1 Influence of substrate concentration

The stopped-flow instrument was used to monitor the first few seconds/minutes of the reaction at 25°C where [3,5-DBP] was varied while [$Cu^{I}PF_6$] and [DBED] were kept constant (Figure 4-1). From the absorbances, the concentrations of **SQ** and DBQ were obtained by solving Equation 4-1 at each time point in Excel. The 400 and 600 nm denominations actually correspond to the maxima of DBQ and **SQ** spectra, where the molar absorptivities are known.

$$\begin{cases} Abs_{400} = \varepsilon_{400}^{DBQ} \, l \, [DBQ] + \varepsilon_{400}^{SQ} \, l \, [SQ] \\ Abs_{600} = \varepsilon_{600}^{DBQ} \, l \, [DBQ] + \varepsilon_{600}^{SQ} \, l \, [SQ] \end{cases}$$

Equation 4-1. System of equation used to solve for the **SQ** and DBQ concentrations of the products.

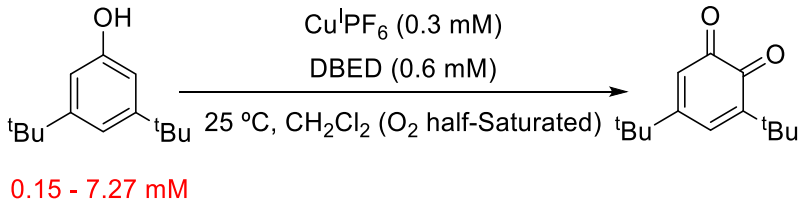

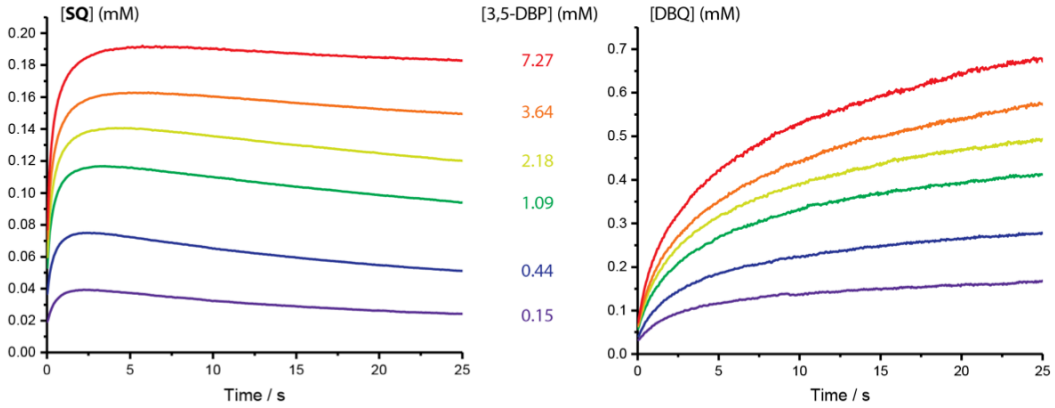

Figure 4-1. Substrate influence at 25°C: stopped-flow reaction of CuIPF6 (0.31 mM), DBED (0.59 mM) and 3,5-DBP (0.15 - 7.27 mM) in O_2-half-saturated DCM shows the formation of both SQ (left) and DBQ (right).

In each experiment, **SQ** forms fast, [**SQ**] reaches a maximum ([**SQ**]$_{max}$) then decreases slowly while DBQ forms gradually. The first striking observation is that, with increase substrate concentration, [**SQ**]$_{max}$ increases up to 61% the total Cu concentration. This is characteristic of a fork mechanism, which is consistent with the competition between steps ② and ⑥ in Scheme 4-1. There are two pathways once the Cu(I) makes the ^{S}**P/O**, the oxidant could either decay to the **BisOH** or bind to the phenolate, making species **A**. The rate of the **BisOH** formation likely only depends on the concentration of the oxidant, whereas the rate of **A** formation is based on both oxidant and phenolate concentrations. Therefore, increasing the concentration of phenol in the system causes formation of more products forming.

To prevent the decay of the **SQ** and to maximize its concentration, the same experiment was performed at −35°C (Figure 4-2). Now $[\mathbf{SQ}]_{max}$ reaches up to 84% of the total Cu concentration (when [3,5-DBP] = 7.27 mM), but gradual decrease of the **SQ** concentration is still observed in all cases. This could be because, when dissociating the substrate, it slowly liberates a small amount of DBED-Cu^{I} complex that faces the fork again.

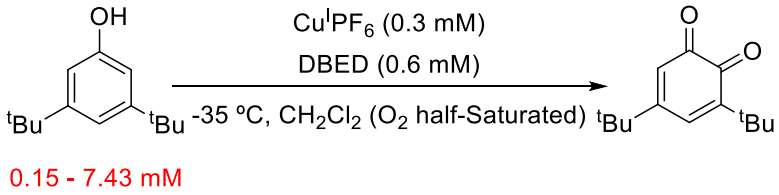

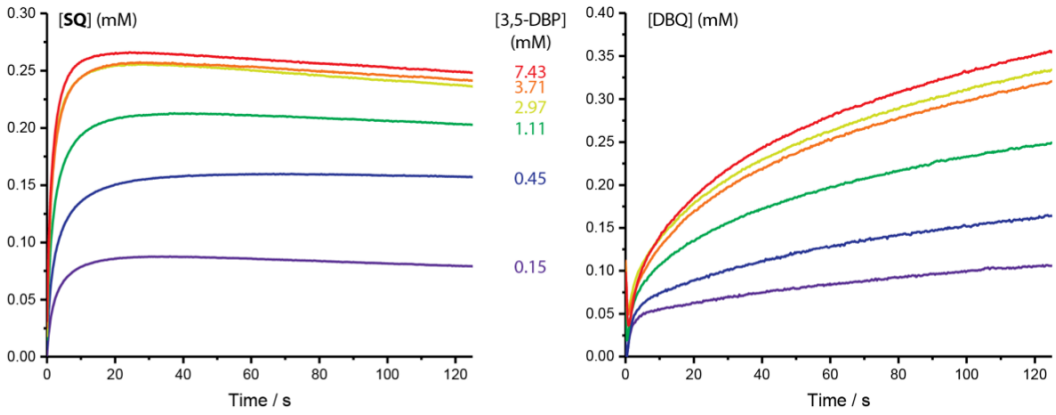

Figure 4-2. Substrate influence at −35°C: stopped-flow reaction of $Cu^{I}PF_6$ (0.323 mM), DBED (0.625 mM) and 3,5-DBP (0.15-7.43 mM) in O_2-half-saturated DCM at −35°C. Formation of **SQ** (left), and DBQ (right).

4.2.2 Influence of DBED concentration

The next experiment was to vary the DBED concentration while $Cu^{I}PF_6$ was kept at 8 mol% of a fixed 3,5-DBP concentration, at −35°C. Thus, [DBED] was varied from 9 to 95 mol% of [3,5-DBP] in order to keep the DBED-to-Cu ratio above 1. The formations of **SQ** and DBQ are represented on Figure 4-3.

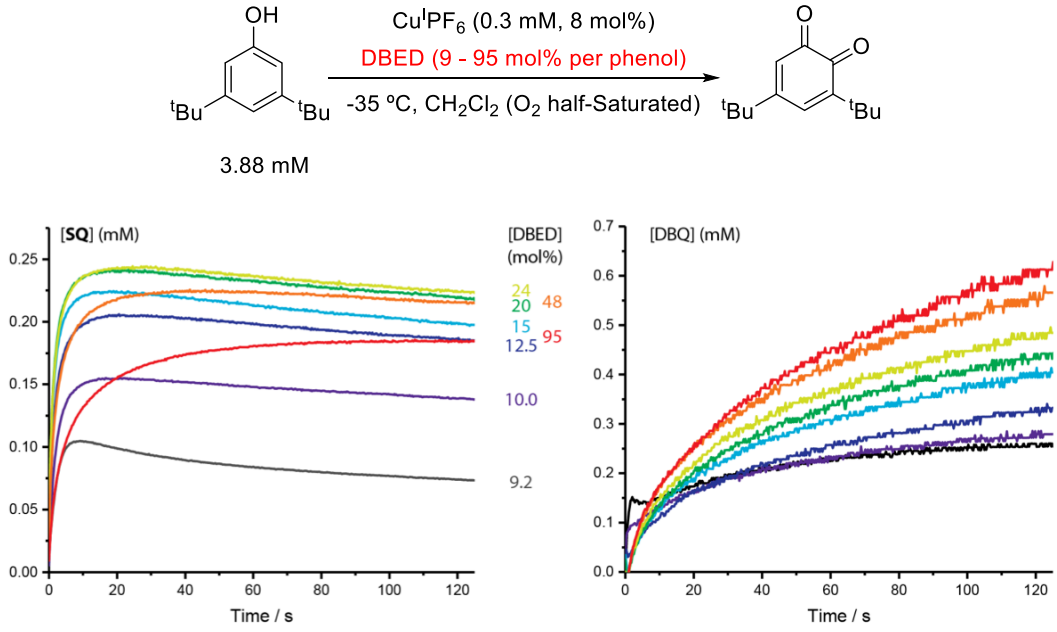

Figure 4-3. DBED influence at −35°C: stopped-flow reaction of $Cu^{I}PF_6$ (0.31 mM), DBED (0.36-3.68 mM, 9-95 mol% per 3,5-DBP) and 3,5-DBP (3.88 mM) in O_2-half-saturated DCM at −35°C. Formation of **SQ** (left), and DBQ (right).

Overall, the trends in **SQ** formation are similar to the experiment above (section 4.2.1), except at high DBED concentrations. Ongoing from 9 to 24 mol% DBED, an increase in the $[\mathbf{SQ}]_{max}$ is observed up to 80% of the total Cu concentration. This is consistent with more DBED allowing more phenolate to form in situ, hence more turnover. With 48% and 95% DBED/3,5-DBP ratio, however, **SQ** formation slows down significantly, a feature we cannot explain yet.

4.2.3 Influence of $Cu^{I}PF_6$ concentration

The $[Cu^{I}PF_6]$ variation experiment was performed at 25°C in the Schlenk flask with the UV-probe (slow mixing). Too keep DBED in excess of $Cu^{I}PF_6$, DBED was kept at the same concentration as the substrate, actually 99.2 mol%. $[Cu^{I}PF_6]$ was varied between 5 mol% and 100 mol% of substrate. Unfortunately, the last experiment is under a default of DBED to Cu and did not proceed well (see below), indicating the importance of the slight excess of DBED to form the phenolate.

Figure 4-4 represents the absorbances at 570 and 400 nm, at which the **SQ** and DBQ species have their maximum absorption, respectively. Figure 4-5 shows the concentration of the product in percentage of yield. It is evident that the reaction achieves better yields at higher $Cu^{I}PF_6$ concentration. In addition, more **SQ** forms when more Cu is present in solution (maxima of the red traces in Figure 4-4). This is consistent with a faster formation of the ^{S}**P** oxidant. However, complete kinetic fitting of this behaviour is currently out of reach until experiments can be done on the stopped-flow instrument, where the pathlength has to be varied, lest the **SQ** absorption saturates.

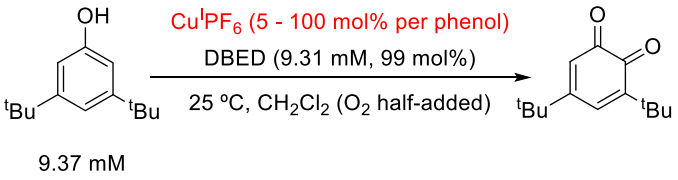

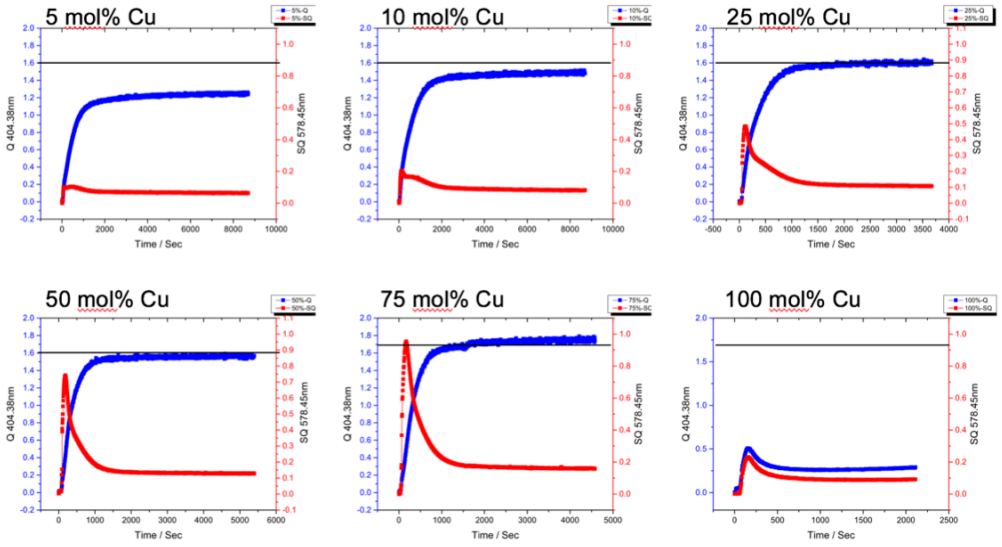

Figure 4-4. $Cu^{I}PF_6$ influence at 25°C: UV-Vis reaction of $Cu^{I}PF_6$ (0.52-9.39 mM, 5-100 mol% per 3,5-DBP), DBED (9.31 mM, 99 mol%) and 3,5-DBP (9.37 mM) in DCM. Time profiles show formation of **SQ** (red) and DBQ (blue). The black line represents 100% yield of DBQ.

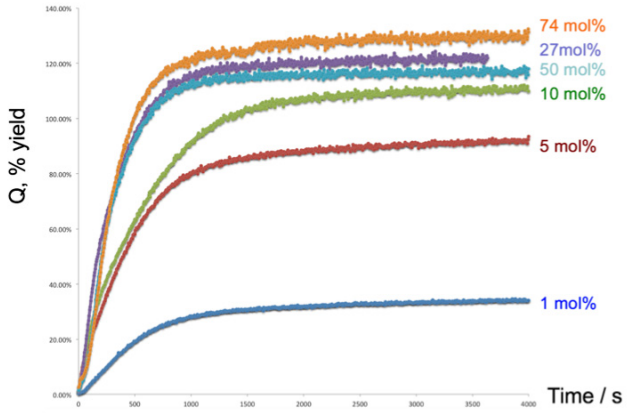

Figure 4-5. Formation of DBQ with varied concentrations of $Cu^{I}PF_6$, expressed as yield of the reaction.

4.3 Reaction Behaviour at –80°C

While the experiments at 25°C and –35°C allowed to monitor the formation of **SQ** and DBQ, and therefore apply to the simplified mechanism of Scheme 2-9, kinetic fitting of the concentrations is made difficult in the absence of knowledge in-between DBED-Cu^{I} and **SQ**. For example, what is the rate expression for steps ①-③ and which one is rate-determining? For this reason, experiments were carried at –80°C. At this temperature, the "decay" of the **SQ** signal after reaching its maximum should not be a problem because **SQ** dissociation is no longer kinetically competent, and neither is ^{S}**P** decomposition (step ⑥). In addition, the other reaction intermediates (^{S}**P**, **A**, **C**) may be studied once all steps are slowed down.

The first low-temperature experiment, stoichiometric at –85°C, allowed us to visualize key intermediate **A**. ^{S}**P** was prepared in situ from a 1:1 $Cu^{I}PF_6$:DBED solution, then reacted with phenol and DBED under N_2 (Figure 4-6). Immediately, an absorption at 435 nm appears, which is characteristic of the **A** species.[42-43] Therefore, ^{S}**P** reacts with 3,5-DBP and a small amount of DBED along the mechanism initially proposed by Stack.[43] and studied in our lab by Mohammad Askari, i.e. step ②.[33] It is noteworthy that **A** was not observed with 4-BP or 4-BP^{-} as reactants. The steric effects imparted by the 3,5-substitution (and the 2,4 substitution in Stack's case) apparently slow down the conversion of **A** to **C**, so that **A** becomes observable. Species **A** slowly

converts into **SQ** in 100% yield with respect to the total Cu concentration. Further introduction of O_2 leads to 100% **SQ**, confirming turnover.

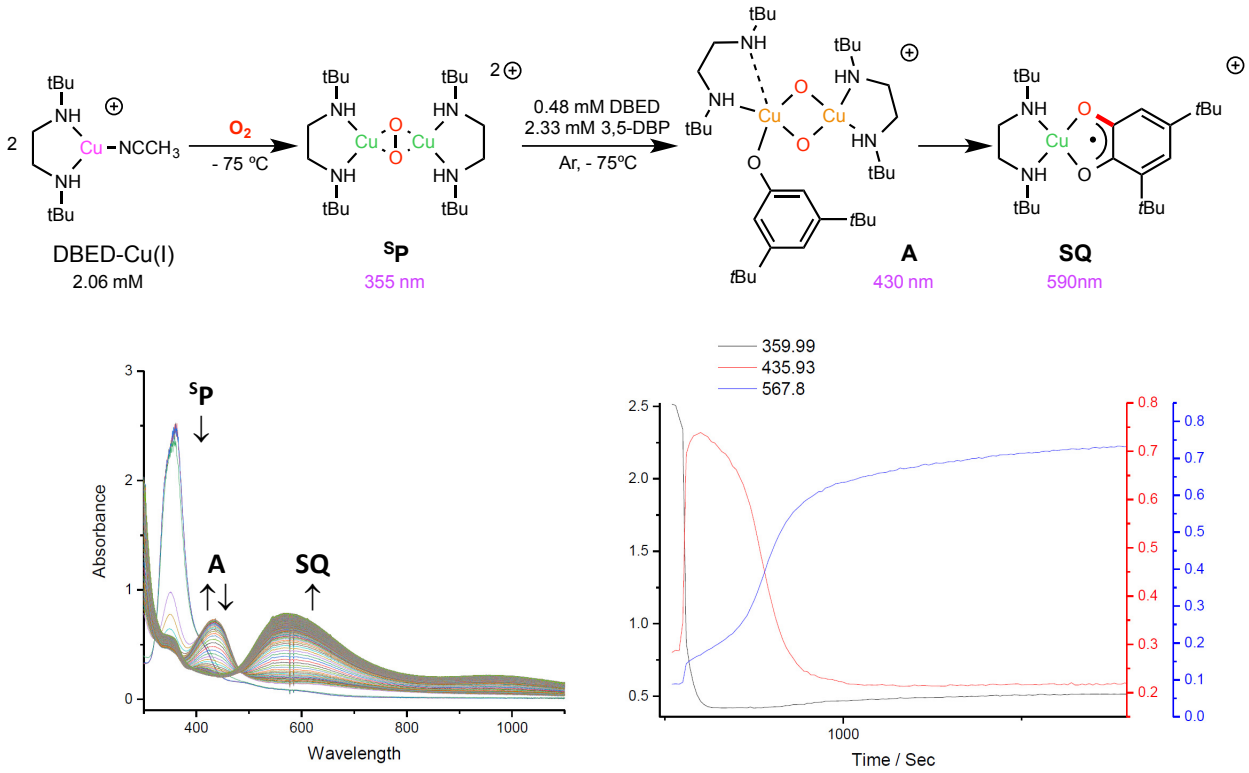

Figure 4-6. UV-Vis of **^{S}P** forms with Cu^IPF_6 (2.06 mM), DBED (2.54 mM) in DCM, decays with 3,5-DBP (2.33 mM) injects into the solution, and **A** forms and decays with **SQ** formation (left) and its time profile (right).

While this experiment is very informative, it begs many questions. The first is related to the quantity of **A**. Species **A** is limited by the phenolate present, therefore the quantity of DBED in excess of Cu. We therefore expect about 0.2 equivalents of **A** to form, which was indeed observed. But then why did *all* the **^{S}P** oxidant disappear (no more absorption at 355 nm)? The second question is why did **SQ** form in more than 50% when the reaction was carried under N_2? According to the mechanism on Scheme 4-1, 1 **^{S}P** molecule should generate 1 **SQ** molecule and 1 $DBEDCu^I$ that shall not turnover with O_2 absent (steps ②, ③ and ④). This reaction was repeated three times, which frustrates the hypothesis of an O_2 leak in the system. We construe

that the consumption of ^{S}**P** may be complicated by other pathways, e.g. protonation and release of H_2O_2, but this type of studies fall beyond the purview of this M.Sc thesis.

Despite the complications observed in this stoichiometric reaction, the use of the very low temperature allowed us to visualize key intermediate **A**, which warrants stopped-flow investigation under catalytically relevant conditions.

4.4 Component Effects at –80°C

4.4.1 Influence of substrate concentration

In a first series of experiments monitored by stopped-flow at –80°C, [3,5-DPB] was varied while [$Cu^{I}PF_6$] and [DBED] were kept constant, similarly to the 25°C experiment above (Figure 4-7). By increasing the concentration of substrate, we were able to observe the raise of the peak at 435 nm which is known intermediate **A**. The concentration of **A** increases in the first 2.5 s of reaction by fast oxidative addition of phenolate to Cu(II) center in ^{S}**P** species (step ②).

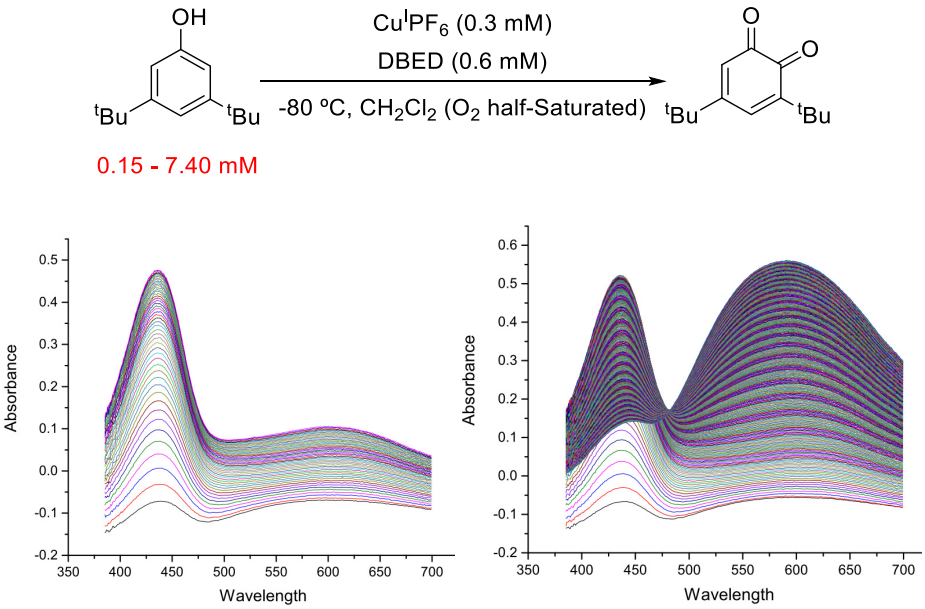

Figure 4-7. UV-Vis of the stopped-flow reaction of $Cu^{I}PF_6$ (0.32 mM), DBED (0.62 mM) and 3,5-DBP (7.40 mM) in O_2-half-saturated DCM at −80°C. Formation of **A** (left) in 2.5s, and **SQ** (right) for 25s.

In each experiment (Figure 4-8), **A** forms fast with increasing the concentration of 3,5-DBP, reaches a maximum concentration ($[\mathbf{A}]_{max}$) then decreases while **SQ** forms gradually. The first striking observation is that, with increasing substrate concentration, $[\mathbf{A}]_{max}$ raises up to 10% with respect to total Cu concentration, and the formation of **A** becomes faster with more [3,5-DBP]. This is consistent with our mechanism proposal: more phenol(ate) will accelerate step ② and produce **A** faster. Another information which we can obtain from the results is that the rate of decrease of [**A**] is not dependent on [3,5-DBP]. This is also consistent with the proposed mechanism, since the steps between **A** and **SQ** do not involve a phenol or phenolate molecule.

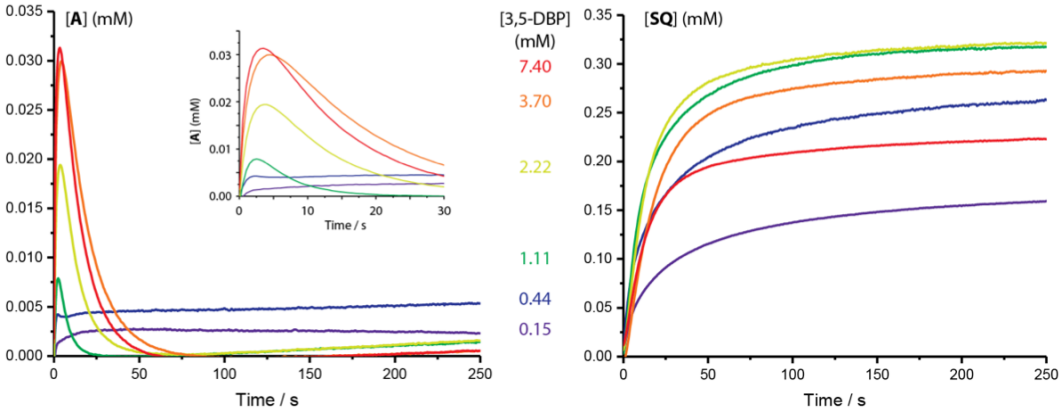

Figure 4-8. Substrate influence at −80°C: stopped-flow reaction of $Cu^{I}PF_6$ (0.32 mM), DBED (0.62 mM) and 3,5-DBP (0.15-7.40 mM) in O_2-half-saturated DCM at −80°C. Formation of **A** (left), and **SQ** (right).

[**SQ**] approaches its maximum ($[\mathbf{SQ}]_{max} = [Cu^{I}PF_6]_{initial}$) when [3,5-DBP] is close to 2.2 mM, i.e. at 15 mol% Cu. At higher phenol concentrations, $[\mathbf{SQ}]_{max}$ decreases, a phenomenon we cannot yet explain. Perhaps the reaction converges to a mixture of **SQ** and **C** at high phenol concentration. Since **C** is globally silent in UV-Vis, we only observe **SQ**, but all the Cu is accounted for. Another hypothesis is that decomposition to **bisOH** occurs. Further work is warranted.

4.4.2 Influence of DBED concentration

In another set of experiments at −80°C, [DBED] was varied while $[Cu^{I}PF_6]$ was kept at 8 mol% of a fixed 3,5-DBP concentration. [DBED] was varied from 9 to 100 mol% of [3,5-DBP] in order to

keep the DBED-to-Cu ratio greater than 1. As above, the UV-Vis spectra revealed the formation of **A** and **SQ** (Figure 4-9).

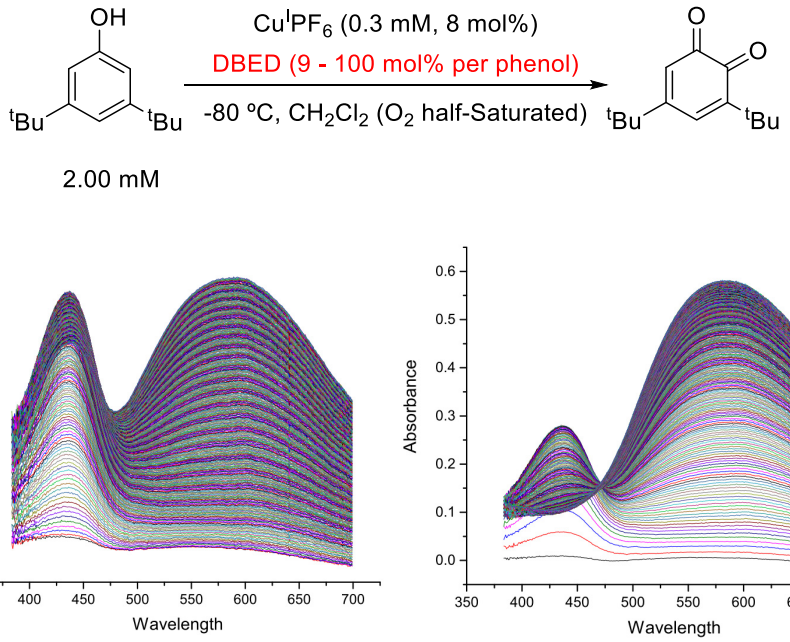

Figure 4-9. UV-Vis reaction of $Cu^{I}PF_6$ (0.17 mM, 8 mol%), DBED (0.31 mM, 15 mol%) and 3,5-DBP (2.00 mM) in O_2-half-saturated DCM at −80°C. Formation of **A** (left) in 25s, and **SQ** (right) for 250 s.

The time-profiling shows the formation of [**A**] forming faster with more [DBED] in the system, as was the case with the phenol effect above (Figure 4-10). The excess of DBED with respect to Cu is responsible for the deprotonation of 3,5-DBP to its phenolate. Therefore, more DBED in the reaction will also drive step ② and the formation of **A** faster. The phenol deprotonation also forms $DBEDH^+$, which is believed to be involved in the transformation from **C** to **SQ** (step ④). As strikingly apparent in Figure 4-10 left, the rate of decay of species **A** is accelerated at higher DBED concentration. This is fully consistent with the involvement of $DBEDH^+$ in-between **A** and **SQ**.

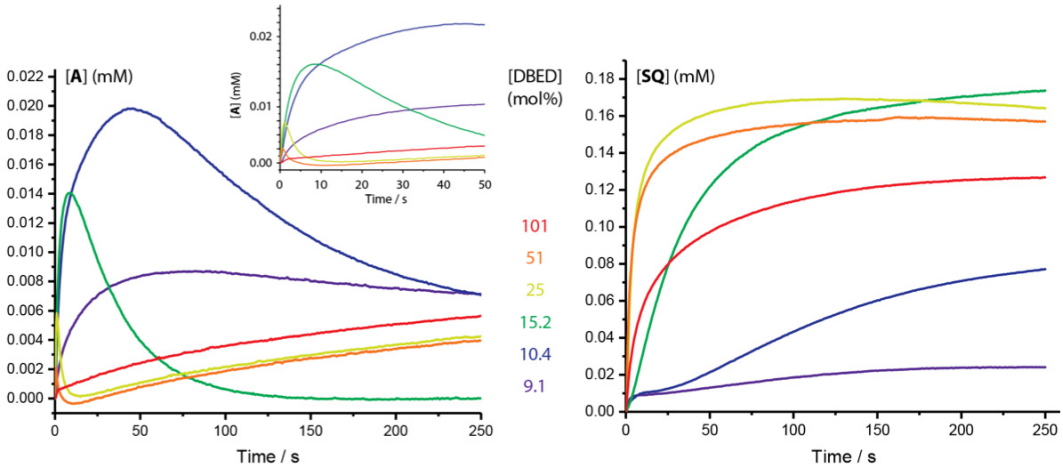

Figure 4-10. DBED influence at −80°C: stopped-flow reaction of $Cu^{I}PF_6$ (0.17 mM), DBED (0.18 – 2.03 mM, 9-101 mol% per 3,5-DBP) and 3,5-DBP (2.00 mM) in O_2-half-saturated DCM at −80°C. Formation of **A** (left), and **SQ** (right).

As was the case in the experiment on the phenol effect, too much DBED is detrimental to the formation of **SQ** (red trace on Figure 4-10 right). This needs to be investigated further.

4.5 Kinetic Isotope Effect (KIE)

As indicated before, the rate-determining step of the reaction at room temperature is believed to be the dissociation of **SQ** into DBQ and DBED-Cu(I). Therefore, no intermediates prior to **SQ** are observed at RT. In order to probe the mechanism and to confirm that the intermediates we observed at low temperature are valid intermediates at room temperature, we probed the product-determining step by isotopic labelling. To this end, the deuterated substrate (3,5-DBP^{HD}) was prepared by a summer intern, Mark Kit, under my supervision (Scheme 4-2).

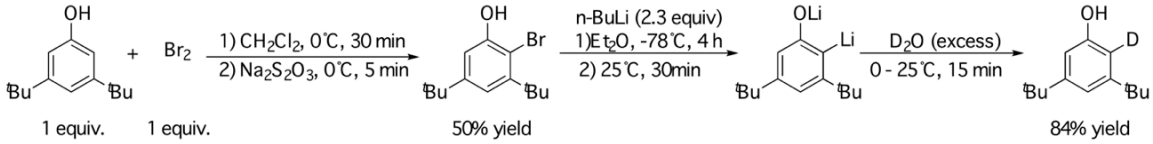

Scheme 4-2. Synthesis of monodeuterated substrate (3,5-DBP^{HD}).

Oxygenation of 3,5-DBP^{HD} displayed an intramolecular KIE = k_H/k_D of 0.87 (see experimental section), which is consistent with previously reported values using 4-BP^{HD} [33] or in tyrosinase.[61-62]

This KIE of 0.87 denotes an inverse isotopic effect,[63] i.e. the reaction involving the C−D bond proceeds faster than the reaction involving the C−H bond. Also, the rate-determining part of the product-determining step does not involve C−H/D cleavage otherwise the KIE would be much higher than 1. These observations are fully consistent with an electrophilic aromatic substitution on 3,5-DBP^{HD}, with a sp^2 carbon of the phenyl ring hybridizing to sp^3 upon C−O bond formation before the C−H/D is deprotonated to recover aromaticity (Scheme 4-3). As shown by Stack and coworkers with stoichiometric models, species **A** possesses all attributes for an intramolecular S_EAr (with KIE = 0.89): the O atoms of the Cu_2O_2 **O** core are electrophilic and positioned near the *ortho* position of the coordinated phenolate.[42-43] Overall, this key experiment gives credit to the intermediary of **A** in the oxygenation pathway *at room temperature*.

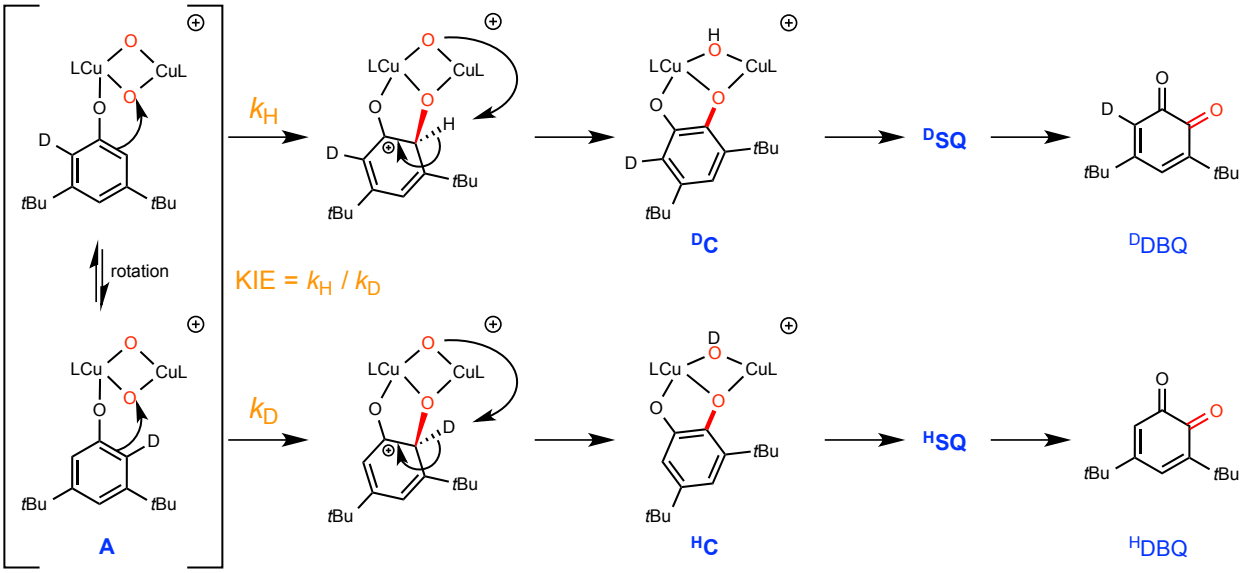

Scheme 4-3. Intramolecular electrophilic aromatic substitution in species **A** and isotopic differentiation.

4.6 Discussion

The above kinetic experiments are the first step towards a full analysis of the reaction mechanism at various temperatures. In order to convey the information gathered at low-temperature to higher temperatures, proper rate modelling is necessary. This means finding a

set of elementary steps, which, taken together, lead to satisfactory fitting of the concentration profiles of all species involved. At room temperature, the reaction sequence from the phenol to **SQ** and to DBQ is reminiscent of a Michaelis-Menten model (Equation 4-2). However, the key difference is that the second step is reversible in our case, making it impossible to find an analytical solution. In addition, Cu channels from mononuclear to binuclear complexes throughout the catalytic cycle, which could make the fit more challenging. Catalyst decomposition to **bisOH** should also be taken into account.

$$E + S \rightleftharpoons ES \longrightarrow E + P$$

$$Cu + ArOH \rightleftharpoons Cu\text{-}SQ \rightleftharpoons Cu + Q$$

Equation 4-2. Comparison between Michaelis-Menten (up) and the simple model for our reaction (down).

Because exact kinetic solutions cannot be expressed, one must rely on developing a system of differential rate equations and employing a software to solve the system and express the results in terms of concentration versus time. Transposing our current mechanism proposal into elementary steps leads to Equation 4-3. Fitting attempts are currently being pursued by Dr. X.

$$\text{①}\begin{cases} LCu + O_2 \longrightarrow LCuO_2 \\ LCuO_2 + LCu \longrightarrow {}^{S}\mathbf{P} \end{cases}$$

$$ArOH + L_{XS} \rightleftharpoons ArO^- + L_{XS}H^+$$

$$\text{②}\ {}^{S}\mathbf{P} + ArO^- \longrightarrow \mathbf{A}$$

$$\text{③}\ \mathbf{A} \longrightarrow \mathbf{C}$$

$$\text{④}\ \mathbf{C} + L_{XS}H^+ \rightleftharpoons \mathbf{SQ} + LCu + L_{XS}$$

$$\text{⑥}\ {}^{S}\mathbf{P} \longrightarrow \mathbf{bisOH}$$

Equation 4-3. Decomposition of the mechanism in elementary steps.

Chapter 5: Conclusion

In conclusion, the possibility to mimic the tyrosinase-like reactivity is highly dependent on the substrate, ligand, Cu source and even solvent. Under very similar catalytic conditions, different phenols will undergo different reactions, with *ortho*-oxygenation and oxidative coupling being the two main pathways. Once a quinone is formed in the medium, it usually undergoes further oxidative coupling(s) that cannot be avoided because the catalytic system is a strong enough oxidant. Substrate 3,5-DBP is the only one that undergoes *ortho*-oxygenation under DBED:$Cu^{I}PF_6$ (8:15 mol%) conditions. It forms DBQ in excellent yield at room temperature within a few hours of exposure to O_2. The UV-Vis spectra at room temperature exhibits a single intermediate, **SQ**, with a concentration profile that allowed us to propose a simplified mechanism in 0. Based on the mechanism, we believe that DBQ is the product of **SQ** dissociation in the last step of turnover, likely the rate-determining step of the reaction. The **SQ** complex is the key to understanding the mechanism of *ortho*-oxygenation with 3,5-DBP because it is the reservoir of Cu(I) for the further steps of the reaction.

In Chapter 3, we discussed ligand screening with mono-, bi-, tri-, and tetradentate ligands, confirming a direct correlation between the presence of the **SQ** intermediate and efficiency of the reaction to perform oxygenation of phenol. Only ligands that impart a twisted **SQ** structure because of their tertiary substituents (e.g. *t*Bu or adamantyl) are supporting efficient *ortho*-oxygenation. The nature of the oxidant is of prime importance: only ligands supporting a ^{S}**P**-type oxidant at low-temperature correlate with high reaction efficiency. The reaction of the ^{S}**P** or **O** oxidant with the in-situ phenolate seems to be the key to achieving selectivity towards substrate oxygenation.

The low temperature stopped-flow experiments (Chapter 1) established different intermediates involved in-between DBED-Cu(I) and **SQ**. Influence of the concentration of phenol, Cu and DBED, highlight key steps of the mechanism. Notably, **A** was observed at low temperatures, which was not the case with 4-BP. The KIE study confirmed that oxygenation at

room temperature proceeds via S_EAr, like tyrosinase does. Full kinetic modelling is very complex and is still in progress.

Future work will revolve on (1) determining the kinetic model of the reactions at many temperatures so as to confirm the proposed mechanism, (2) surveying the reaction of many ^{S}**P** and **O** oxidants with phenolates to probe for the source of selectivity, (3) determining the redox potentials of ^{S}**P** and **O** oxidants at low temperature in order to see how ligands modify the outer-sphere electron-transfer pathway, (4) once the mechanism is well understood, identifying the role of other phenol substrates with different electronic structures (substituents), and (5) understanding how the C–O coupling occurs.

Overall, our mechanistic understanding will guide researchers in harnessing the oxidative abilities of Cu/O_2 moieties and developing new catalytic systems that are inspired by the efficiency of tyrosinase. Aerobic catalysis with copper precursors is still in its infancy and, being bio-inspired, will find much interest due to its green-chemistry aspects.

Chapter 6: Experimental Section

6.1 General Conditions

Chemicals and solvents were purchased from Sigma Aldrich, Alfa Aesar or Strem Chemicals. Inhibitor-free solvents were dried using a MBraun SPS 800, transferred to an inert-atmosphere glove box (MBraun Labmaster, <1 ppm O_2 and H_2O, filled with a dry N_2 atmosphere), further degassed under vacuum and stored over activated molecular sieves (4 Å). *N*,*N*'-di-*tert*-butylethylenediamine (DBED) was distilled over CaH_2 under N_2 and stored in the glovebox. The copper(I) salt $[Cu(CH_3CN)_4](PF_6)$, abbreviated $Cu^{I}PF_6$, was purchased from commercial sources or made via a literature procedure.[64] All copper(I) complexes were stored inside the glovebox.

Unless otherwise noted, reactions were performed in oven-dried glassware under a positive pressure of nitrogen using standard synthetic inert-atmosphere techniques. Bulk oxidation reactions were set-up in the glovebox in 10 mL, oven-dried Radley tubes equipped with a Teflon-coated stir bar. The reaction vessels were then connected to a cylinder of O_2, purged at least three times with O_2 and then over-pressurized to +1.0 atm.

UV-Visible spectra were recorded on a B&W Tek iTrometer equipped with fiber-optic cables connected to a Hellma full-quartz dip-probe having a 1.0 mm pathlength. The probe was immersed in the solution inside a custom-made Schlenk flask. Temperature was maintained with external cooling baths: acetone/dry ice (−75 °C inside the solution), acetone/liquid nitrogen (−85 °C), pentane/liquid nitrogen (−115 °C). Spectra for mixtures or evolving solutions are reported in apparent ε, i.e. molar extinction coefficients with respect to the total Cu concentration.

Low-temperature stopped-flow experiments were carried out in the Département de Chimie at the Université de Montréal on a Hi-Tech CSF-61DX2 instrument (TgK Scientific) equipped with a diode-array detector over the 300-700 nm range. The UV-Vis cuvette (pathlengths of 1.5 or 10 mm) was cooled by immersion in an ethanol bath cooled with liquid N_2. Syringe 1 was filled with a CH_2Cl_2 solution containing 3,5-DBP, DBED and $Cu^{I}PF_6$ in desired concentrations that was prepared in an MBraun Labmaster glovebox. Syringe 2 was filled with CH_2Cl_2 that was O_2-

saturated at atmospheric pressure and room temperature. Concentrations were corrected for the 2-fold dilution upon mixing.

^{1}H-NMR spectra were collected on a Varian Innova 500 MHz instrument at 25 °C.

6.2 UV-Vis Experiments at Room Temperature

In the glovebox, Cu^{I}PF6 (0.02 mmol, 9.5 mM) dissolved in DCM was added into a solution of DAdED (0.04 mmol, 18.9 mM), and a transparent colorless mixture solution was obtained. 3,5-DBP (0.25 mmol, 124 mM) was dissolved in DCM. The 3,5-DBP and CuL (8:15 mol%) solution were mixed together into a 2 mL volumetric flask (brought to 2 mL with DCM) to make the stock solution. 6 mL of DCM was charged into the UV-Vis probe cell in the glovebox, transferred outside then connected into the UV-Vis fiber-optics. 600 µL of the stock solution was injected into the UV-Vis cell, and then O_2 was introduced. Spectra were collected every 5 seconds for 4 hours at 25°C. The final concentrations are [3,5-DBP] = 11.3 mM, [Cu] = 0.9 mM, [DAdED] = 1.7 mM, and the pathlength of the UV probe is 0.1 cm (Figure 6-1). The same method was applied to DtOED (Figure 6-2), DTrED, TEED (Figure 6-4), BMPD and TEPD (Figure 6-3).

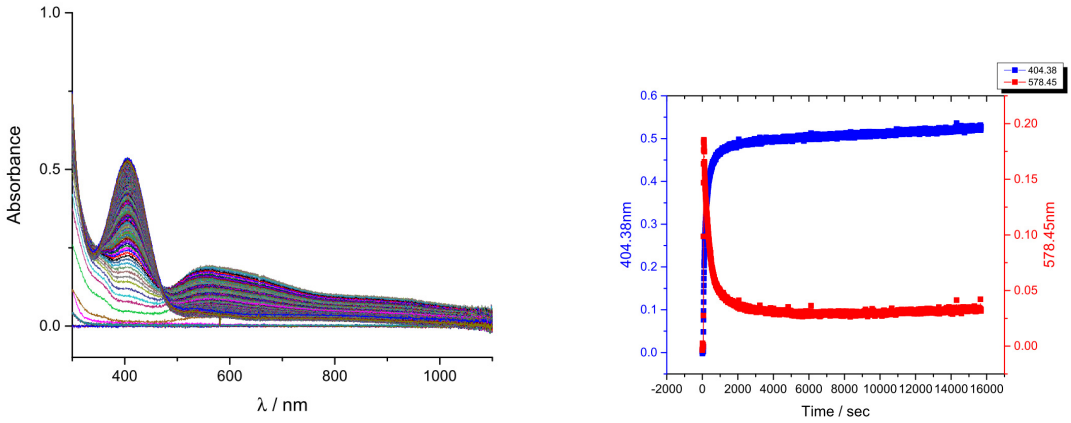

Figure 6-1. (Left) UV-Vis spectra during the reaction of 3,5-DBP (11.3 mM) with Cu^{I}PF$_6$ (8 mol%), DAdED (15 mol%) and O_2 (1 atm) in DCM at 25°C for 4 h (pathlength 1.0 mm). (Right) time profile of the absorbances where the DBQ (blue) and the **SQ** intermediate (red) absorb.

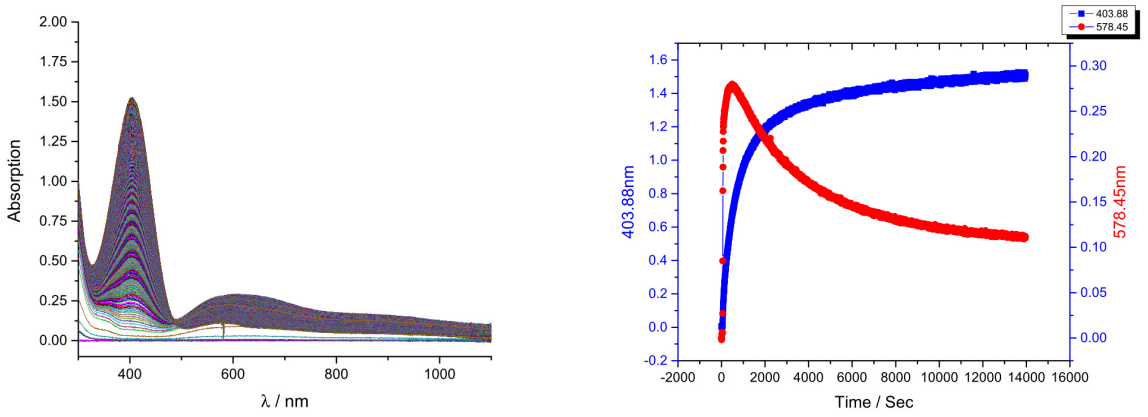

Figure 6-2. (Left) UV-Vis spectra during the reaction of 3,5-DBP (11.6 mM) with $Cu^{I}PF_6$ (8 mol%), DtOED (15 mol%) and O_2 (1 atm) in DCM at 25°C for 4 h (pathlength 1.0 mm). (Right) time profile of the absorbances where the DBQ (blue) and the **SQ** intermediate (red) absorb.

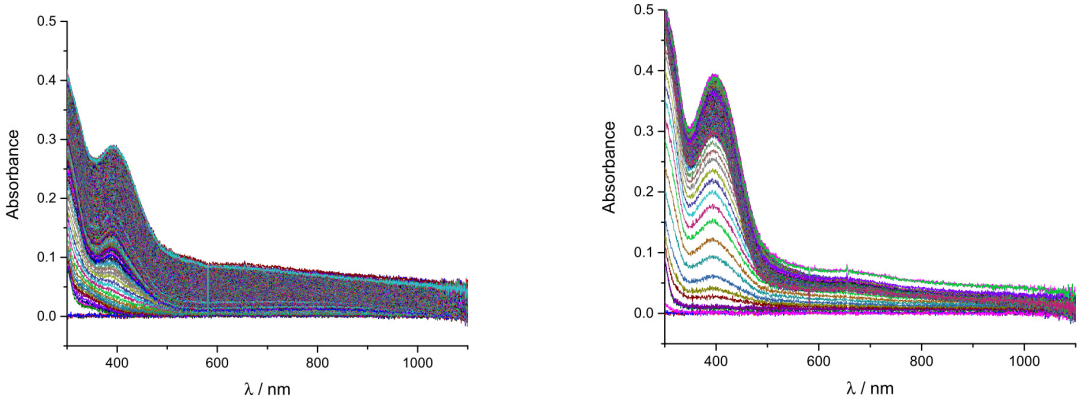

Figure 6-3. (Left) UV-Vis spectra during the reaction of 3,5-DBP (13.8 mM) with $Cu^{I}PF_6$ (8 mol%), BMPD (15 mol%) and O_2 (1 atm) in DCM at 25°C for 4 h (pathlength 1.0 mm). (Right) UV-Vis spectra during the reaction of 3,5-DBP (13.8 mM) with $Cu^{I}PF_6$ (8 mol%), TEPD (15 mol%) and O_2 (1 atm) in DCM at 25°C for 4 h (pathlength 1.0 mm).

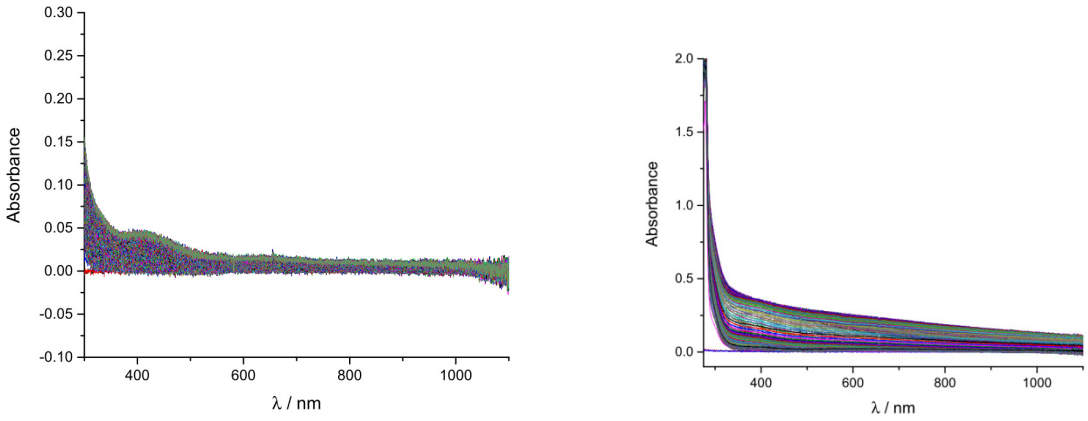

Figure 6-4. (Left) UV-Vis spectra during the reaction of 3,5-DBP (11.1 mM) with $Cu^{I}PF_6$ (8 mol%), DTrED (15 mol%) and O_2 (1 atm) in DCM at 25°C for 4 h (pathlength 1.0 mm). (Right) UV-Vis spectra during the reaction of 3,5-DBP (10.2 mM) with $Cu^{I}PF_6$ (8 mol%), TEED (15 mol%) and O_2 (1 atm) in DCM at 25°C for 4 h (pathlength 1.0 mm).

6.3 Low-Temperature Stabilities

In the glovebox a stock solution of $Cu^{I}PF_6$ and DtOED is prepared (16.9 mmol each) in 3 mL DCM. 7 mL DCM was charged into the UV-Vis probe cell in the glovebox, transferred outside then connected into the UV-Vis fiber-optics probe then cooled down to −78°C using a dry ice/acetone bath. 600 µL of the stock solution was injected into the UV-Vis cell, and then O_2 was introduced. Spectra were collected every 5 seconds for 4 hours at low temperature (Figure 6-5). The final concentration of Cu was 1.334 mM, and the pathlength of the UV probe is 0.1 cm. The same method was applied to DAdED (Figure 6-6), BMPD and DTrED (Figure 6-7).

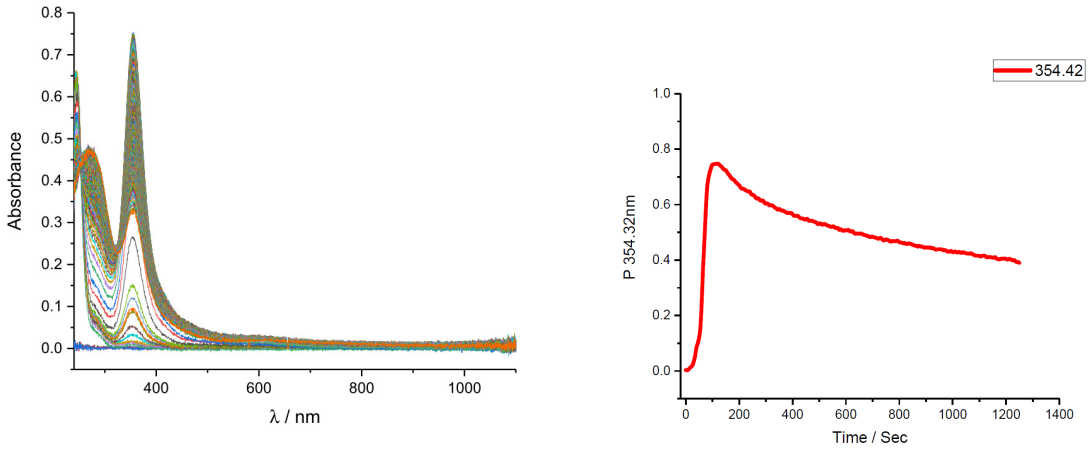

Figure 6-5. Low-temperature formation and decay of DtOED-^{S}**P** complexes with [Cu^{I}PF$_6$] = 1.334mM at −75°C in DCM monitored by UV-Vis spectroscopy (left), and its time profile (right).

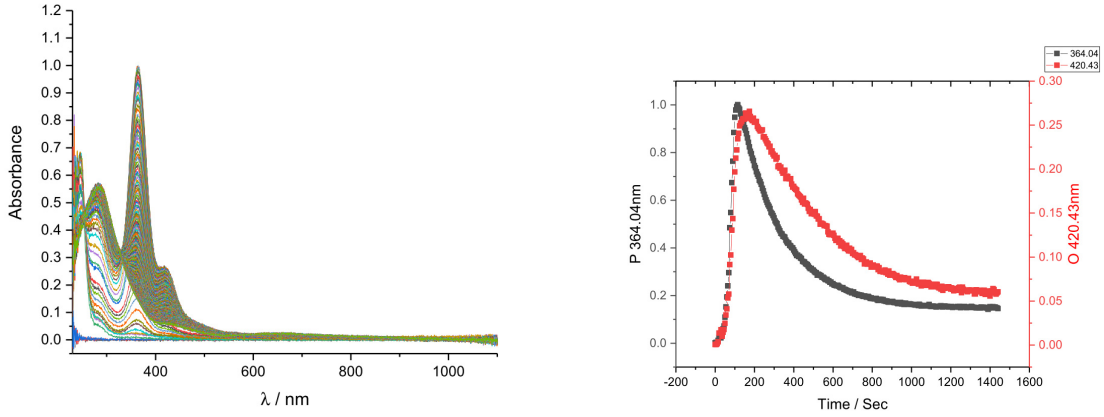

Figure 6-6. Low-temperature formation and decay of DAdED-^{S}**P** and/or **O** complexes at −75°C in DCM monitored by UV-Vis spectroscopy (left, [Cu^{I}PF$_6$] = 1.036mM), and its time profile (right).

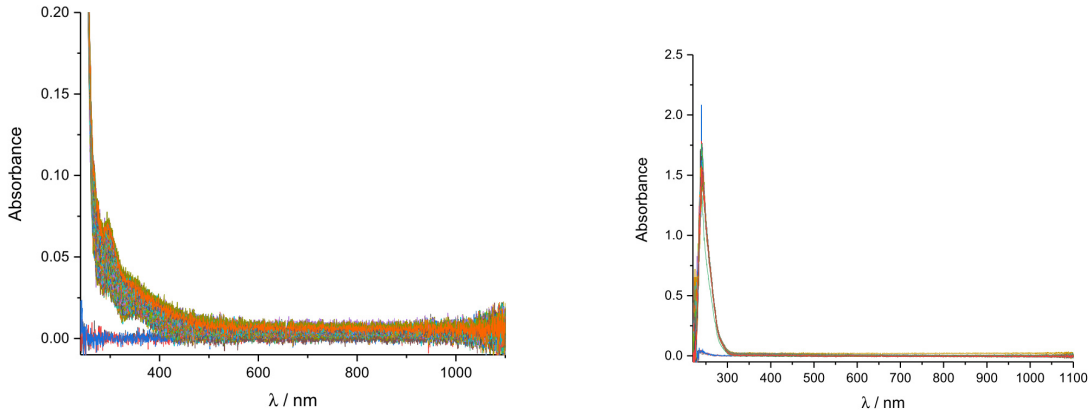

Figure 6-7. Low-temperature formation and decay of BMPD-^{S}**P** and/or **O** complexes (left, [Cu^{I}PF$_6$] = 1.334mM) and DTrED (right, [Cu^{I}PF$_6$] = 1.504mM) at −75°C in DCM monitored by UV-Vis spectroscopy.

6.4 Crystal Structures of the SQ species

This **L-SQ** species were made independently by mixing equimolar amounts of L, Cu^{I}PF$_6$ and DBQ in THF (Scheme 6-1 for DBED) and isolated by layered crystallization with pentane or diethyl ether in the glovebox at −30°C for two days.

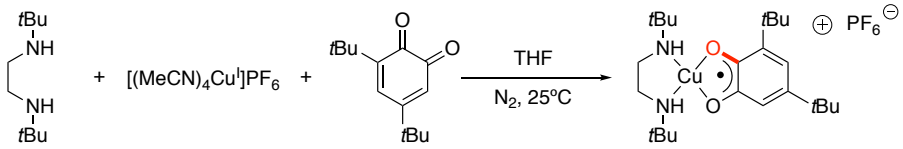

Scheme 6-1. Formation of semiquinone with equimolar Cu^{I}PF$_6$, DBED and DBQ.

X-ray crystallographic analysis was performed using the Cu-Kα microfocus or Mo-Kα source of a Bruker APEX-DUO diffractometer. The frames were integrated with the Bruker SAINT software package using a narrow-frame algorithm. Data were corrected for absorption effects using the multi-scan method (SADABS or TWINABS). The structures were solved by direct methods and refined using the Bruker APEX2 or APEX3 software package (SHELXL instructions). Non-hydrogen atoms were refined with anisotropic thermal parameters. Hydrogen atoms were generated in idealized positions, riding on the carrier atoms, with isotropic thermal parameters. The molecular structures for additional complexes **TMED-SQ** and **DiBED-SQ** are given in Figure 6-8.

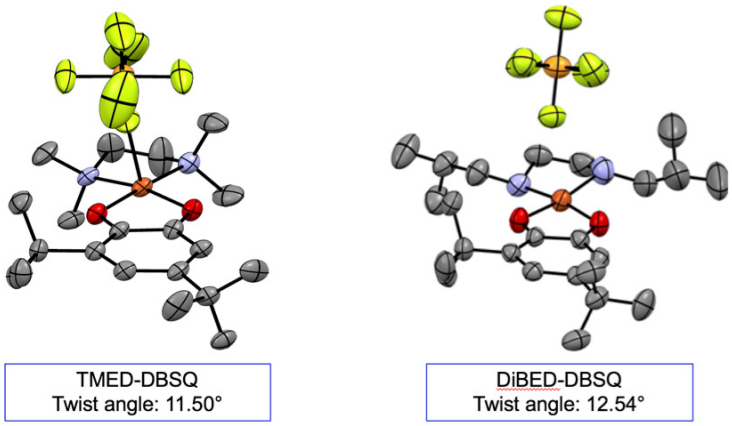

Figure 6-8. ORTEP at 50% ellipsoid probability of **TMED-SQ** and **DiBED-SQ**. Hydrogen atoms were omitted for clarity.

6.5 Stopped-Flow experiments

6.5.1 Substrate influence followed by Stopped-Flow Experiment at 25°C

Two stock solutions were prepared in the glovebox, one for the $Cu^{I}PF_6$-DBED (8:15%), and another one is for the 3,5-DBP (1.49 mmol, 148 mM) in DCM. Seven sample solutions were prepared by mixed 500 µL of the $Cu^{I}PF_6$-DBED solution with 20, 60, 150, 300, 400, 500 and 1000 µL of the 3,5-DBP stock solution to achieve the final concentrations of [$Cu^{I}PF_6$] = 0.31 mM, [DBED] = 0.59 mM, and [3,5-DBP] = 0.15, 0.44, 1.09, 2.18, 3,64 and 7.27 mM. The sample solution was transferred into a syringe and connected onto one end of the Y-junction. The other syringe contained O_2-saturated DCM. Spectra were collected every 50 ms for a total duration of 2.5 or 25 s, or every 0.5 s for a total duration of 250 s.

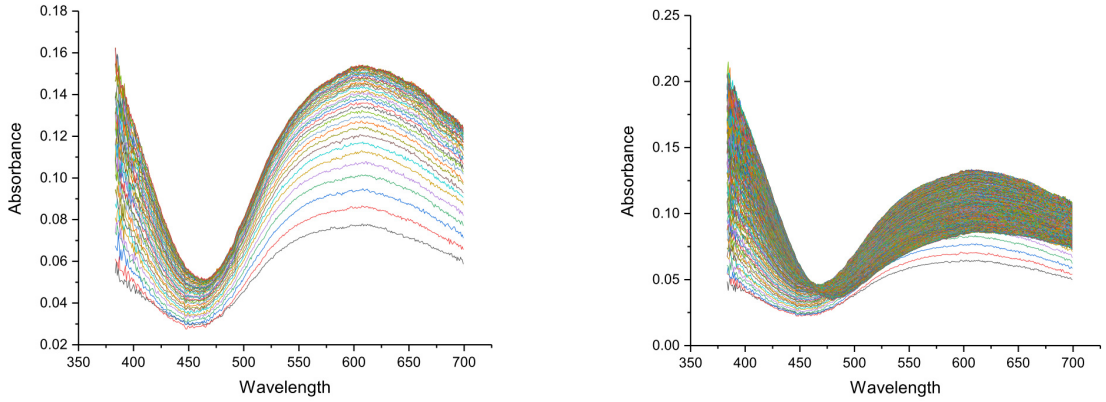

Figure 6-9. UV-Vis reaction of $Cu^{I}PF_6$ (0.31 mM, 8 mol%), DBED (0.59 mM, 15 mol%) and 3,5-DBP (0.15 mM) in O_2-half-saturated DCM at 25°C. Formation of **SQ** (580 nm) and DBQ (400 nm) for 2.5s (left), and 25s (right).

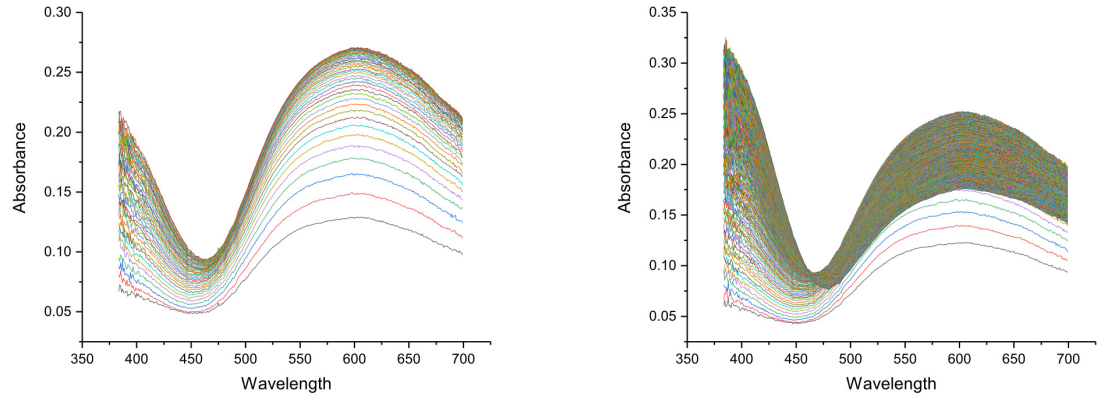

Figure 6-10. UV-Vis reaction of $Cu^{I}PF_6$ (0.31 mM, 8 mol%), DBED (0.59 mM, 15 mol%) and 3,5-DBP (0.44 mM) in O_2-half-saturated DCM at 25°C. Formation of **SQ** (580 nm) and DBQ (400 nm) for 2.5s (left), and 25s (right).

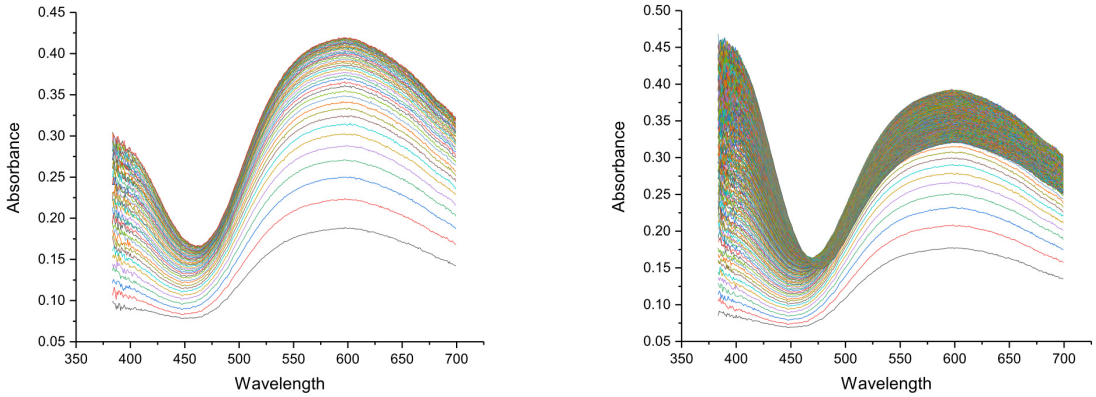

Figure 6-11. UV-Vis reaction of $Cu^{I}PF_6$ (0.31 mM, 8 mol%), DBED (0.59 mM, 15 mol%) and 3,5-DBP (1.09 mM) in O_2-half-saturated DCM at 25°C. Formation of **SQ** (580 nm) and DBQ (400 nm) for 2.5s (left), and 25s (right).

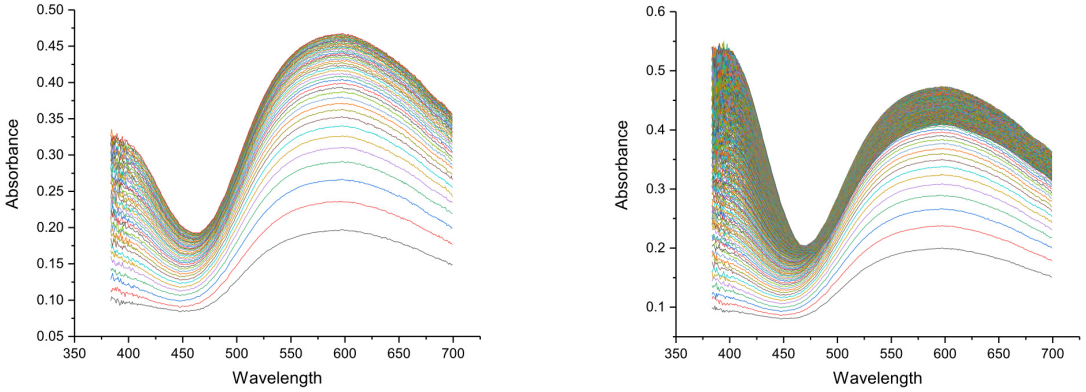

Figure 6-12. UV-Vis reaction of $Cu^{I}PF_6$ (0.31 mM, 8 mol%), DBED (0.59 mM, 15 mol%) and 3,5-DBP (2.18 mM) in O_2-half-saturated DCM at 25°C. Formation of **SQ** (580 nm) and DBQ (400 nm) for 2.5s (left), and 25s (right).

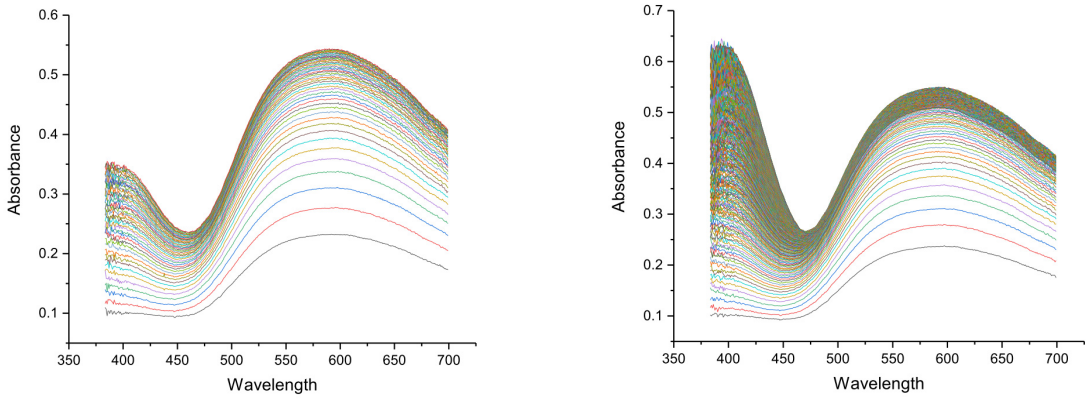

Figure 6-13. UV-Vis reaction of $Cu^{I}PF_6$ (0.31 mM, 8 mol%), DBED (0.59 mM, 15 mol%) and 3,5-DBP (3.64 mM) in O_2-half-saturated DCM at 25°C. Formation of **SQ** (580 nm) and DBQ (400 nm) for 2.5s (left), and 25s (right).

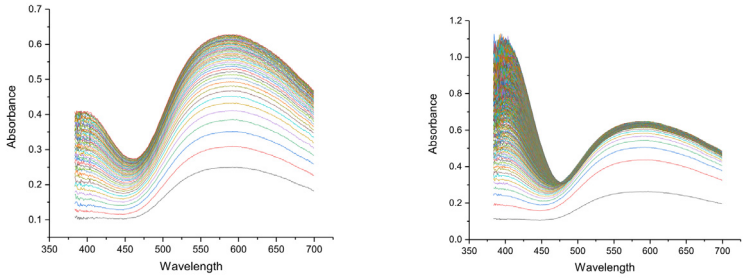

Figure 6-14. UV-Vis reaction of $Cu^{I}PF_6$ (0.31 mM, 8 mol%), DBED (0.59 mM, 15 mol%) and 3,5-DBP (7.27 mM) in O_2-half-saturated DCM at 25°C. Formation of **SQ** (580 nm) and DBQ (400 nm) for 2.5s (left), and 25s (middle), and 125s (right).

6.5.2 Substrate influence followed by Stopped-Flow Experiment at –35°C

Two stock solutions were prepared in the glovebox, one for the $Cu^{I}PF_6$-DBED (8:15%), and another one for 3,5-DBP (1.49 mmol, 148mM) in DCM. Seven sample solutions were prepared by mixing 500 µL of the $Cu^{I}PF_6$-DBED solution with 20, 60, 150, 300, 400, 500 and 1000 µL of the 3,5-DBP stock solution to achieve the final concentrations of [$Cu^{I}PF_6$] = 0.32mM, [DBED] = 0.63mM, and [3,5-DBP] = 0.15, 0.45, 1.11, 2.23, 2.97, 3,71 and 7.43 mM. The sample solution was transferred into a syringe and connected onto one end of the Y-junction. The other syringe

contained O_2-saturated DCM. Spectra were collected every 50 ms for a total duration of 2.5 or 25 s, or every 0.5 s for a total duration of 250 s.

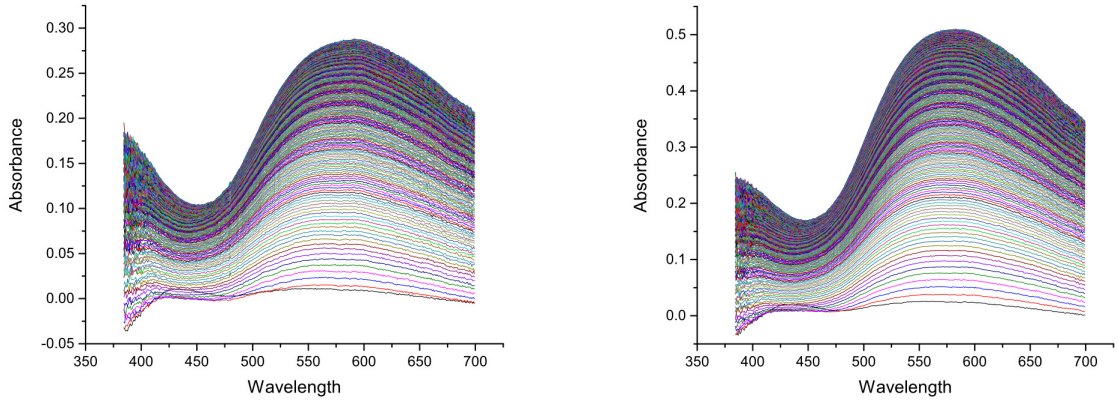

Figure 6-15. UV-Vis reaction of $Cu^{I}PF_6$ (0.32 mM, 8 mol%), DBED (0.63 mM, 15 mol%) and 3,5-DBP (0.15 mM (left), 0.45 mM (right)) in O_2-half-saturated DCM at −35°C. Formation of **SQ** (580 nm) and DBQ (400 nm) for 25 s.

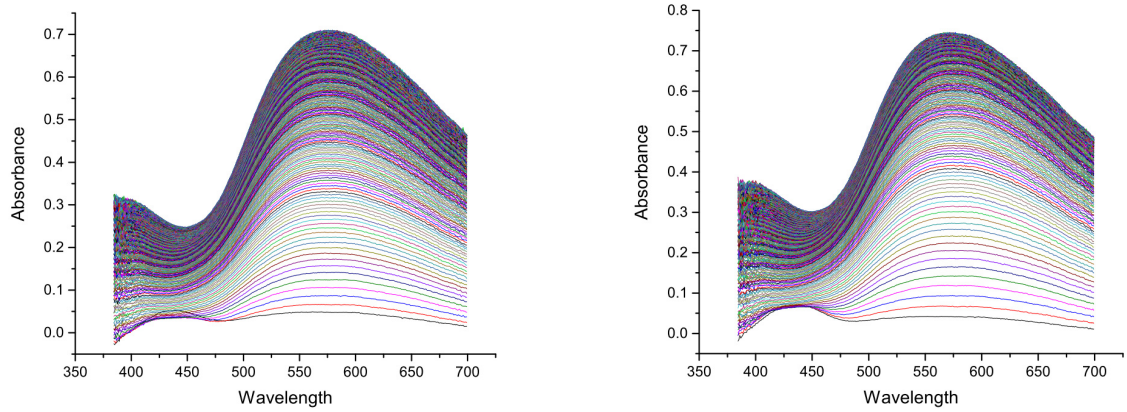

Figure 6-16. UV-Vis reaction of $Cu^{I}PF_6$ (0.32 mM, 8 mol%), DBED (0.63 mM, 15 mol%) and 3,5-DBP (1.11 mM (left), 2.23 mM (right)) in O_2-half-saturated DCM at −35°C. Formation of **SQ** (580 nm) and DBQ (400 nm) for 25 s.

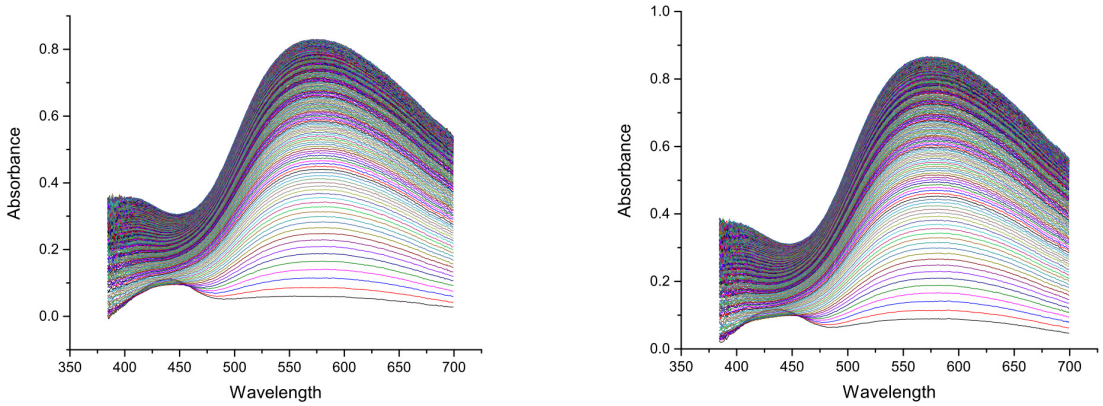

Figure 6-17. UV-Vis reaction of $Cu^{I}PF_6$ (0.32 mM, 8 mol%), DBED (0.63 mM, 15 mol%) and 3,5-DBP (2.97 mM (left), 3.71 mM (right)) in O_2-half-saturated DCM at −35°C. Formation of **SQ** (580 nm) and DBQ (400 nm) for 25 s.

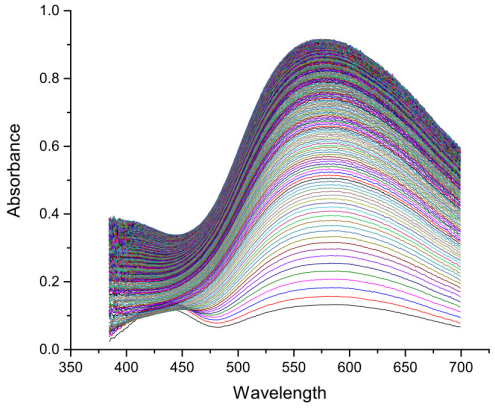

Figure 6-18. UV-Vis reaction of $Cu^{I}PF_6$ (0.32 mM, 8 mol%), DBED (0.63 mM, 15 mol%) and 3,5-DBP (7.43 mM) in O_2-half-saturated DCM at −35°C. Formation of **SQ** (580 nm) and DBQ (400 nm) for 25 s.

6.5.3 Substrate influence followed by Stopped-Flow Experiment at –80°C

Two stock solutions were prepared in the glovebox, one for the $Cu^{I}PF_6$-DBED (8:15%), and another one for 3,5-DBP (1.48 mmol, 148mM) in DCM. Seven sample solutions were prepared by mixed 500 µL of the $Cu^{I}PF_6$-DBED solution with 20, 60, 150, 300, 500 and 1000 µL of the 3,5-DBP stock solution to achieve the final concentration of [$Cu^{I}PF_6$] = 0.32 mM, [DBED] = 0.62mM, and [3,5-DBP] = 0.15, 0.44, 1.11, 2.22, 2.97, 3,70 and 7.40 mM. The sample solution was

transferred into a syringe and connected onto one end of the Y-junction. The other syringe contained O_2-saturated DCM. Spectra were collected every 50 ms for a total duration of 2.5 or 25 s, or every 0.5 s for a total duration of 250 s.

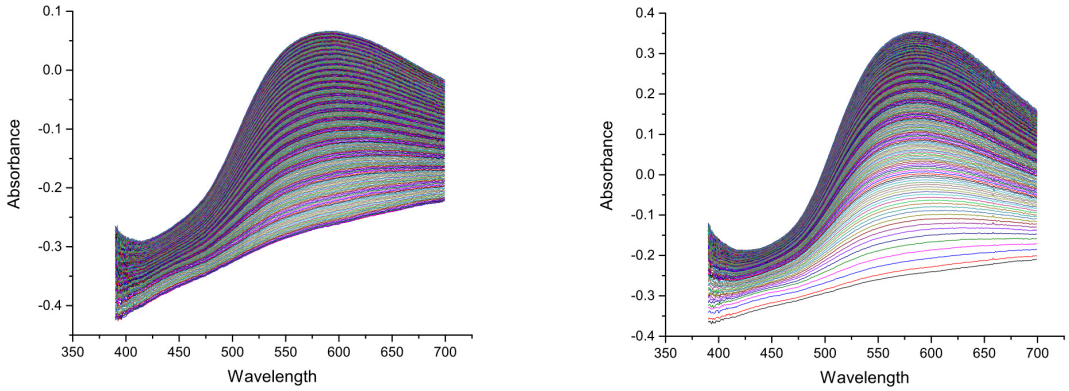

Figure 6-19. UV-Vis reaction of $Cu^{I}PF_6$ (0.32 mM, 8 mol%), DBED (0.63 mM, 15 mol%) and 3,5-DBP (0.15 mM) in O_2-half-saturated DCM at −80°C. Formation of **SQ** (580 nm) and **A** (~430 nm) for 25 s (left), and 250 s (right).

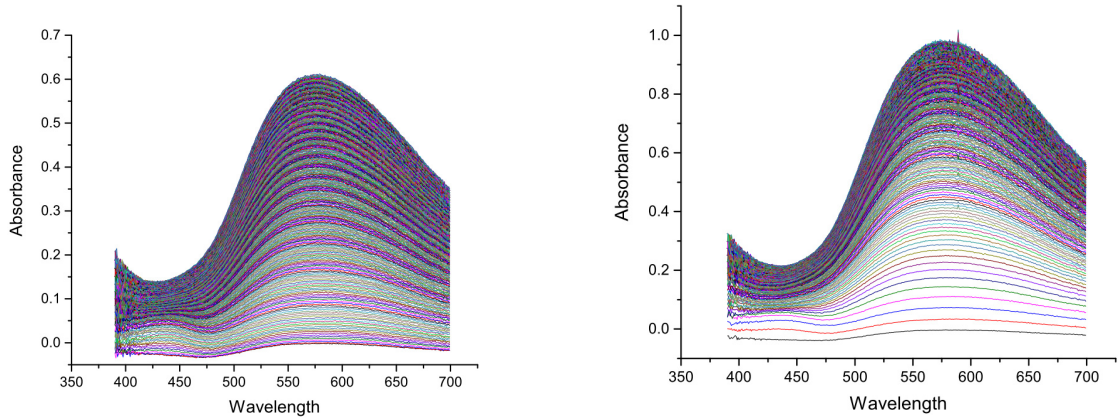

Figure 6-20. UV-Vis reaction of $Cu^{I}PF_6$ (0.32 mM, 8 mol%), DBED (0.63 mM, 15 mol%) and 3,5-DBP (0.44 mM) in O_2-half-saturated DCM at −80°C. Formation of **SQ** (580 nm) and **A** (~430 nm) for 25 s (left), and 250 s (right).

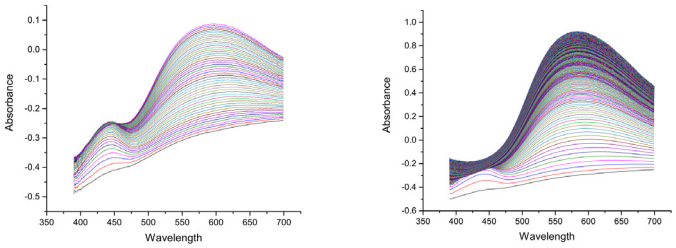

Figure 6-21. UV-Vis reaction of $Cu^{I}PF_6$ (0.32 mM, 8 mol%), DBED (0.63 mM, 15 mol%) and 3,5-DBP (1.11 mM) in O_2-half-saturated DCM at −80°C. Formation of **SQ** (580 nm) and **A** (~430 nm) for 5 s (left), 25 s (middle), and 250 s (right).

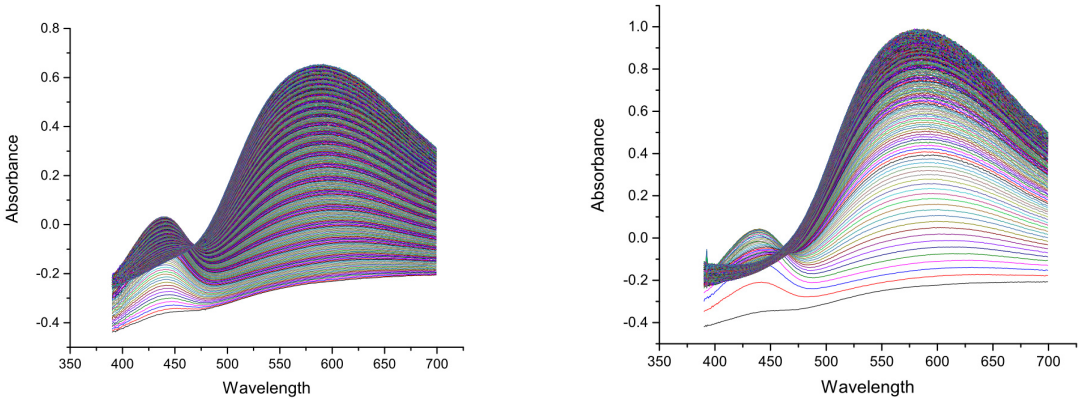

Figure 6-22. UV-Vis reaction of $Cu^{I}PF_6$ (0.32 mM, 8 mol%), DBED (0.63 mM, 15 mol%) and 3,5-DBP (2.22 mM) in O_2-half-saturated DCM at −80°C. Formation of **SQ** (580 nm) and **A** (~430 nm) for 25 s (left) and 250 s (right).

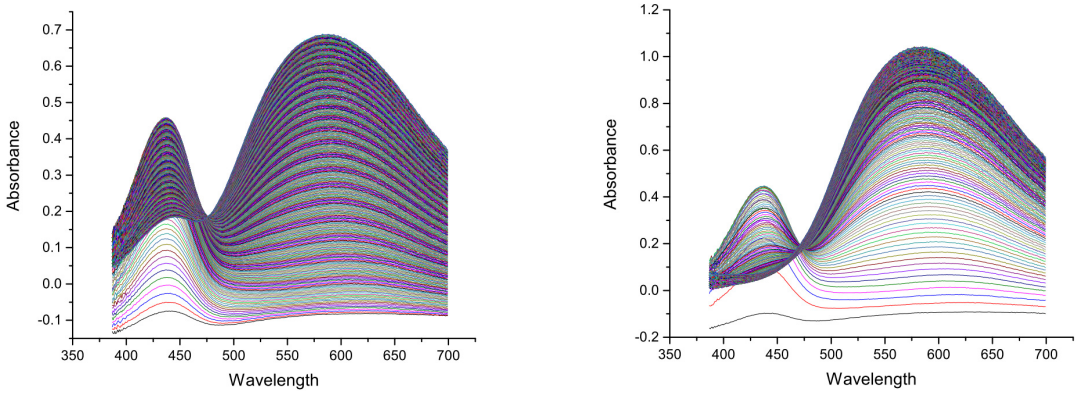

Figure 6-23. UV-Vis reaction of $Cu^{I}PF_6$ (0.32 mM, 8 mol%), DBED (0.63 mM, 15 mol%) and 3,5-DBP (3.70 mM) in O_2-half-saturated DCM at −80°C. Formation of **SQ** (580 nm) and **A** (~430 nm) for 25 s (left) and 250 s (right).

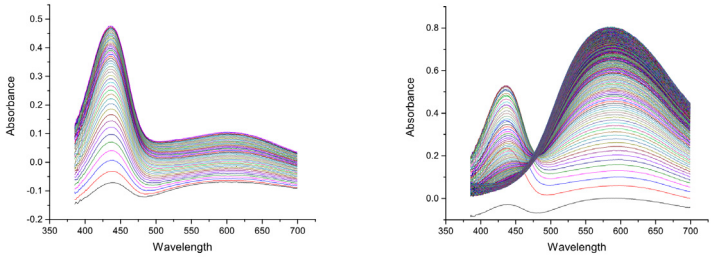

Figure 6-24. UV-Vis reaction of $Cu^{I}PF_6$ (0.32 mM, 8 mol%), DBED (0.63 mM, 15 mol%) and 3,5-DBP (7.4 mM) in O_2-half-saturated DCM at −80°C. Formation of **A** (~430 nm) and **SQ** (580 nm) for 2.5 s (left), 25 s (middle), and 250 s (right).

6.5.4 DBED influence followed by Stopped-Flow Experiment at –35°C

Two stock solutions were prepared in the glovebox, one for the $Cu^{I}PF_6$-DBED (8:8.1%) with 3,5-DBP (1.55mmol, 0.16M), and another one for DBED (0.13 mmol, 12.9mM) in DCM. Eight sample solutions were prepared by mixed 500 µL of the $Cu^{I}PF_6$-DBED solution with 20, 40, 100, 160, 270, 380, 960 and 2100 µL of the DBED stock solution to achieve the final concentration of [$Cu^{I}PF_6$] = 0.309 mM, [3,5-DBP] = 3.877 mM, and [DBED] = 0.36, 0.39, 0.48, 0.58, 0.75, 0.93, 1.86, and 3.68 mM (9.17, 9.99, 12.46, 14.93, 19.46, 23.98, 47.86 and 94.78 mol% respectively). The sample solution was transferred into a syringe and connected onto one end of the Y-

junction. The other syringe contained O_2-saturated DCM. Spectra were collected every 50 ms for a total duration of 25 s, or every 0.25 s for a total duration of 125 s.

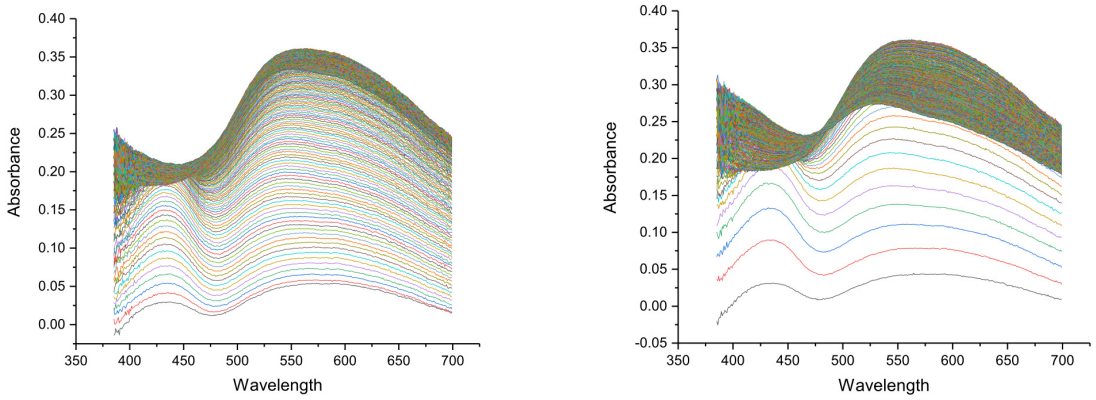

Figure 6-25. UV-Vis reaction of $Cu^{I}PF_6$ (0.31 mM, 8 mol%), DBED (0.36 mM, 9 mol%) and 3,5-DBP (3.88 mM) in O_2-half-saturated DCM at −35°C. Formation of **SQ** (580 nm) and **A** (~430 nm) for 25 s (left) and 125 s (right).

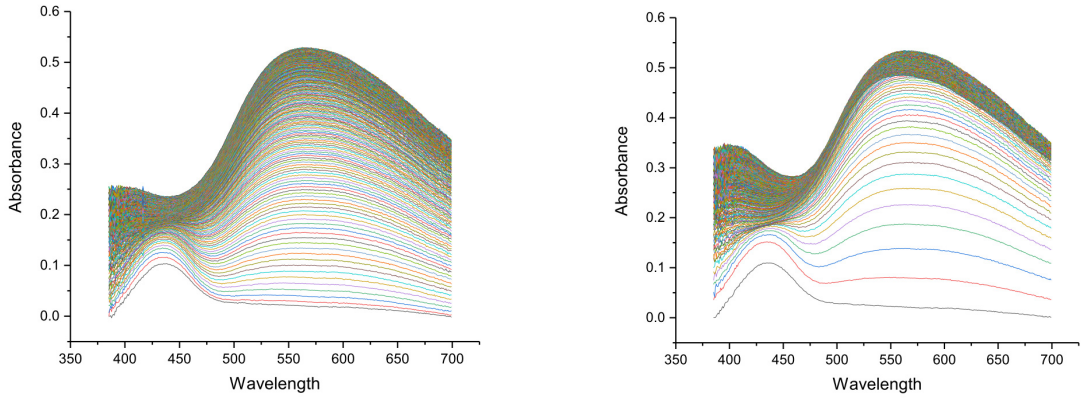

Figure 6-26. UV-Vis reaction of $Cu^{I}PF_6$ (0.31 mM, 8 mol%), DBED (0.39 mM, 10 mol%) and 3,5-DBP (3.88 mM) in O_2-half-saturated DCM at −35°C. Formation of **SQ** (580 nm) and **A** (~430 nm) for 25 s (left) and 125 s (right).

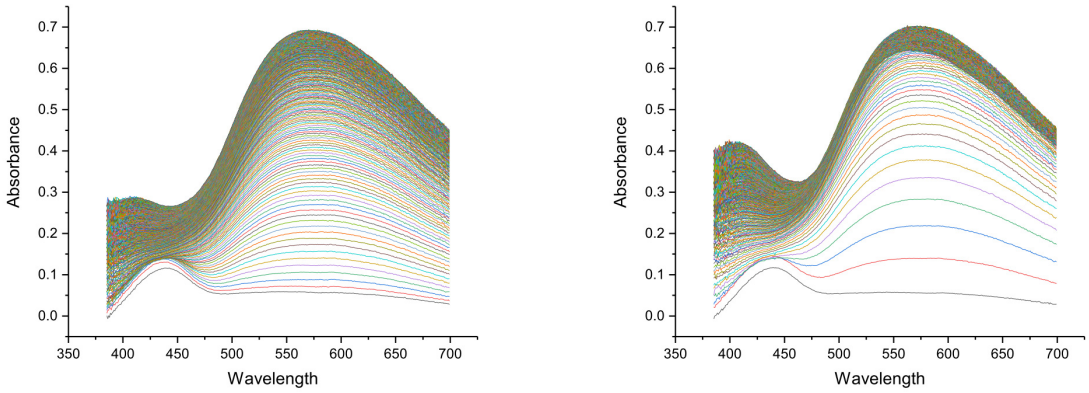

Figure 6-27. UV-Vis reaction of $Cu^{I}PF_6$ (0.31 mM, 8 mol%), DBED (0.47 mM, 15 mol%) and 3,5-DBP (3.88 mM) in O_2-half-saturated DCM at −35°C. Formation of **A** (~430 nm), **SQ** (580 nm) and DBQ (404 nm) for 25 s (left) and 125 s (right).

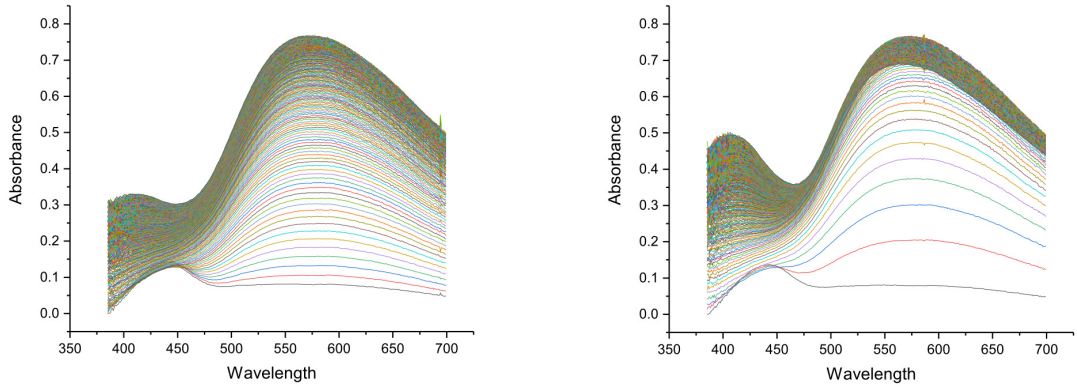

Figure 6-28. UV-Vis reaction of $Cu^{I}PF_6$ (0.31 mM, 8 mol%), DBED (0.59 mM, 15 mol%) and 3,5-DBP (3.88 mM) in O_2-half-saturated DCM at −35°C. Formation of **A** (~430 nm), **SQ** (580 nm) and DBQ (404 nm) for 25 s (left) and 125 s (right).

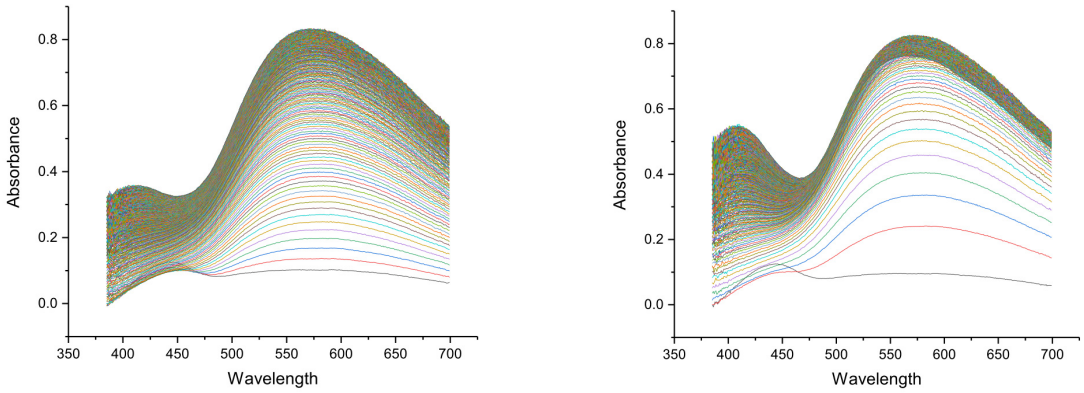

Figure 6-29. UV-Vis reaction of $Cu^{I}PF_6$ (0.31 mM, 8 mol%), DBED (0.79 mM, 20 mol%) and 3,5-DBP (3.88 mM) in O_2-half-saturated DCM at −35°C. Formation of **A** (~430 nm), **SQ** (580 nm) and DBQ (404 nm) for 25 s (left) and 125 s (right).

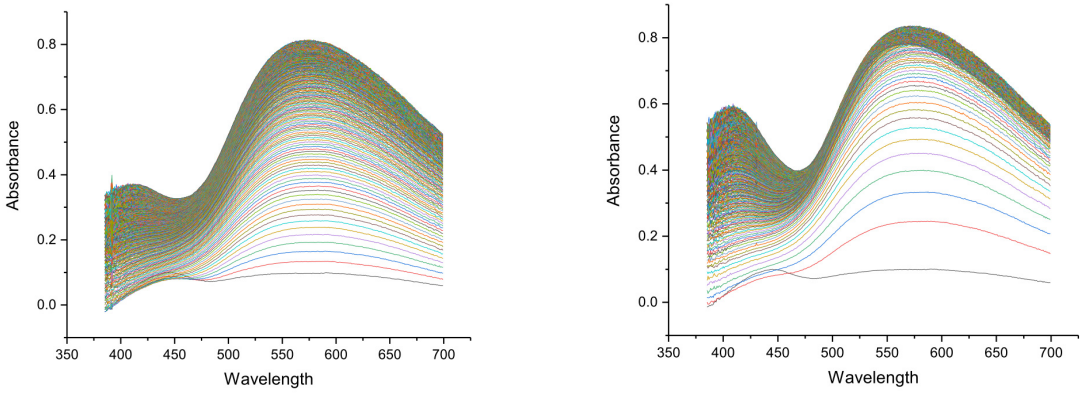

Figure 6-30. UV-Vis reaction of $Cu^{I}PF_6$ (0.31 mM, 8 mol%), DBED (0.97 mM, 25 mol%) and 3,5-DBP (3.88 mM) in O_2-half-saturated DCM at −35°C. Formation of **A** (~430 nm), **SQ** (580 nm) and DBQ (404 nm) for 25 s (left) and 125 s (right).

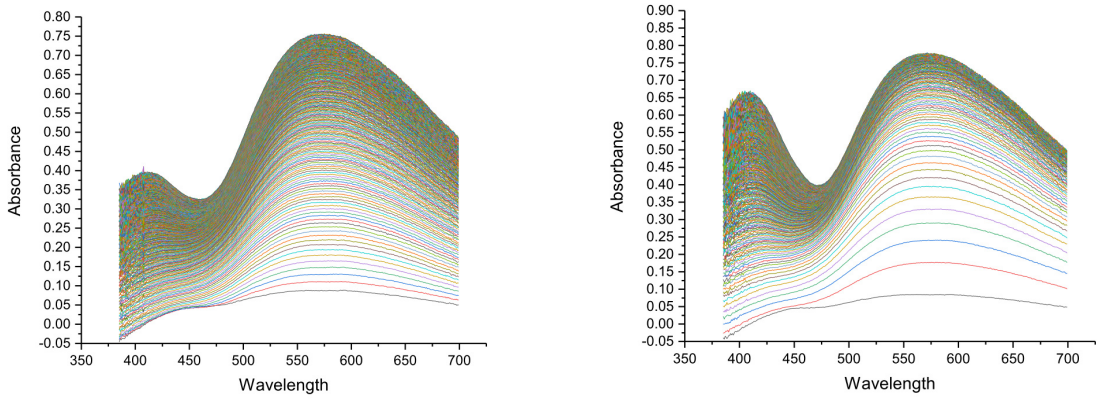

Figure 6-31. UV-Vis reaction of $Cu^{I}PF_6$ (0.31 mM, 8 mol%), DBED (1.92 mM, 50 mol%) and 3,5-DBP (3.88 mM) in O_2-half-saturated DCM at −35°C. Formation of **A** (~430 nm), **SQ** (580 nm) and DBQ (404 nm) for 25 s (left) and 125 s (right).

100% 25s [DBED]=3.89mM

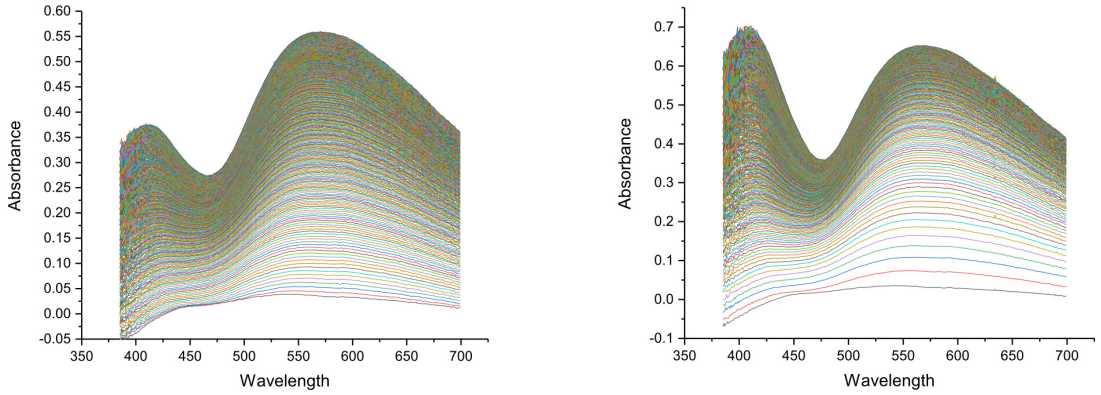

Figure 6-32. UV-Vis reaction of $Cu^{I}PF_6$ (0.31 mM, 8 mol%), DBED (3.89 mM, 100 mol%) and 3,5-DBP (3.88 mM) in O_2-half-saturated DCM at −35°C. Formation of **A** (~430 nm), **SQ** (580 nm) and DBQ (404 nm) for 25 s (left) and 125 s (right).

6.5.5 DBED influence followed by Stopped-Flow Experiment at –80°C

Two stock solutions were prepared in the glovebox, one for the $Cu^{I}PF_6$-DBED (8:8.1%) with 3,5-DBP (1.00mmol, 0.10M), and another one for DBED (0.18 mmol, 17.6 mM) in DCM. Six sample

solutions prepared by mixed 400 µL of the $Cu^{I}PF_6$-DBED solution with 10, 40, 150, 380, 960 and 2100 µL of the DBED stock solution to achieve the final concentration of [$Cu^{I}PF_6$] = 0.174 mM, [3,5-DBP] = 2.002 mM, and [DBED] = 0.18, 0.21, 0.31, 0.51, 1.02 and 2.03 mM (9.08, 10.4, 15.3, 25.4, 51.0 and 101 mol% respectively). The sample solution was transferred into a syringe and connected onto one end of the Y-junction. The other syringe contained O_2-saturated DCM. Spectra were collected every 50 ms for a total duration of 25 s, or every 0.5 s for a total duration of 250 s.

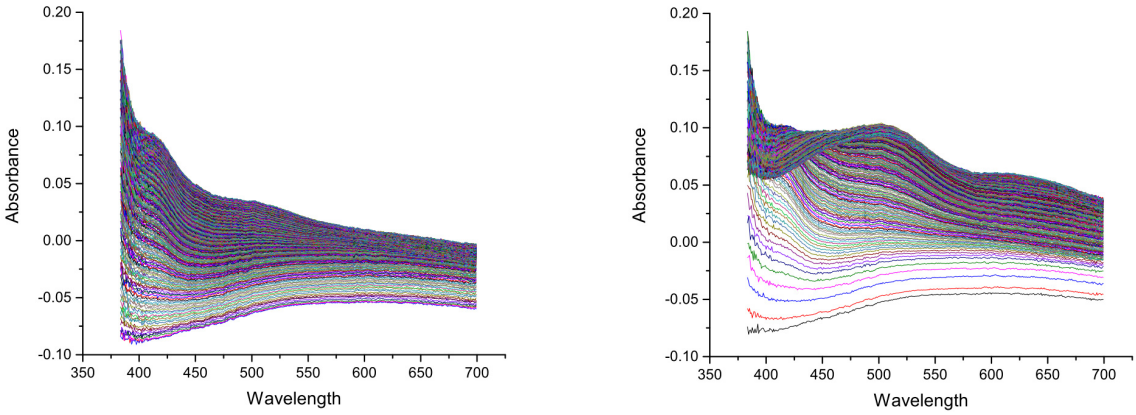

Figure 6-33. UV-Vis reaction of $Cu^{I}PF_6$ (0.17 mM, 8 mol%), DBED (0.18 mM, 9 mol%) and 3,5-DBP (2.00 mM) in O_2-half-saturated DCM at −80°C. Formation of **SQ** (580 nm) and DBQ (404 nm) for 25s (left) and 250s (right).

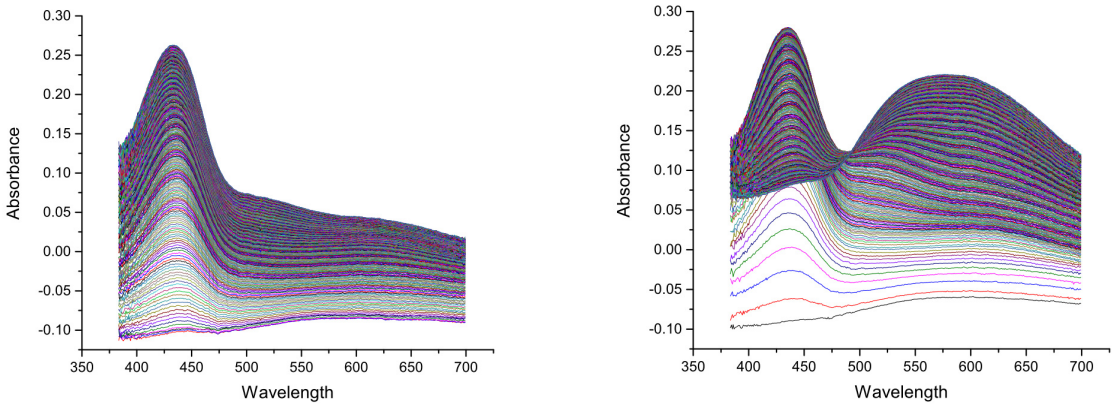

Figure 6-34. UV-Vis reaction of $Cu^{I}PF_6$ (0.17 mM, 8 mol%), DBED (0.21 mM, 10 mol%) and 3,5-DBP (2.00 mM) in O_2-half-saturated DCM at −80°C. Formation of **A** (~430 nm), **SQ** (580 nm) and DBQ (404 nm) for 25 s (left) and 250 s (right).

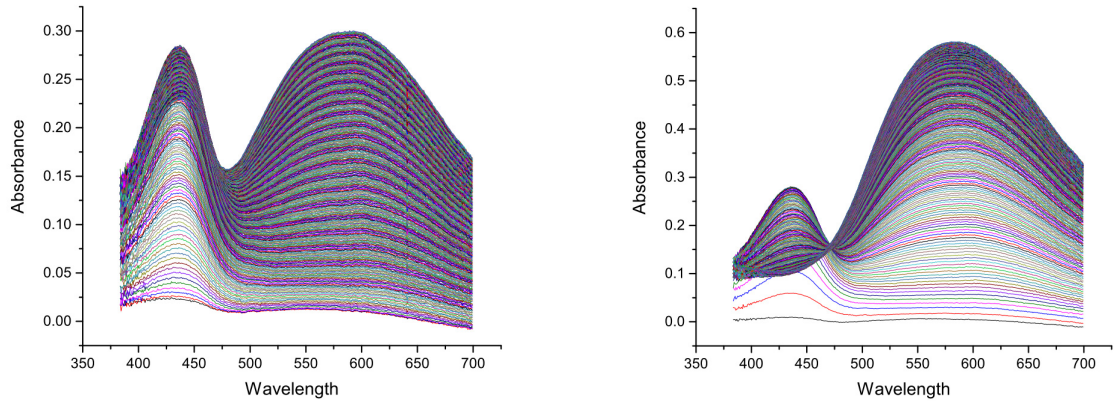

Figure 6-35. UV-Vis reaction of $Cu^{I}PF_6$ (0.17 mM, 8 mol%), DBED (0.31 mM, 15 mol%) and 3,5-DBP (2.00 mM) in O_2-half-saturated DCM at −80°C. Formation of **A** (~430 nm), **SQ** (580 nm) and DBQ (404 nm) for 25 s (left) and 250 s (right).

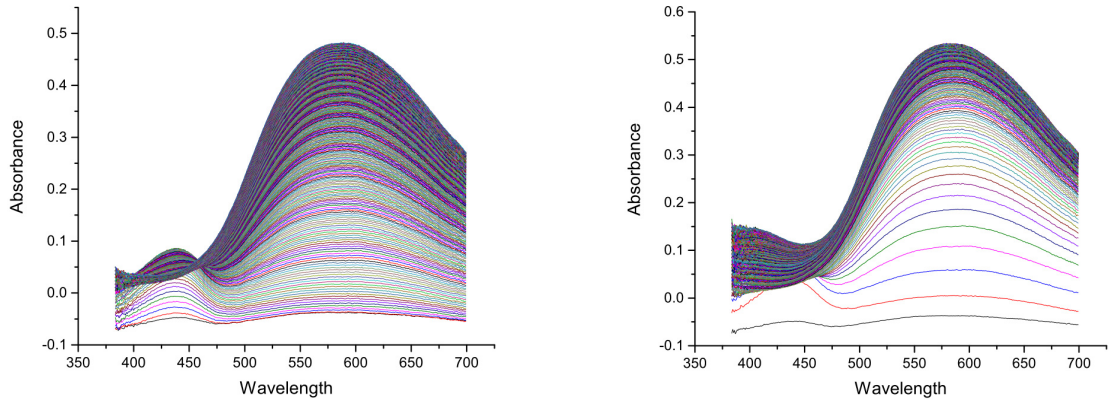

Figure 6-36. UV-Vis reaction of $Cu^{I}PF_6$ (0.17 mM, 8 mol%), DBED (0.51 mM, 25 mol%) and 3,5-DBP (2.00 mM) in O_2-half-saturated DCM at −80°C. Formation of **A** (~430 nm), **SQ** (580 nm) and DBQ (404 nm) for 25 s (left) and 250 s (right).

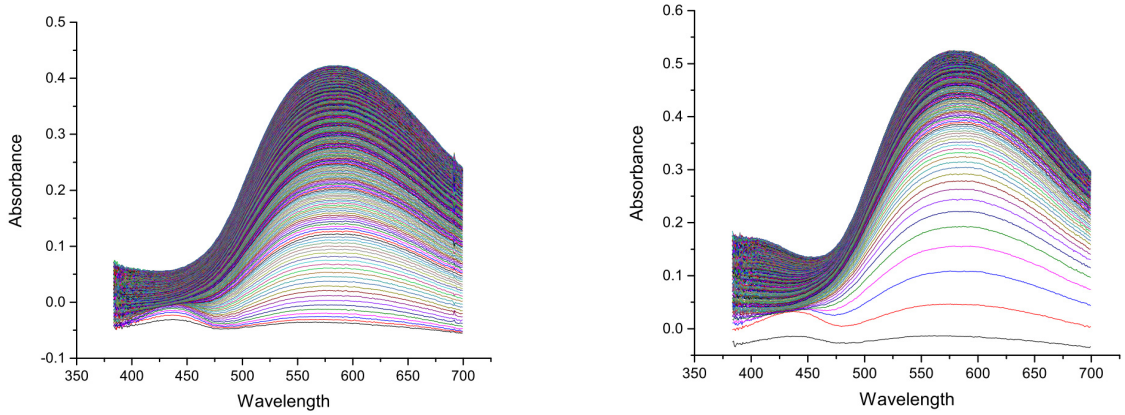

Figure 6-37. UV-Vis reaction of $Cu^{I}PF_6$ (0.17 mM, 8 mol%), DBED (1.02 mM, 50 mol%) and 3,5-DBP (2.00 mM) in O_2-half-saturated DCM at −80°C. Formation of **A** (~430 nm), **SQ** (580 nm) and DBQ (404 nm) for 25 s (left) and 250 s (right).

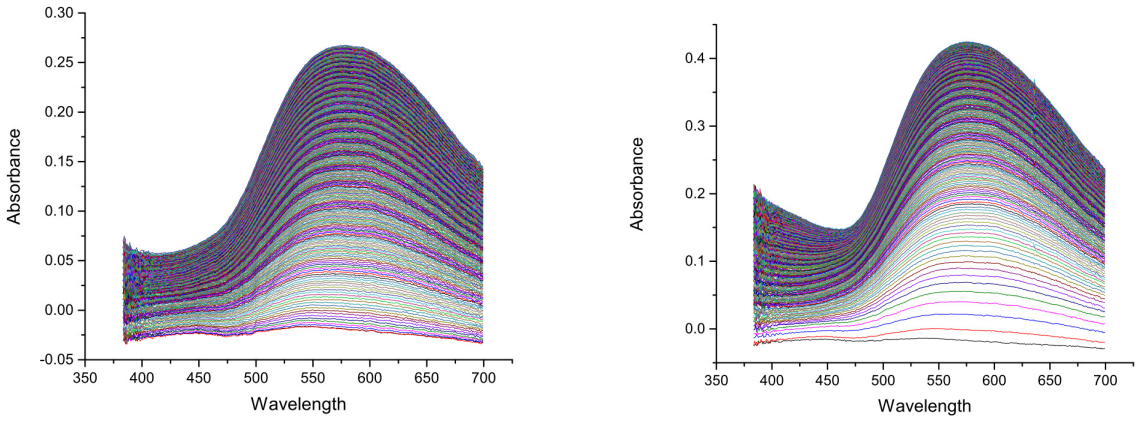

Figure 6-38. UV-Vis reaction of $Cu^{I}PF_6$ (0.17 mM, 8 mol%), DBED (2.03 mM, 100 mol%) and 3,5-DBP (2.00 mM) in O_2-half-saturated DCM at −80°C. Formation of **A** (~430 nm), **SQ** (580 nm) and DBQ (404 nm) for 25 s (left) and 250 s (right).

6.6 Kinetic Isotope Effect

6.6.1 Synthesis

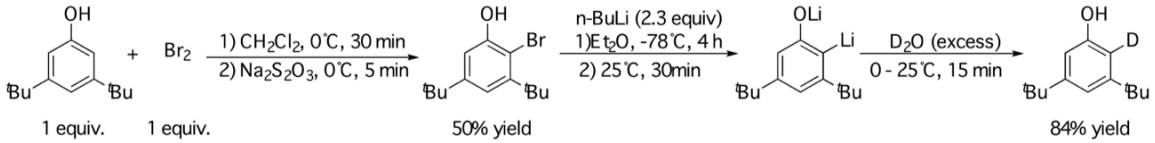

Scheme 6-2. Synthesis of 2-deuterio-3,5-di-*tert*-butylphenol.

2-bromo-3,5-di-*tert*-butylphenol.[65,66] In a 250 mL single-necked round-bottom flask equipped with magnetic stir bar, 3,5-di-*tert*-butylphenol (2.070 g, 10.06 mmol) was dissolved in 50 mL of dichloromethane (DCM). The reaction flask was cooled in an ice-water bath to 0°C, then of Br_2 (0.510 mL, 10.06 mmol) dissolved in 5 mL of DCM was added dropwise over 30 minutes. After 30 minutes of additional stirring, 100 mL of N/10 $Na_2S_2O_3$ was added. After an additional 5 minutes of stirring, the filtrate was passed through a Celite bed, which was washed with an additional 10 mL of DCM. The filtrate was washed with 50 mL of N/10 $Na_2S_2O_3$ and the organic layer (DCM) was collected, dried over Na_2SO_4 and the solvent evaporated under reduced pressure. The dried product was stored under nitrogen and then further separated in a flash

column (2 column volumes (CVs) at 100% hexanes; 2 CVs at 0.5% EtOAc in hexanes; 2 CVs at 1% EtOAc in hexanes; 2 CVs at 1.5% EtOAc in hexanes ; 10 CVs at 2% EtOAc in hexanes). The pure fractions (by TLC) were combined, concentrated under reduced pressure and an ^{1}HNMR spectrum was collected to access purity. ^{1}H-NMR (300 MHz, $CDCl_3$): δ 7.05(d,1H), 6.99 (d,1H), 5.94 (s,1H), 1.53 (s,9H), 1.31 (s,9H) ppm.

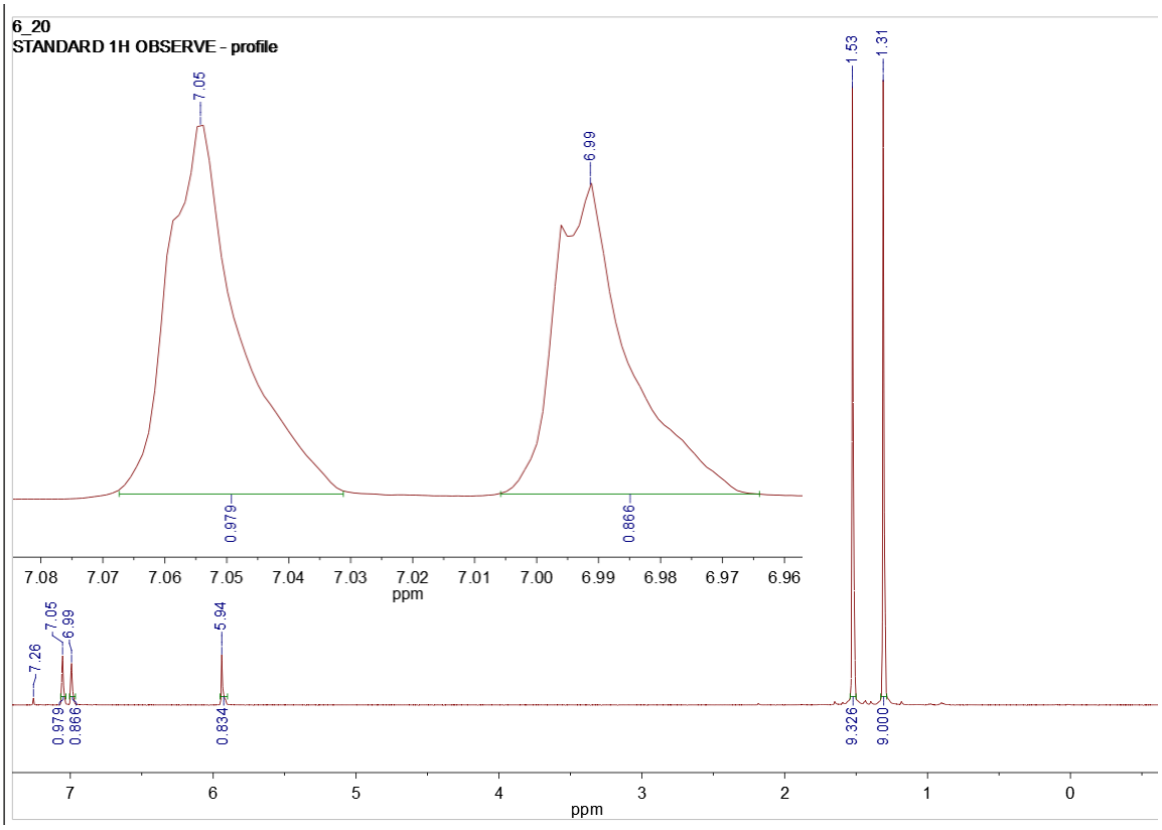

Figure 6-39. ^{1}H-NMR spectrum of 2-bromo-3,5-di-*tert*-butylphenol.

2-deuterio-3,5-di-*tert*-butylphenol. In the glovebox, the 1439.6 mg of purified 2-bromo-3,5-ditertbutylphenol (5.047 mmol) were added to an oven dried 200 mL Schlenk flask equipped with a Teflon-coated magnetic stir bar. 60 mL of dry diethyl ether was added. The flask was capped, transported out of the glovebox and connected to a Schlenk line. The line and flask were purged with a vacuum and then kept under nitrogen gas. This was done an additional three times. While the flask was cooled to –78°C in an acetone-dry ice bath, a bottle of *n*-BuLi

under nitrogen was titrated with *N*-benzylbenzamide to determine exact concentration (2.3 M). With the use of an oven-dried cannula, 2.3 equiv. of *n*-BuLi were added slowly. The reaction mixture was stirred under nitrogen for 4 hours. The mixture was warmed to room temperature and mixed for an additional 30 minutes. The flask was then cooled to 0°C in an ice-water bath when a large excess (2.5 mL) of D_2O was slowly added over 5 minutes, forming a white precipitate. The reaction mixture was then stirred for an additional 10 minutes at room temperature. Work-up: the pH of the mixture was made acidic by the addition of 10 M HCl. The aqueous layer was extracted from ether three separate times. The organic layer was collected. Fresh diethyl ether was added to the aqueous layer and the aqueous layer was separated for three additional times. The organic layer was combined with the previously isolated organic layer. The fractions were dried over $MgSO_4$ and concentrated under reduced pressure. The coloured crystals were recrystallized three times in hexanes, yielding the following ^{1}H-NMR spectrum. ^{1}H-NMR (500 MHz, $CDCl_3$): δ 6.99 (d,1H), 6.69 (d,1H), 4.70 (s,1H), 1.30 (s,18H) ppm.

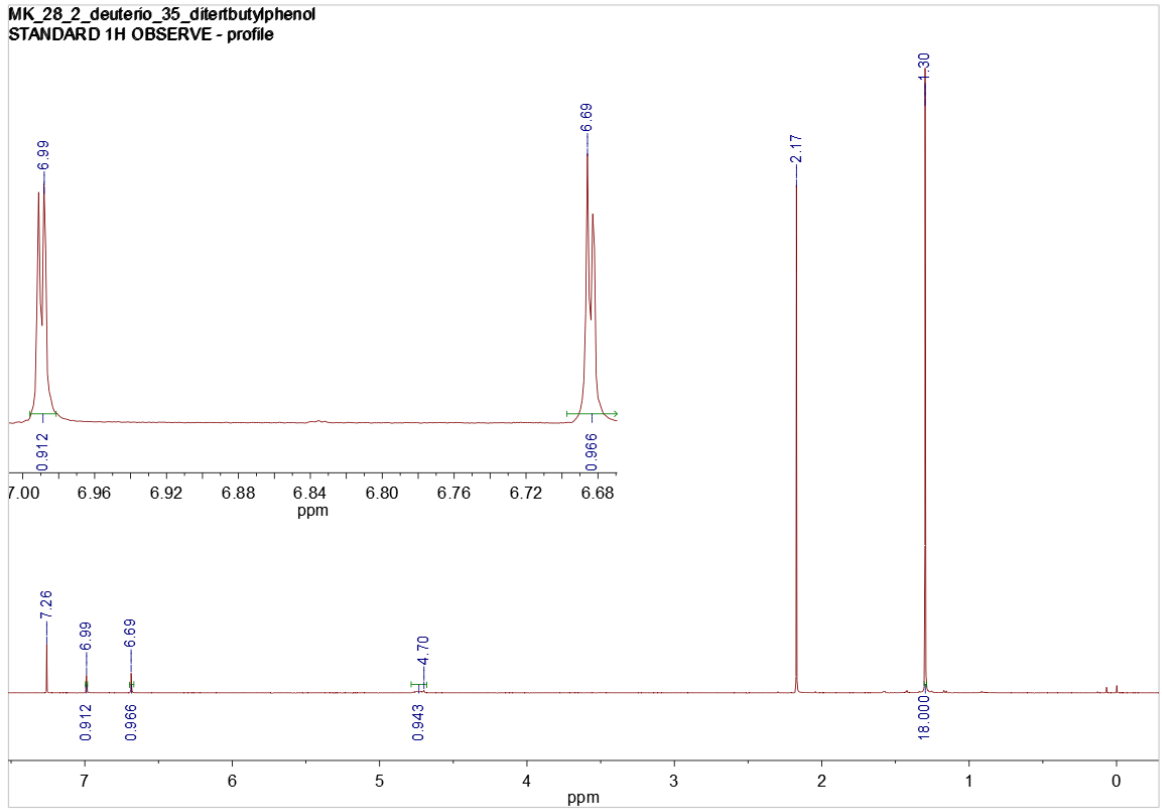

Figure 6-40. ^{1}H-NMR spectrum of 2-deuterio-3,5-di-*tert*-butylphenol.

6.6.2 Reaction of 2-deuterium-3,5-di-*tert*-butylphenol

In the glovebox, a solution of DBED (8.1 mg, 0.047 mmol, 18 mol%) and $Cu^{I}PF_6$ (7.7 mg , 0.021 mmol, 8 mol%) in 1 mL of DCM was prepared in a 20 mL vial. In an oven-dried Radley tube was added first 2-deuterium-3,5-di-*tert*-butylphenol (55.5 mg, 0.268 mmol) then the DBED/$Cu^{I}PF_6$ solution. The vial content was washed with 2 mL of DCM and added into the Radley tube. This was repeated to afford a final phenol concentration of 0.05 M. The tube was capped, transported out of the glovebox and connected to the oxygen tank. The line was purged several times and the solution was spun at room temperature for 5 hours. A colour change from pink to green was observed. Work-up was performed by adding 4 mL of a sodium bisulfate solution (10% by weight). The organic layer was extracted, dried over $MgSO_4$, and concentrated under

reduced pressure. To assess the amount of quinone produced, 4.0 mg of an internal standard, hexamethylbenzene, was added, yielding the following ^{1}H-NMR spectrum on Figure 6-41.

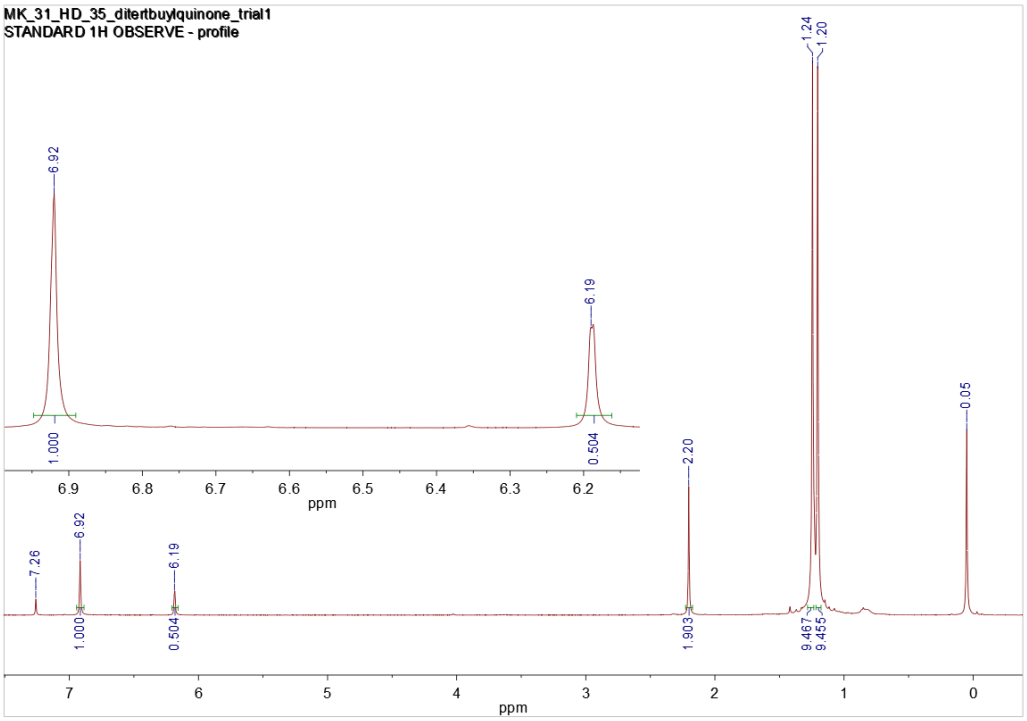

Figure 6-41. ^{1}H-NMR spectrum (500 MHz, $CDCl_3$) of the mixture of ^{H}DBQ and ^{D}DBQ obtained after reaction of 2-deuterium-3,5-di-*tert*-butylphenol. δ 6.92 (s,1H), 6.19 (d,H/D),1.24 (s,9H), 1.20 (s,9H) ppm.

6.6.3 Determination of the KIE

The ^{H}DBQ/^{D}DBQ mixture was analyzed in HPLC-grade methanol by mass spectrometry on the electrospray ionization chamber of the Q-TOF instrument at CBAMS, using the $[DBQNa]^{+}$ peaks at m/z 243.15 and 244.16, respectively. An examples of KIE calculation is provided in (Figure 6-42). The experiments were carried out five independent times, including using different sources or deuterated phenol. The 244.16 peak heights were corrected from the +1 component for $[^{H}DBQNa]^{+}$ (^{13}C contributions, as well as a small amount of reduction/protonation ion, determined on pure DBQ samples beforehand). The ratio of the corrected peaks yielded the ^{H}DBQ/^{D}DBQ ratio obtained. The purity (deuterium incorporation) of the initial phenol was also taken in consideration, since the non-deuterated phenol only yields ^{H}DBQ. The KIE corresponds

to products only stemming from the deuterated phenol, and was calculated according to formula:

$$KIE = \frac{1}{Purity\left(\frac{^{H}DBQ}{^{D}DBQ} + 1\right) - 1}$$

Equation 6-1. Calculation equation of kinetic isotope effect.

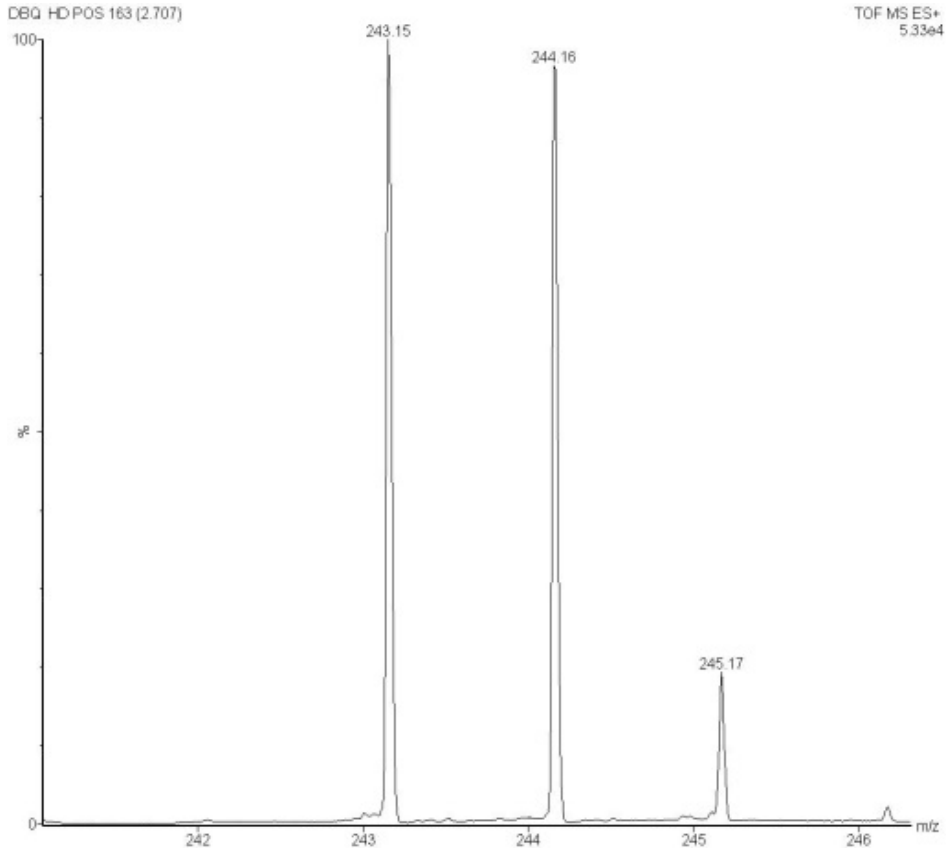

Figure 6-42. ESI-MS of the crude $^{H/D}$DBQ mixture at positive mode in HPLC-grade methanol ($[DBQNa]^+$ region). KIE calculation for this example was done as follows:

Peak Location:	243.15	244.16	245.17
Peak Intensity:	76860	73990	14890
Corrected 244.16 intensity:		56618	
Deuterium Incorporation (purity):	95.13%		

D-phenol to ^{D}DBQ = 44.59%, D-phenol to ^{H}DBQ = 55.41%

KIE = 0.8047

Chapter 7: References

1. Sugumaran, M., Comparative biochemistry of eumelanogenesis and the protective roles of phenoloxidase and melanin in insects. *Pigment Cell Res* **2002,** *15* (1), 2-9.

2. Solomon, E. I.; Heppner, D. E.; Johnston, E. M.; Ginsbach, J. W.; Cirera, J.; Qayyum, M.; Kieber-Emmons, M. T.; Kjaergaard, C. H.; Hadt, R. G.; Tian, L., Copper Active Sites in Biology. *Chem. Rev.* **2014,** *114* (7), 3659-3853.

3. Micillo, R.; Panzella, L.; Koike, K.; Monfrecola, G.; Napolitano, A.; d'Ischia, M., "Fifty Shades" of Black and Red or How Carboxyl Groups Fine Tune Eumelanin and Pheomelanin Properties. *International Journal of Molecular Sciences* **2016,** *17* (5).

4. Shosuke, I., A Chemist's View of Melanogenesis. *Pigment Cell Research* **2003,** *16* (3), 230-236.

5. Sugumaran, M., Reactivities of Quinone Methides versus o-Quinones in Catecholamine Metabolism and Eumelanin Biosynthesis. *International Journal of Molecular Sciences* **2016,** *17* (9), 1576.

6. Allen, S. E.; Walvoord, R. R.; Padilla-Salinas, R.; Kozlowski, M. C., Aerobic Copper-Catalyzed Organic Reactions. *Chem. Rev.* **2013,** *113* (8), 6234-6458.

7. Solomon, E. I.; Ginsbach, J. W.; Heppner, D. E.; Kieber-Emmons, M. T.; Kjaergaard, C. H.; Smeets, P. J.; Tian, L.; Woertink, J. S., Copper dioxygen (bio)inorganic chemistry. *Faraday Discuss.* **2011,** *148* (0), 11-39.

8. Hoffmann, A.; Citek, C.; Binder, S.; Goos, A.; Rübhausen, M.; Troeppner, O.; Ivanović-Burmazović, I.; Wasinger, E. C.; Stack, T. D. P.; Herres-Pawlis, S., Catalytic Phenol Hydroxylation with Dioxygen: Extension of the Tyrosinase Mechanism beyond the Protein Matrix. *Angew. Chem., Int. Ed.* **2013,** *52* (20), 5398-5401.

9. Matoba, Y.; Kumagai, T.; Yamamoto, A.; Yoshitsu, H.; Sugiyama, M., Crystallographic Evidence That the Dinuclear Copper Center of Tyrosinase Is Flexible during Catalysis. *J. Biol. Chem.* **2006,** *281* (13), 8981-8990.

10. Mirica, L. M.; Ottenwaelder, X.; Stack, T. D. P., Structure and Spectroscopy of Copper−Dioxygen Complexes. *Chem. Rev.* **2004,** *104* (2), 1013-1046.

11. Cahoy, J.; Holland, P. L.; Tolman, W. B., Experimental Studies of the Interconversion of μ-η2:η2-Peroxo- and Bis(μ-oxo)dicopper Complexes. *Inorg. Chem.* **1999,** *38* (9), 2161-2168.

12. Henson, M. J.; Mukherjee, P.; Root, D. E.; Stack, T. D. P.; Solomon, E. I., Spectroscopic and Electronic Structural Studies of the Cu(III)2 Bis-μ-oxo Core and Its Relation to the Side-On Peroxo-Bridged Dimer. *J. Am. Chem. Soc.* **1999,** *121* (44), 10332-10345.

13. Citek, C.; Lyons, C. T.; Wasinger, E. C.; Stack, T. D. P., Self-assembly of the oxy-tyrosinase core and the fundamental components of phenolic hydroxylation. *Nat. Chem.* **2012,** *4* (4), 317-322.

14. Hay, A. S.; Blanchard, H. S.; Endres, G. F.; Eustance, J. W., Polymerization by oxidative coupling. *J. Am. Chem. Soc.* **1959,** *81* (23), 6335-6336.

15. Rolff, M.; Schottenheim, J.; Decker, H.; Tuczek, F., Copper-O2 reactivity of tyrosinase models towards external monophenolic substrates: molecular mechanism and comparison with the enzyme. *Chem. Soc. Rev.* **2011,** *40* (7), 4077-4098.

16. Elwell, C. E.; Gagnon, N. L.; Neisen, B. D.; Dhar, D.; Spaeth, A. D.; Yee, G. M.; Tolman, W. B., Copper–Oxygen Complexes Revisited: Structures, Spectroscopy, and Reactivity. *Chem. Rev.* **2017,** *117* (3), 2059-2107.

17. Würtele, C.; Gaoutchenova, E.; Harms, K.; Holthausen, M. C.; Sundermeyer, J.; Schindler, S., Crystallographic Characterization of a Synthetic 1:1 End-On Copper Dioxygen Adduct Complex. *Angew. Chem., Int. Ed.* **2006,** *45* (23), 3867-3869.

18. Fujisawa, K.; Tanaka, M.; Moro-oka, Y.; Kitajima, N., A Monomeric Side-On Superoxocopper(II) Complex: Cu(O2)(HB(3-tBu-5-iPrpz)3). *J. Am. Chem. Soc.* **1994,** *116* (26), 12079-12080.

19. Kitajima, N.; Fujisawa, K.; Morooka, Y.; Toriumi, K., .mu.-.eta.2:.eta.2-Peroxo binuclear copper complex, [Cu(HB(3,5-(Me2CH)2pz)3)]2(O2). *J. Am. Chem. Soc.* **1989,** *111* (24), 8975-8976.

20. Kitajima, N.; Koda, T.; Iwata, Y.; Morooka, Y., Reaction aspects of a .mu.-peroxo binuclear copper(II) complex. *J. Am. Chem. Soc.* **1990,** *112* (24), 8833-8839.

21. Solomon, E. I.; Tuczek, F.; Root, D. E.; Brown, C. A., Spectroscopy of Binuclear Dioxygen Complexes. *Chem. Rev.* **1994,** *94* (3), 827-856.

22. Stack, T. D. P., Complexity with simplicity: a steric continuum of chelating diamines with copper(i) and dioxygen. *Dalton Trans.* **2003,** (10), 1881-1889.

23. Halfen, J. A.; Mahapatra, S.; Wilkinson, E. C.; Kaderli, S.; Young, V. G., Jr.; Que, L., Jr.; Zuberbuhler, A. D.; Tolman, W. B., Reversible cleavage and formation of the dioxygen O-O bond within a dicopper complex. *Science* **1996,** *271* (5254), 1397-400.

24. Mahadevan, V.; Henson, M. J.; Solomon, E. I.; Stack, T. D. P., Differential Reactivity between Interconvertible Side-On Peroxo and Bis-μ-oxodicopper Isomers Using Peralkylated Diamine Ligands. *J. Am. Chem. Soc.* **2000,** *122* (41), 10249-10250.

25. Garcia-Bosch, I.; Cowley, R. E.; Díaz, D. E.; Peterson, R. L.; Solomon, E. I.; Karlin, K. D., Substrate and Lewis Acid Coordination Promote O–O Bond Cleavage of an Unreactive L2CuII2(O22–) Species to Form L2CuIII2(O)2 Cores with Enhanced Oxidative Reactivity. *J. Am. Chem. Soc.* **2017,** *139* (8), 3186-3195.

26. Ottenwaelder, X.; Rudd, D. J.; Corbett, M. C.; Hodgson, K. O.; Hedman, B.; Stack, T. D. P., Reversible O−O Bond Cleavage in Copper−Dioxygen Isomers: Impact of Anion Basicity. *J. Am. Chem. Soc.* **2006,** *128* (29), 9268-9269.

27. Storr, T.; Verma, P.; Pratt, R. C.; Wasinger, E. C.; Shimazaki, Y.; Stack, T. D. P., Defining the Electronic and Geometric Structure of One-Electron Oxidized Copper−Bis-phenoxide Complexes. *J. Am. Chem. Soc.* **2008,** *130* (46), 15448-15459.

28. Citek, C.; Gary, J. B.; Wasinger, E. C.; Stack, T. D. P., Chemical Plausibility of Cu(III) with Biological Ligation in pMMO. *J. Am. Chem. Soc.* **2015,** *137* (22), 6991-6994.

29. Gary, J. B.; Citek, C.; Brown, T. A.; Zare, R. N.; Wasinger, E. C.; Stack, T. D. P., Direct Copper(III) Formation from O2 and Copper(I) with Histamine Ligation. *J. Am. Chem. Soc.* **2016,** *138* (31), 9986-9995.

30. Keown, W.; Gary, J. B.; Stack, T. D. P., High-valent copper in biomimetic and biological oxidations. *J. Biol. Inorg. Chem.* **2017,** *22* (2), 289-305.

31. Osako, T.; Ohkubo, K.; Taki, M.; Tachi, Y.; Fukuzumi, S.; Itoh, S., Oxidation Mechanism of Phenols by Dicopper−Dioxygen (Cu2/O2) Complexes. *J. Am. Chem. Soc.* **2003,** *125* (36), 11027-11033.

32. Emil, R.; Wolfgang, K.; Biprajit, S.; B., U. V.; Jürgen, P.; Roger, G.; Wolf-Dietrich, E.; A., S. G.; Uwe, B.; Elias, K.; Christian, L.; Hartmut, H.; Shih-Fan, H.; Bernd, P.; Sabine, L., Selective Catalytic Oxidation of C-H Bonds with Molecular Oxygen. *ChemCatChem* **2013,** *5* (1), 82-112.

33. Askari, M. S.; Esguerra, K. V. N.; Lumb, J.-P.; Ottenwaelder, X., A Biomimetic Mechanism for the Copper-Catalyzed Aerobic Oxygenation of 4-tert-Butylphenol. *Inorg. Chem.* **2015,** *54* (17), 8665-8672.

34. Rolff, M.; Schottenheim, J.; Peters, G.; Tuczek, F., The First Catalytic Tyrosinase Model System Based on a Mononuclear Copper(I) Complex: Kinetics and Mechanism. *Angew. Chem., Int. Ed.* **2010,** *49* (36), 6438-6442.

35. Réglier, M.; Jorand, C.; Waegell, B., Binuclear copper complex model of tyrosinase. *Chem. Commun.* **1990,** (24), 1752-1755.

36. Casella, L.; Gullotti, M.; Radaelli, R.; Di Gennaro, P., A tyrosinase model system. Phenol ortho-hydroxylation by a binuclear three-coordinate copper(I) complex and dioxygen. *Chem. Commun.* **1991,** (22), 1611-1612.

37. Schottenheim, J.; Fateeva, N.; Thimm, W.; Krahmer, J.; Tuczek, F., Catalytic Conversion of Monophenols to Ortho-Quinones in a Tyrosinase-Like Fashion: Towards More Biomimetic and More Efficient Model Systems. *Zeitschrift für anorganische und allgemeine Chemie* **2013,** *639* (8‐9), 1491-1497.

38. Wilfer, C.; Liebhäuser, P.; Erdmann, H.; Hoffmann, A.; Herres-Pawlis, S., Biomimetic Hydroxylation Catalysis Through Self-Assembly of a Bis(pyrazolyl)methane Copper–Peroxo Complex. *Eur. J. Inorg. Chem.* **2015,** *2015* (3), 494-502.

39. Santagostini, L.; Gullotti, M.; Monzani, E.; Casella, L.; Dillinger, R.; Tuczek, F., Reversible Dioxygen Binding and Phenol Oxygenation in a Tyrosinase Model System. *Chem.--Eur. J.* **2000,** *6* (3), 519-522.

40. Sanyal, I.; Mahroof-Tahir, M.; Nasir, M. S.; Ghosh, P.; Cohen, B. I.; Gultneh, Y.; Cruse, R. W.; Farooq, A.; Karlin, K. D., Reactions of dioxygen (O2) with mononuclear copper(I) complexes: temperature-dependent formation of peroxo- or oxo- (and dihydroxo-) bridged dicopper(II) complexes. *Inorg. Chem.* **1992,** *31* (21), 4322-4332.

41. Itoh, S.; Kumei, H.; Taki, M.; Nagatomo, S.; Kitagawa, T.; Fukuzumi, S., Oxygenation of Phenols to Catechols by A (μ-η2:η2-Peroxo)dicopper(II) Complex: Mechanistic Insight into the Phenolase Activity of Tyrosinase. *J. Am. Chem. Soc.* **2001,** *123* (27), 6708-6709.

42. Mirica, L. M.; Vance, M.; Rudd, D. J.; Hedman, B.; Hodgson, K. O.; Solomon, E. I.; Stack, T. D. P., Tyrosinase Reactivity in a Model Complex: An Alternative Hydroxylation Mechanism. *Science* **2005,** *308* (5730), 1890-1892.

43. Op't Holt, B. T.; Vance, M. A.; Mirica, L. M.; Heppner, D. E.; Stack, T. D. P.; Solomon, E. I., Reaction Coordinate of a Functional Model of Tyrosinase: Spectroscopic and Computational Characterization. *J. Am. Chem. Soc.* **2009,** *131* (18), 6421-6438.

44. Decker, H.; Dillinger, R.; Tuczek, F., How Does Tyrosinase Work? Recent Insights from Model Chemistry and Structural Biology. *Angew. Chem., Int. Ed.* **2000,** *39* (9), 1591-1595.

45. W., B.; E., H., The oxidation of phenols with copper ‐ amine catalysts and its relation to the mode of action of tyrosinase: I. The catalytic oxidation of monohydric phenols to orthoquinone derivatives. *Recueil des Travaux Chimiques des Pays-Bas* **1955,** *74* (8), 937-955.

46. Bulkowski, J. E. Binucleating Ligand-Metal Complexes as Oxidation Catalysts. U.S. Patent 4,545,937, 1985.

47. Esguerra, K. V. N.; Fall, Y.; Petitjean, L.; Lumb, J.-P., Controlling the Catalytic Aerobic Oxidation of Phenols. *J. Am. Chem. Soc.* **2014,** *136* (21), 7662-7668.

48. Hay, A. S., The SPE international award address—1975 polymerization by oxidative coupling—an historical review. *Polym. Eng. Sci.* **1976,** *16* (1), 1-10.

49. Mirica, L. M.; Vance, M.; Rudd, D. J.; Hedman, B.; Hodgson, K. O.; Solomon, E. I.; Stack, T. D. P., A Stabilized μ-η2:η2 Peroxodicopper(II) Complex with a Secondary Diamine Ligand and Its Tyrosinase-like Reactivity. *J. Am. Chem. Soc.* **2002,** *124* (32), 9332-9333.

50. Mirica, L. M.; Rudd, D. J.; Vance, M. A.; Solomon, E. I.; Hodgson, K. O.; Hedman, B.; Stack, T. D. P., μ-η2:η2-Peroxodicopper(II) Complex with a Secondary Diamine Ligand: A Functional Model of Tyrosinase. *J. Am. Chem. Soc.* **2006,** *128* (8), 2654-2665.

51. Esguerra, K. V. N.; Fall, Y.; Lumb, J.-P., Catalytic aerobic oxidation of halogenated phenols. *Inorg. Chim. Acta* **2017**.

52. Kwon, O.; Virgel N. Esguerra, K.; Glazerman, M.; Petitjean, L.; Xu, Y.; Ottenwaelder, X.; Lumb, J.-P., Development of 3,5-Di-tert-butylphenol as a Model Substrate for Biomimetic Aerobic Copper Catalysis. *Synlett* **2017,** *28* (3), 1548-1553.

53. Esguerra, K. V. N.; Fall, Y.; Lumb, J.-P., A Biomimetic Catalytic Aerobic Functionalization of Phenols. *Angew. Chem., Int. Ed.* **2014,** *53* (23), 5877-5881.

54. Verma, P.; Weir, J.; Mirica, L.; Stack, T. D. P., Tale of a Twist: Magnetic and Optical Switching in Copper(II) Semiquinone Complexes. *Inorg. Chem.* **2011,** *50* (20), 9816-9825.

55. Askari, M. S.; Rodriguez-Solano, L. A.; Proppe, A.; McAllister, B.; Lumb, J. P.; Ottenwaelder, X., Catalytic aerobic oxidation of phenols to ortho-quinones with air-stable copper precatalysts. *Dalton Trans.* **2015,** *44* (27), 12094-12097.

56. Yamazaki, S.-i.; Itoh, S., Kinetic Evaluation of Phenolase Activity of Tyrosinase Using Simplified Catalytic Reaction System. *J. Am. Chem. Soc.* **2003,** *125* (43), 13034-13035.

57. Mirica, L. M.; Stack, T. D. P., A Tris(μ-hydroxy)tricopper(II) Complex as a Model of the Native Intermediate in Laccase and Its Relationship to a Binuclear Analogue. *Inorg. Chem.* **2005,** *44* (7), 2131-2133.

58. Lewis, E. A.; Tolman, W. B., Reactivity of Dioxygen−Copper Systems. *Chem. Rev.* **2004,** *104* (2), 1047-1076.

59. Morioka, C.; Tachi, Y.; Suzuki, S.; Itoh, S., Significant Enhancement of Monooxygenase Activity of Oxygen Carrier Protein Hemocyanin by Urea. *J. Am. Chem. Soc.* **2006,** *128* (21), 6788-6789.

60. Herres-Pawlis, S.; Verma, P.; Haase, R.; Kang, P.; Lyons, C. T.; Wasinger, E. C.; Flörke, U.; Henkel, G.; Stack, T. D. P., Phenolate Hydroxylation in a Bis(μ-oxo)dicopper(III) Complex: Lessons from the Guanidine/Amine Series. *J. Am. Chem. Soc.* **2009,** *131* (3), 1154-1169.

61. Fujieda, N.; Yabuta, S.; Ikeda, T.; Oyama, T.; Muraki, N.; Kurisu, G.; Itoh, S., Crystal structures of copper-depleted and copper-bound fungal pro-tyrosinase: insights into endogenous cysteine-dependent copper incorporation. *J. Biol. Chem.* **2013,** *288* (30), 22128-40.

62. Suzuki, K.; Shimokawa, C.; Morioka, C.; Itoh, S., Monooxygenase Activity of Octopus vulgaris Hemocyanin. *Biochemistry* **2008,** *47* (27), 7108-7115.

63. Anslyn, E. V.; Dougherty, D. A., *Modern Physical Organic Chemistry*. University Science Books: **2005**.

64. Kubas, G. J., *Inorg. Synth.* **1990,** *28*, 68-70.

65 Zhang, H.; Kwong, F. Y.; Tian, Y.; Chan, K. S., Base and Cation Effects on the Suzuki Cross-Coupling of Bulky Arylboronic Acid with Halopyridines: Synthesis of Pyridylphenols. *J. Org. Chem.* **1998,** *63* (20), 6886-6890.

66 Bhonde, V. R.; O'Neill, B. T.; Buchwald, S. L., An Improved System for the Aqueous Lipshutz-Negishi Cross-Coupling of Alkyl Halides with Aryl Electrophiles. *Angew. Chem., Int. Ed.* **2016,** *55* (5), 1849-53.